NASA CR-152465

REPORT NO. P77-20
HAC REF. NO. D7036

FINAL REPORT
NAS 5–23621

METEOROLOGICAL RADAR FACILITY (MRF) SLOT CONDUCTANCE INVESTIGATIONS

JANUARY 1977

Prepared for: National Aeronautics and Space Administration
Goddard Space Flight Center
Greenbelt Road, Maryland 20771

AEROSPACE GROUPS
HUGHES
HUGHES AIRCRAFT COMPANY
CULVER CITY, CALIFORNIA

SECURITY CLASSIFICATION OF THIS PAGE *(When Data Entered)*

REPORT DOCUMENTATION PAGE		READ INSTRUCTIONS BEFORE COMPLETING FORM
1. REPORT NUMBER	2. GOVT. ACCESSION NO.	3. RECIPIENT'S CATALOG NUMBER
4. TITLE *(and Subtitle)* Meteorological Radar Facility (MRF) Slot Conductance Investigations		5. TYPE OF REPORT & PERIOD COVERED Final Report 21 June-21 December 1976 6. PERFORMING ORG. REPORT NUMBER P77-20; HAC Ref. D7036
7. AUTHOR(s) A. E. Ratkevich		8. CONTRACT OR GRANT NUMBER(s) NAS 5-23621
9. PERFORMING ORGANIZATION NAME AND ADDRESS Antenna Department Radar System Group Hughes Aircraft Company Culver City, California 90230		10. PROGRAM ELEMENT, PROJECT, TASK AREA & WORK UNIT NUMBERS
11. CONTROLLING OFFICE NAME AND ADDRESS National Aeronautics and Space Administration Goddard Space Flight Center Greenbelt, Maryland 20771		12. REPORT DATE January 1977 13. NUMBER OF PAGES 85
14. MONITORING AGENCY NAME & ADDRESS*(if different from Controlling Office)*		15. SECURITY CLASS. *(of this report)* Unclassified 15a. DECLASSIFICATION/DOWNGRADING SCHEDULE N/A

16. DISTRIBUTION STATEMENT *(of this Report)*

Distribution per Contract Article I. B. (Item 2)

17. DISTRIBUTION STATEMENT *(of the abstract entered in Block 20, if different from Report)*

18. SUPPLEMENTARY NOTES

19. KEY WORDS *(Continue on reverse side if necessary and identify by block number)*

- Non-resonsant short longitudinal shunt slots
- Admittance Measurements
- Very long traveling wave array
- X-band

20. ABSTRACT *(Continue on reverse side if necessary and identify by block number)*

A preliminary Meteorological Radar Facility (MRF) array design was completed in support of the slot conductance measurement program. Three different slot measurement techniques were evaluated. This resulted in the selection of the probe comparison measurement technique as the principal experimental method with the impedance measurement technique selected to measure a few higher conductance slots to be used as reference slots. The impedance of 43 slots in 0.9 x 0.4 inch standard waveguide and of 40 slots in 0.835 x 0.4 inch waveguide was measured. Also, impedance measurements

DD FORM 1 JAN 73 1473 EDITION OF 1 NOV 65 IS OBSOLETE

Unclassified

SECURITY CLASSIFICATION OF THIS PAGE *(When Data Entered)*

20. Abstract (Continued)

were made of a few slots using image planes to simulate mutual coupling effects. The measured and theoretical conductance, susceptance, and radiation phase data are presented in graphic form as a function of slot displacement for constant slot length and of slot length for constant slot displacement. It is concluded that the proposed MRF array design approach is a feasible one.

PREFACE

This document is the final report for the Meteorological Radar Facility (MRF) Slot Conductance Investigations Program and is submitted in accordance with the requirements of Contract NAS5-23621 from the National Aeronautics and Space Administration. The report covers the work performed by the Hughes Aircraft Company from June through December, 1976. The Technical Officer is L.R. Dod of the National Aeronautics and Space Administration, whose guidance on this program is gratefully acknowledged. The Hughes effort was conducted within the Antenna Department of the Radar Microwave Laboratory, Radar Systems Group, and was supervised by Charles K. Watson under the general direction of Charles A. Strider. The design, analysis, and test was the responsibility of Adam E. Ratkevich, Project Engineer; significant guidance was provided by Swegn D. Hamren, Program Manager; the majority of the tests and computations were made by Steve E. Panaretos; important contributions were made by Norman C. Olsen in the analysis, and by Leland I. Auslender in preparation of this manuscript.

CONTENTS

LIST OF ILLUSTRATIONS

LIST OF ILLUSTRATIONS (Continued)

LIST OF ILLUSTRATIONS (Continued)

LIST OF TABLES

1.0 INTRODUCTION

This contractual effort consists of experimental study tasks that, together with related design considerations, address the technology that is pertinent to the array antenna subsystem of the Meteorological Radar Facility (MRF). Both a subscale antenna, nominally 4 by 5 meters in dimensions, and a full-scale antenna, nominally 4 by 18 meters, are being considered. The study is being limited to questions pertinent to the microwave design. Mechanical and thermal design questions are not being considered.

The design study tasks, which encompass various microwave design considerations, were added to what may be considered essentially an experimental study for four reasons:

1. To provide continuity with the earlier MRF antenna study, done in connection with Contract No. NAS5-22468.
2. To provide direction with regard to the most useful range of slot conductance measurements to be made.
3. To provide a practical guide concerning the best way in which the measured data can be presented and used for the MRF slot array design.
4. To clarify what further microwave study tasks may be necessary before design of the MRF slot array can begin.

With regard to the last objective, it is to be stressed that an accurate evaluation of mutual coupling effects and its incorporation into the design of the MRF planar array may be a major analytical or experimental effort in itself, and the results of evaluation undertaken in the present study will serve as a preliminary assessment.

This final report covers three main topics: experimental investigations, supporting microwave design considerations, and experimental results and conclusions.

2.0 DESIGN AND TASK DESCRIPTION

The antenna as presently considered operates at X-band at a nominal frequency of 10 GHz. It consists of a narrow transmitting array less than 3 cm wide and a receiving antenna, nominally 4 meters wide, that fills the remainder of the aperture. The lengths of the antennas will be either 5 or 18 meters.

The receiving antenna consists of 180 parallel traveling-wave arrays that run the length of the antenna. Each traveling-wave array is a waveguide with shunt reactive longitudinal radiating slots cut in the broadwall of the guide. Approximately 328 slots are used in each 5-meter array and approximately 1180 in each 18-meter array. Because of the many slots in each longitudinal array, the coupling of each slot to the waveguide is very low. The slots are offset to one side of the centerline of the guide, and the coupling is controlled by both the offset and the slot length. The longitudinal slot spacing is approximately 0.600 inch. The traveling-wave arrays are placed side by side with a centerline-to-centerline spacing of 0.875 inch. The slot spacing and number of arrays have been slightly revised from those of the earlier study.

The transmitting antenna consists of one or two traveling-wave arrays like the receiving arrays described above and located parallel to them with a gap, possibly loaded, for isolation.

The maximum of each traveling-wave receiver pattern is situated on a conical surface that is at an angle of approximately 45 degrees from a plane perpendicular to the axis of the array. The response of the combination of 180 arrays in azimuth to provide multiple beams on the cone is not determined in the antenna itself. Rather, each longitudinal array provides an input to an individual receiver and the desired patterns in azimuth, 86 in number, are generated in the system processor by means of the digitized received signals. The angle at which the elevation pattern maximum occurs is controlled by the wave velocity in the radiating waveguide, which is determined by the waveguide width. At present, a tilt angle of 45 degrees is assumed. This angle is provided by an internal waveguide width of 0.835 inch

at 10 GHz. The aperture excitation and sidelobe level in the elevation plane are controlled by the coupling of the slots, i. e., by the slot lengths and offsets. The sidelobe level design is assumed to be a 25-dB Taylor, $\bar{n}=3$, design.

The study includes the following specific contractual tasks.

1. Formulation of the techniques and design of the experiment to make those measurements of low-conductance, short, shunt slots that are of interest for the design of the MRF slot array.
2. Fabrication of test fixtures and slot configurations appropriate to these measurements.
3. Measurement of slot admittances versus slot lengths and versus slot displacements from the waveguide centerline.
4. Comparison of the measured results with theoretical predictions and extraction of data for standard X-band waveguide and for the waveguide size that at that time appears advisable for application to the antenna of the Meteorological Radar Facility.

In addition, a number of supportive design studies are included.

3.0 MICROWAVE DESIGN CONSIDERATIONS

3.1 APERTURE DESIGN

3.1.1 Array Lattice Selection

The planar array aperture will consist of a rectangular lattice of slot radiating elements, the shunt slots being cut in the broadwalls of vertically running waveguides that are mounted side by side. The coordinate system for the MRF planar array is shown in Figure 1. The array is to be designed for one-dimensional scan along the arc defined by the direction cosine angle, α_y = constant. The direction cosine angle, α_y, will be approximately 45 degrees. The limits on the slot element spacings in the rectangular lattice are related to the traveling-wave linear array tilt angle, $90^o - \alpha_y$, and the scan angle extremes, $\theta x = \pm 35$ degrees. It can be shown by a grating lobe diagram study that the element-spacing limits for the MRF array are determined by the following worst case scan conditions:

1. Beam broadside in XZ plane ($\theta_x = 0^o$), beam tilted by 45 degrees from broadside in the YZ plane ($90^o - \alpha_y = 45^o$). A grating lobe

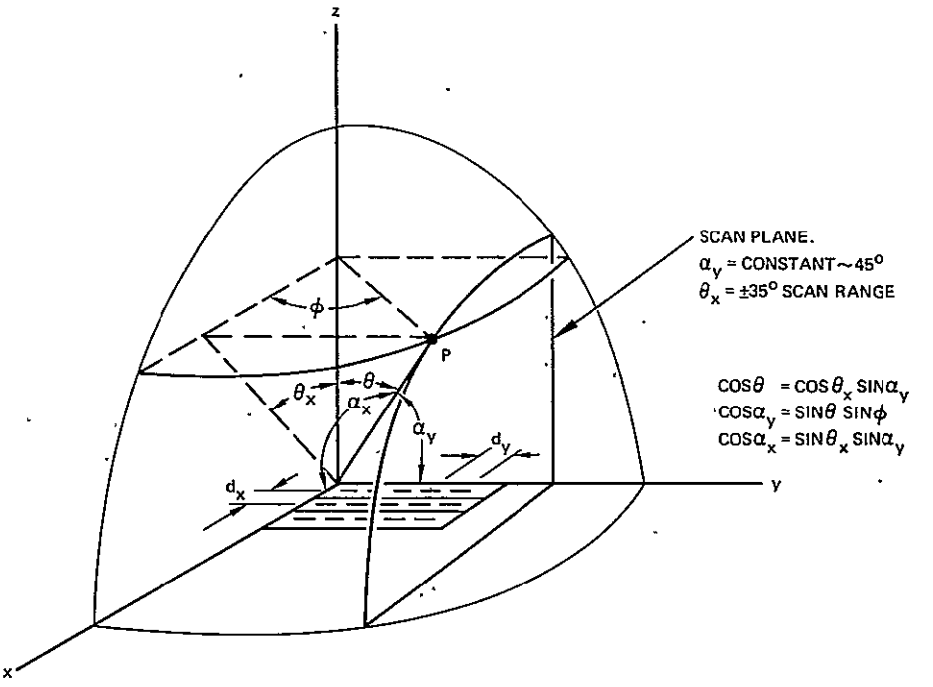

Figure 1. Coordinate system for MRF planar array.

occurs in the YZ plane when the d_y slot spacing satisfies the following equation:

$$\frac{d_y}{\lambda}(\cos \alpha_{yg} - \cos \alpha_y) = -1$$

where

$(90^\circ - \alpha_y)$ = linear array beam tilt angle

α_{yg} = grating lobe angle

For a design angle of $\alpha_y = 45$ degrees and at 10 GHz, a grating lobe just begins to occur in visible space ($\alpha_{yg} = 180^\circ$) for $d_y = 0.691$ inch. In general, quite adequate performance can be achieved with a scannable array designed with a 10-percent lattice, i.e., a lattice whose spacing is 90 percent of the grating-lobe spacing. By this criterion, a linear-array slot spacing of $0.9 \times 0.691 = 0.622$ inch would be used. This spacing is 3.5 percent larger than the previously assumed spacing of 0.600 inch and would decrease the number of slots required for each 5- and 18-meter linear array from 328 to 316 and from 1180 to 1139, respectively.

2. Beam scanned to its maximum scan angle in its scan plane ($\theta_x = \pm 35^\circ$, $\alpha_y = 45^\circ$). A grating lobe occurs in the scan plane, as defined in Figure 1, when the d_x slot spacing satisfies the following equation.

$$\frac{d_x}{\lambda}(\cos \alpha_{xg} - \cos \alpha_x) = -1$$

where

α_x = direction cosine scan angle referenced to the x-axis

α_{xg} = grating lobe angle

For a design angle of $\alpha_y = 45^\circ$ and a beam scan angle of $\theta_x = 35^\circ$, then $\alpha_x = 66.07$ degrees and, at 10 GHz, a grating lobe just begins to occur in visible space ($\alpha_{xg} = 135^\circ$ and $\sin \theta_g = \sqrt{(\cos \alpha_{xg})^2 + (\cos \alpha_y)^2} = 1$) for $d_x = 1.061$ inches.

The design spacing in d_x will be close to 0.875 inch (an 18-percent lattice), which is appreciably less than this maximum spacing limit of 1.061 inches.

3.1.2 Aperture Impedance Considerations

A planar array built up from a number of slotted waveguide sections presents an aperture similar to that of an open-ended waveguide array; the slots cut through the waveguide walls are themselves short sections of waveguide. A computer program is available that accurately determines the active-element impedance of open-ended waveguides arranged in an infinite-extent, doubly-periodic grid; the program accounts completely for the effects of mutual coupling. The values obtained are also very good approximations to those prevailing for elements (other than edge elements) in large finite arrays. The method of analysis utilized is basically that outlined in Amitay.[1]

The active-element impedance of the slot radiators will change with scan angle because of the same mechanism as for the open-ended waveguide radiators, i.e., because of the change in mutual coupling. Because the geometry on the aperture side of the array is the same for slot radiators as for open-ended waveguide radiators (same lattice and radiating aperture dimensions), and because the mutual coupling is determined by this geometry, the mutual coupling effects for the two cases should also be the same. It is believed, therefore, that a useful estimate of the variation of slot active-element impedance with scan can be obtained by use of the waveguide array computer program. Because the open-ended waveguides analyzed by this program are assumed to be terminated in matched generators, however, and those of the slots are not so terminated, it cannot be used to determine the actual values of slot element impedance.

The waveguide array program was utilized to calculate the reflection coefficients as a function of scan angle for slot lengths of 0.400 and 0.480 inches. The program was modified to permit the use of independently fed cutoff slots and to translate the reflection coefficients, computed at the aperture plane, through the cutoff slots to the inside wall of the waveguide. E- and H-plane lattice dimensions of 0.875 and 0.600 inches, respectively, were used, as was a slot width of 0.062 inches, a radiating guide wall thickness of 0.020 inches, an α_y of 45 degrees, and a frequency of 10.0 GHz. Figure 2 indicates the coordinate system used in the calculations as well as

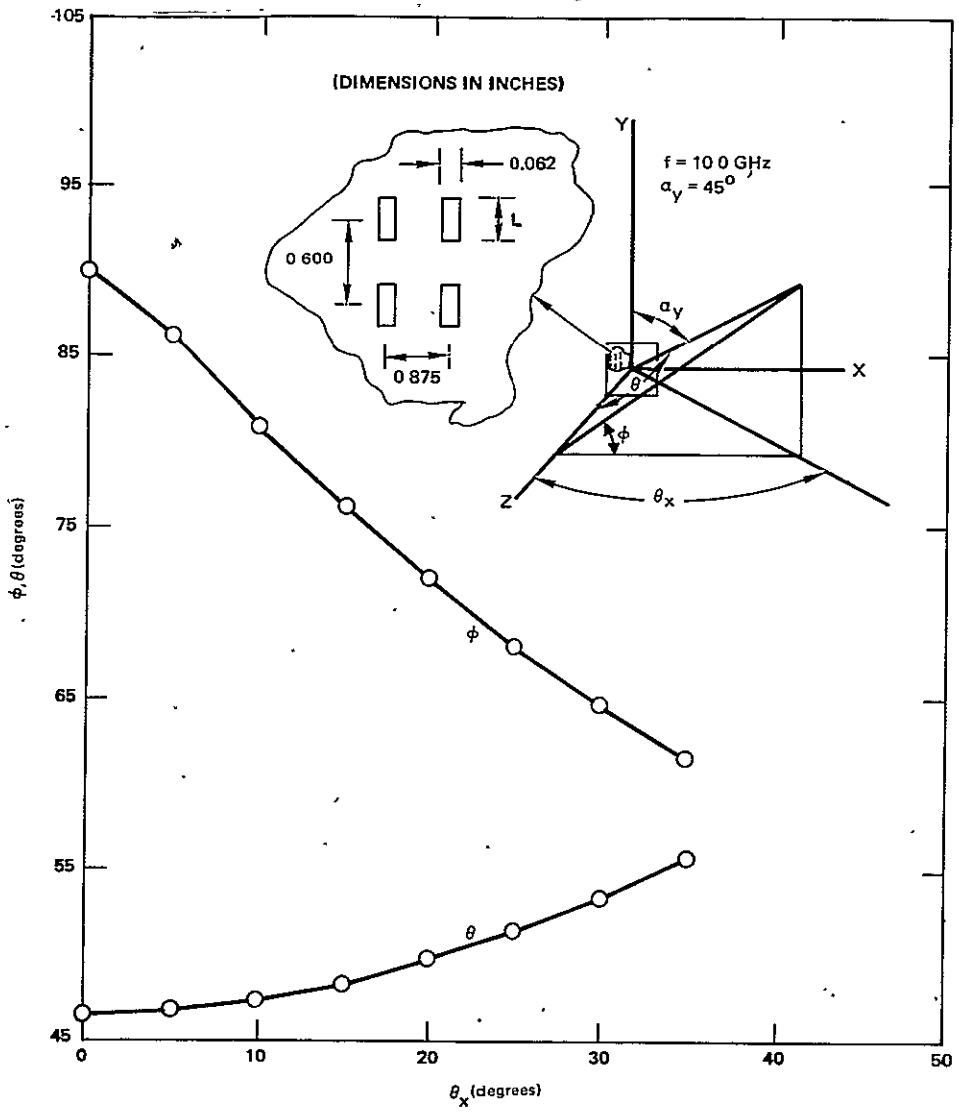

Figure 2. Coordinate system utilized for reflection coefficient calculations.

the relationship between θ_x, θ, and ϕ Figures 3a and 3b indicate the computed reflection coefficients versus θ_x for slots 0.400 and 0.480 inches in length. As can be seen from the figures, a change of approximately 2.1 percent in magnitude and 0.6 degrees in phase was computed for the 0.400-inch slot, and 3.3 percent in magnitude and 1.0 degrees in phase for the 0.480 inch slot. It is felt, therefore, that no significant change in slot active-element impedance should occur as a result of scanning the beam over the angular range intended.

3.2 SLOT CONDUCTANCE REQUIREMENTS

Accurate derivation of the slot conductance distribution for the MRF traveling-wave linear slot arrays necessitates four design stages: (1) derivation of the conductances, for a range of load powers, for the simplified case of resonant slots (zero reactance) with no interactions between slots[2][3]; (2) derivation of the conductances, for a selected load power, for the case of resonant slots including internal interaction between slots[4]; (3) investigation of the effects on the array performance when the conductances derived in stage two are applied to reactive slots[5]; and (4) evaluation of the MRF conductance requirements under external (mutual coupling) interaction effects.

The first three of these four stages were completed for the 5-meter array. For the 18-meter array, only the first stage design was implemented. In this first stage, the approximate resonant slot conductance requirements were derived for the cases of 328 and 1180 slots and for 5-, 2.5-, and 1-percent power to the load. The cases of 5-percent load power with aluminum waveguide losses included were also computed. The computations were carried out point-by-point for each slot. These first stage conductance requirements are plotted in Figures 4 and 5 for, respectively, the 5 and 18 meter arrays. The results are approximate because both internal and external interactions between slots were not included in the computations. This data is convenient for the selection of a particular design for a given percentage of power to the load. On the basis of the data in Figures 4 and 5, the design case of 2.5-percent load power would be selected, the objective being a design for

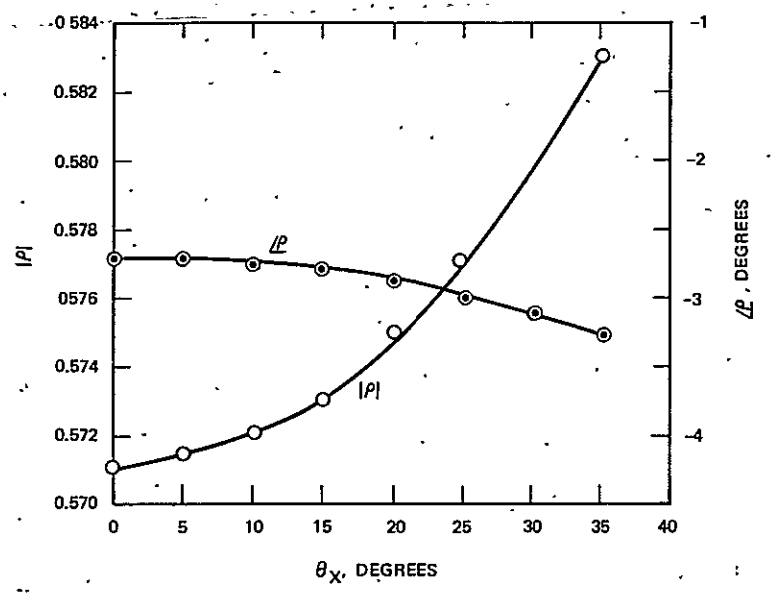

a. L = 0.400 INCHES

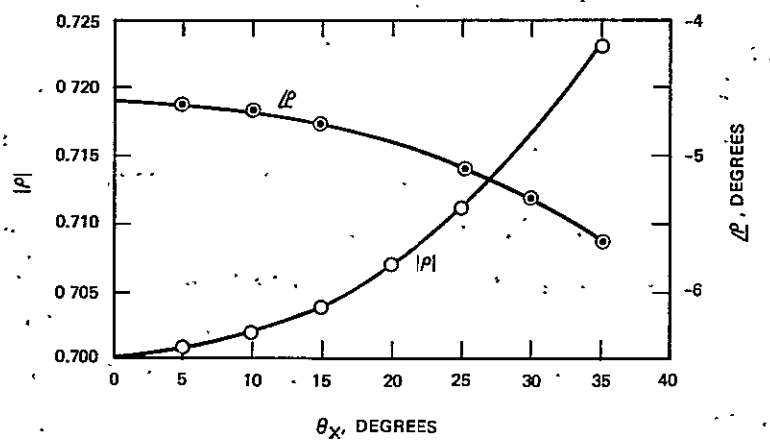

b. L = 0.480 INCHES

Figure 3. Reflection coefficient as a function of scan angle for two configurations of slots.

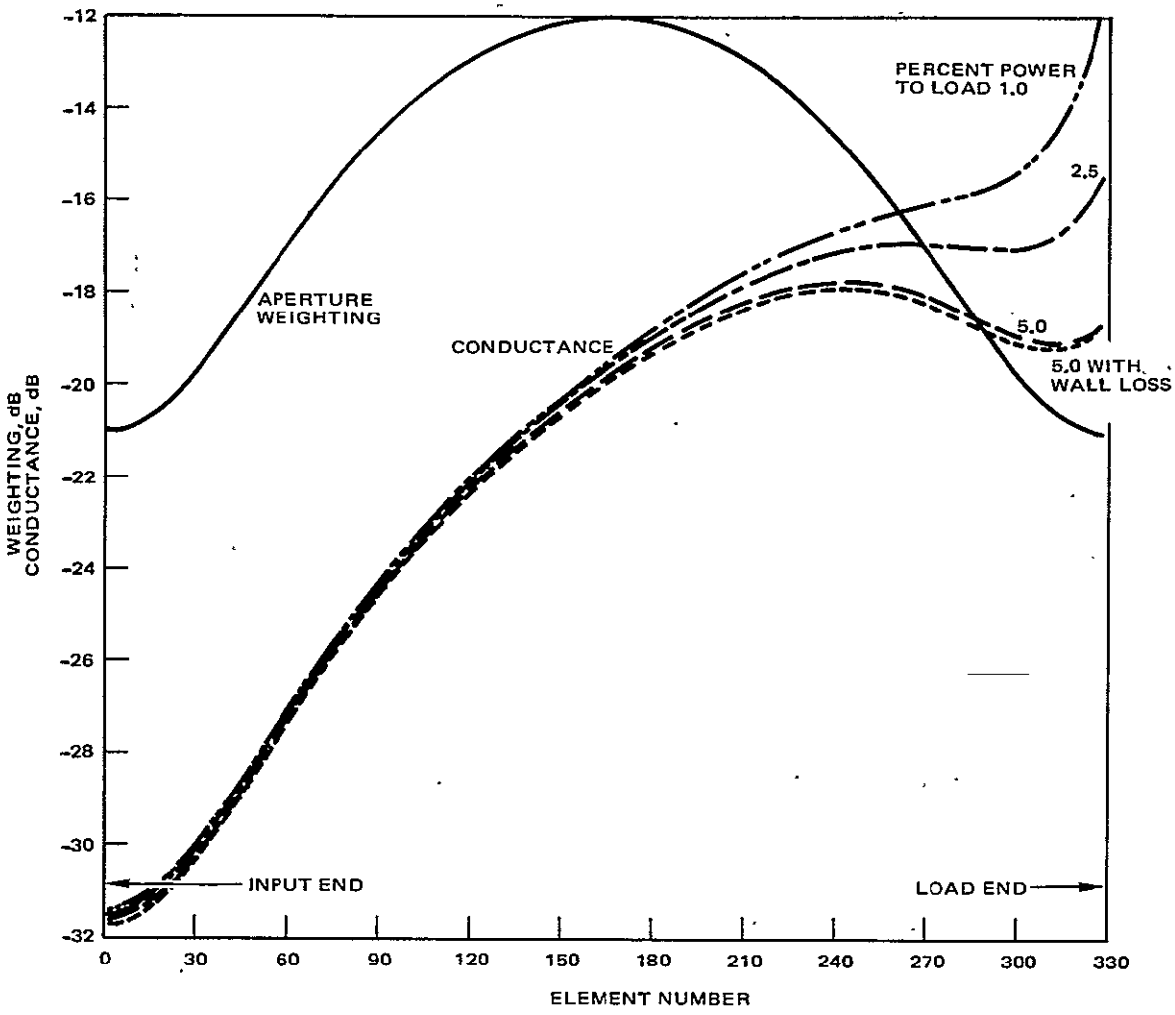

Figure 4. Traveling-wave array conductance curves for 328 slots with a 25-dB Taylor weighting ($\bar{n}$ = 3).

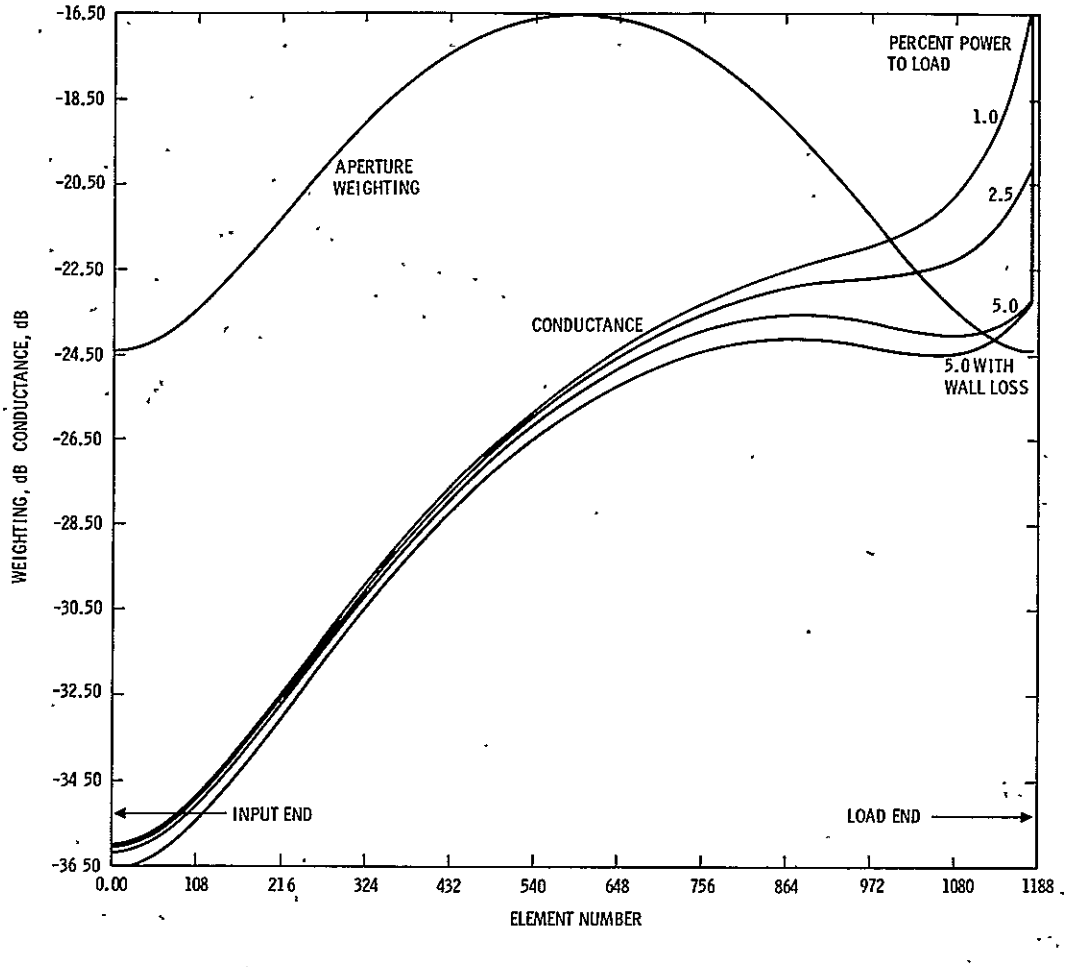

Figure 5. Traveling-wave array conductance curves for 1180 slots with a 25-dB Taylor weighting ($\bar{n} = 3$).

a minimum amount of power to the load while avoiding any rapid rise in design conductance at the load end of the line, such as occurs for the case of 1-percent load power. In addition, although the 1-percent load-power case is the most efficient, the net improvement in gain over the 2.5-percent load-power case is negligible. For these two cases, the gain loss is, respectively, 0.04 and 0.11 dB, or a difference of 0.07 dB.

In the second design stage, with the 2.5-percent load power case selected, the conductance requirements for the 5-meter array were derived for the resonant slot case in which the internal interactions between slots are accounted for. For the MRF array, where the conductance values are very low, the internal reflections by the resonant slots are also very low; hence, internal interaction effects are very small and there is little difference between the first and second stage designs.

In the third stage, the effect of the use of non-resonant (reactive) rather than resonant slots was evaluated. For a fixed slot displacement of 0.30 inch and for slot lengths that provided the required conductances, the computed slot reactances were added to the slot conductances, and the consequent aperture distribution was obtained by means of a computerized model of a reactive traveling-wave feed, linear-array system.* The comparative aperture distributions for the second-stage and third-stage designs are shown in Figure 6; the effect of the increased internal reflections due to the slot

*A linear traveling wave feed can be modeled quite accurately by use of a scattering matrix formulation. Each of the slot-couplers (three-ports) and interconnecting waveguides (two-ports) is represented by a scattering matrix whose elements are determined either by measurement or by an analysis of their equivalent circuit representations. The feed line load and the slot-coupler output port mismatches are treated as reflection coefficients at the appropriate ports. A computer program has been written to perform the matrix manipulations necessary to determine the input VSWR, power into the feed line load, and the excitations at the slot-coupler output ports as a function of output port (antenna port) mismatch.

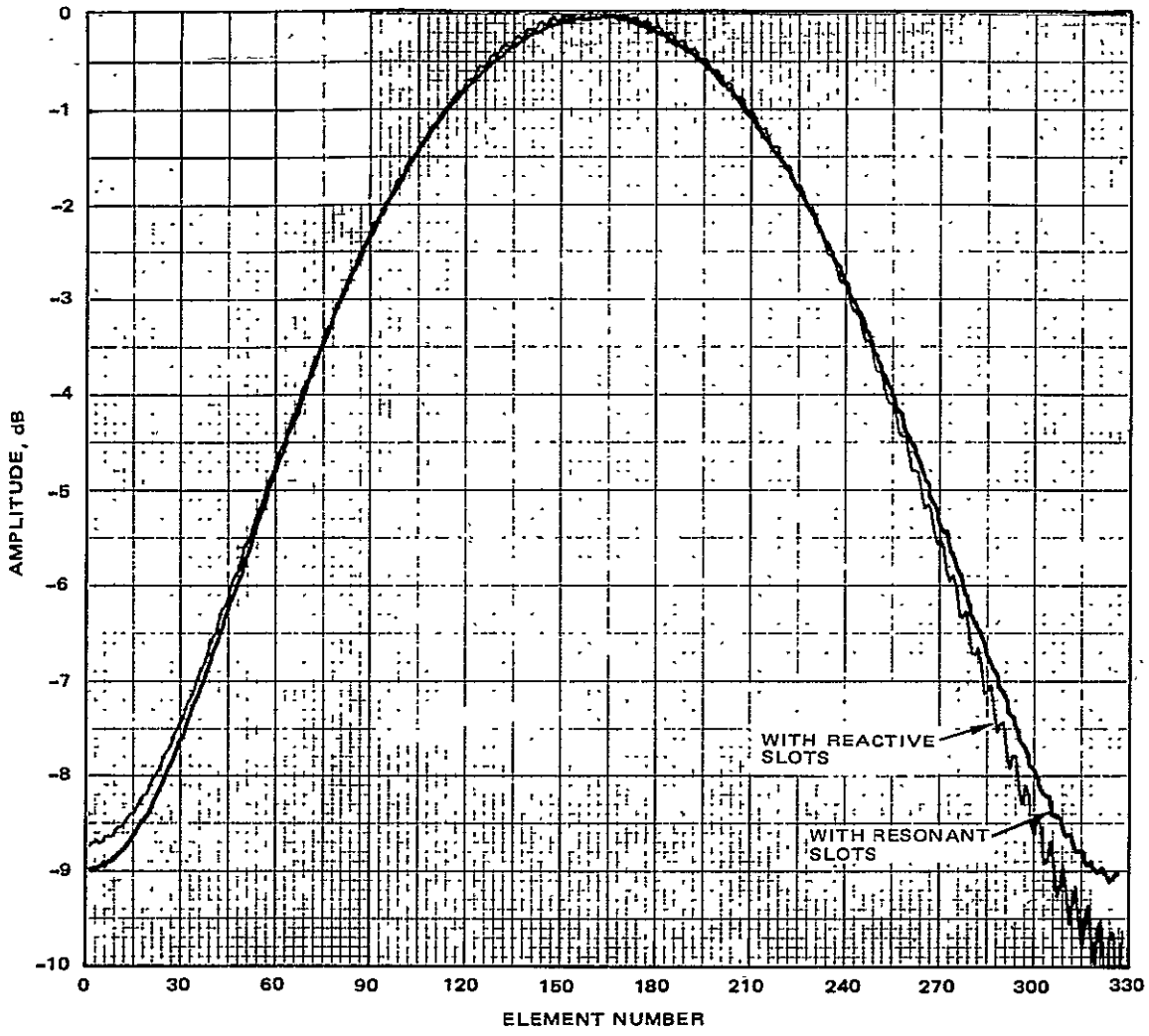

Figure 6. Aperture distributions for 5-meter, traveling-wave linear array.

reactances is clearly evident. If these small oscillations in the aperture amplitude distribution result in an unacceptable side lobe structure in the elevation-plane pattern, then the second-stage design procedure would have to be iterated. For each iteration, an estimate of the slot reactance for each of the 328 slots would be made, and the slot conductance requirements would then be derived under the conditions of internal interactions due to these high slot reactances. A computerized model of this design procedure was not available; in addition, there is not much difference in the sidelobe structure for the

elevation-plane pattern resulting from the aperture distribution shown in Figure 6 for the reactive slots and for the ideal case pattern, so that the iterative design procedure was not undertaken. A comparison of the resonant-slot pattern (Figure 7a) with the reactive-slot pattern (Figure 7b) shows that the principal effect of the small modulation on the amplitude distribution is the -42 dB sidelobe that occurs in a direction looking above the horizon. The beam broadening that occurs for this reactive slot case (Figure 7b) is due to a phase-error effect that can be corrected for and which is discussed in Section 3.4.2.

The fourth design stage involves the determination of mutual coupling effects on the slot admittances. The conductance curves shown in Figures 4 and 5 are for the case in which internal and external interactions are neglected. Internal interactions result only in small modulations on the conductance curves so that their effect on the aperture distribution, when not corrected for, is small. External interactions (or mutual coupling) can have a much broader effect on the slot conductances and, consequently, on the aperture distribution. Some of the possible consequences of these effects, if not corrected for, are reviewed in Section 3.3. Also, some slot measurements were made using image planes (see Section 5.4) to simulate the effect of mutual coupling and thereby permit an approximate assessment of the impact of mutual coupling on the design.

3.3 SLOT CONDUCTANCE ERROR EFFECTS

Conductance errors that will lead to aperture distribution errors can occur due to mutual coupling effects, slot measurement errors, and array fabrication errors.[6][7] Mutual coupling effects have been found to increase the effective slot conductance by a factor of as much as 2 to 1 compared with the isolated slot conductance; consequently, even where some efforts are made to account for mutual coupling in the MRF array design, mutual coupling is expected to present the primary error source. A summary of the range of errors that might occur under mutual coupling effects is given in Table 1. Errors in the calibration of the lower range of conductance values (conductances in the range from 0.0001 to 0.001) are expected to present the second largest error source. Both of these error sources are expected to result in incremental

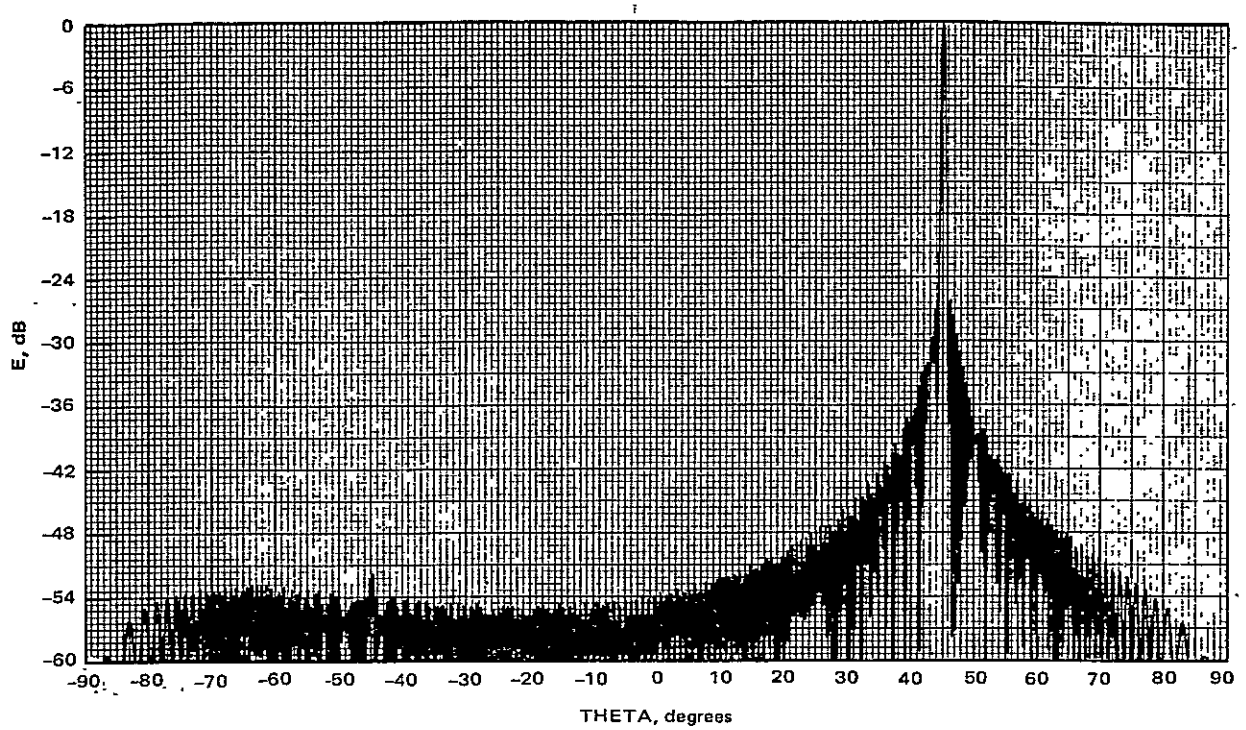

a. With resonant (zero reactance) slots

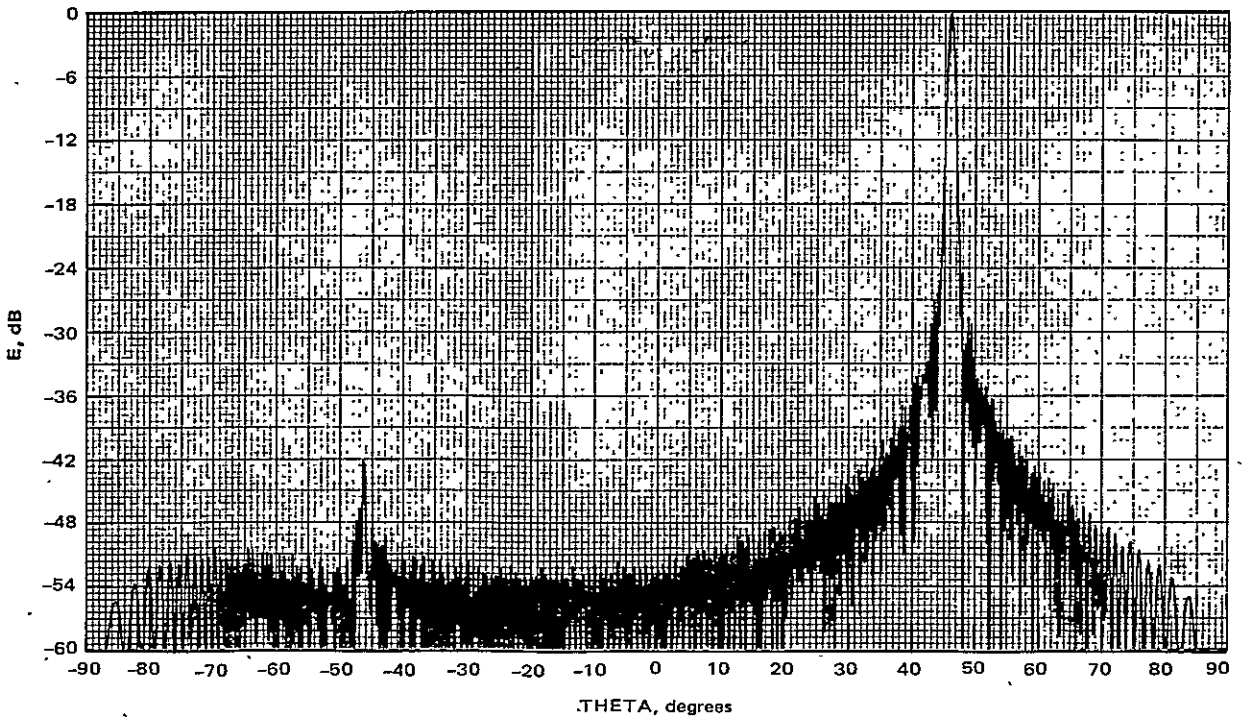

b. With reactive slots

Figure 7. Elevation-plane patterns at 10 GHz for 5-meter linear traveling-wave array (constant displacement and variable length design).

TABLE I. SLOT-CONDUCTANCE DESIGN-ERROR CASES DUE TO MUTUAL-COUPLING EFFECTS

Case	Assumed Error Effects	Design Goal	Design Input	Actual Error Effect	Effective Error[d] Case (See Table 2)
1	$1X^a$	g	g	$1X^a$	$g_e = g$ (no error)
2	$1X^a$	g	g	$2X^b$	$g_e = 2g$
3	$1X^a$	g	g	$0.5X^c$	$g_e = 0.5g$
4	$2X^b$	g	g/2	$2X^b$	$g_e = g$ (no error)
5	$2X^b$	g	g/2	$1X^a$	$g_e = 0.5g$
6	$2X^b$	g	g/2	$0.5X^c$	$g_e = 0.25g$

a. Case where mutual coupling effects are negligible

b. Case where mutual coupling effects double the design input conductance

c. Case where mutual coupling effects halve the design input conductance

d. g = ideal case design conductance, g_e = effective error case conductance

error effects; i.e., the conductance errors will not be random in magnitude or location but will tend to show up as nearly uniform changes over large areas of the array. The effects of random manufacturing errors[6][7] are expected to be of secondary importance, compared to incremental errors, because of the large size of the MRF array. The type of conductance error effect for which evaluation is most important, therefore, is the incremental conductance error.

Three types of incremental conductance errors were evaluated for the five meter array; each is discussed briefly.

1. The case in which the first 87 elements on the input end of the array (the region of lowest conductance values) are in error by the linear relation:

$$g_e = g + g(88-N)/87 \qquad (1)$$

where

N = slot number 1 to 87

g = ideal design conductance

g_e = conductance including errors

Equation (1) represents a condition in which the actual conductance (g_e) is equal to twice the design conductance (g) at the input end (N = 1) and changes linearly to the error-free values ($g_e = g$) at N = 88. This would represent a situation where large measurement errors occur in the testing of the low conductance slots.

2. The case in which the actual conductance over the full array is uniformly greater than the design conductance by the ratios: $g_e = g + 0.1g$, $g + 0.25g$, $g + 0.75g$, and $g + 1.0g$. The last equation represents an extreme situation in which mutual coupling, having been ignored in the design, tends to double the effective conductance. This situation is defined in Table 1 under case 2.

3. The case in which the actual conductance over the full array is uniformly less than the design conductance by the ratios: $g_e = g - 0.1g$, $g - 0.25g$, $g - 0.5g$ and $g - 0.75g$. This case would represent the situation in which mutual coupling effects have either been over-compensated for, or have been ignored in the design, while the actual effect is to decrease the conductance. The last condition ($g_e = g - 0.75g$) represents the extreme error case in which it has been assumed that mutual coupling doubles the effective conductance while, in reality, mutual coupling halves

the effective conductance. This situation is defined in Table 1 under case 6. The next to the last equation can occur under either undercompensation (case 3 in Table 1) or over-compensation (case 5 in Table 1).

The evaluation of each of these cases for the 5-meter array is presented in Figures 8 through 13 and in Table 2. The aperture distributions for the errorless 25-dB Taylor design and for the linear-error case, Equation (1), are shown in Figure 8. The corresponding linear array elevation-plane patterns are shown in Figure 11 and the relative gains and beamwidths are given in Table 2. The effect of this type of error on gain, beamwidth, and elevation-plane pattern sidelobe performance is seen to be negligible when compared with the no-error pattern. For the case illustrated in Figure 9, in which the actual conductances are uniformly greater than the design conductances, it can be seen that the dominant effect is an increased degree of amplitude taper on the load end of the traveling-wave linear array. The corresponding effects on the elevation-plane patterns (Figure 12 and Table 2) are seen to be small; i.e., there is a slight lowering of the sidelobe structure, a small beam broadening, and a small gain loss. Where the actual conductances are uniformly less than the design conductances, Figure 10, the dominant effect is a decreased amplitude taper on the load end of the array. The corresponding effects on the elevation-plane patterns (Figure 13 and Table 2) are also seen to be small (there is a small increase of the sidelobe structure, a small beam narrowing, and a small gain loss) except for $g_e = 0.25g$. For $g_e = 0.25g$ there is a rapid increase of the amount of power to the load, resulting in a loss of 1.9 dB in net gain.

On the basis of these results it is concluded that the beam pattern performance remains acceptable for a wide range of conductance design errors. Only when the effective conductance, including mutual coupling effects, is less than half the desired value does the extra power being dissipated in the load that terminates the traveling-wave feed become excessive.

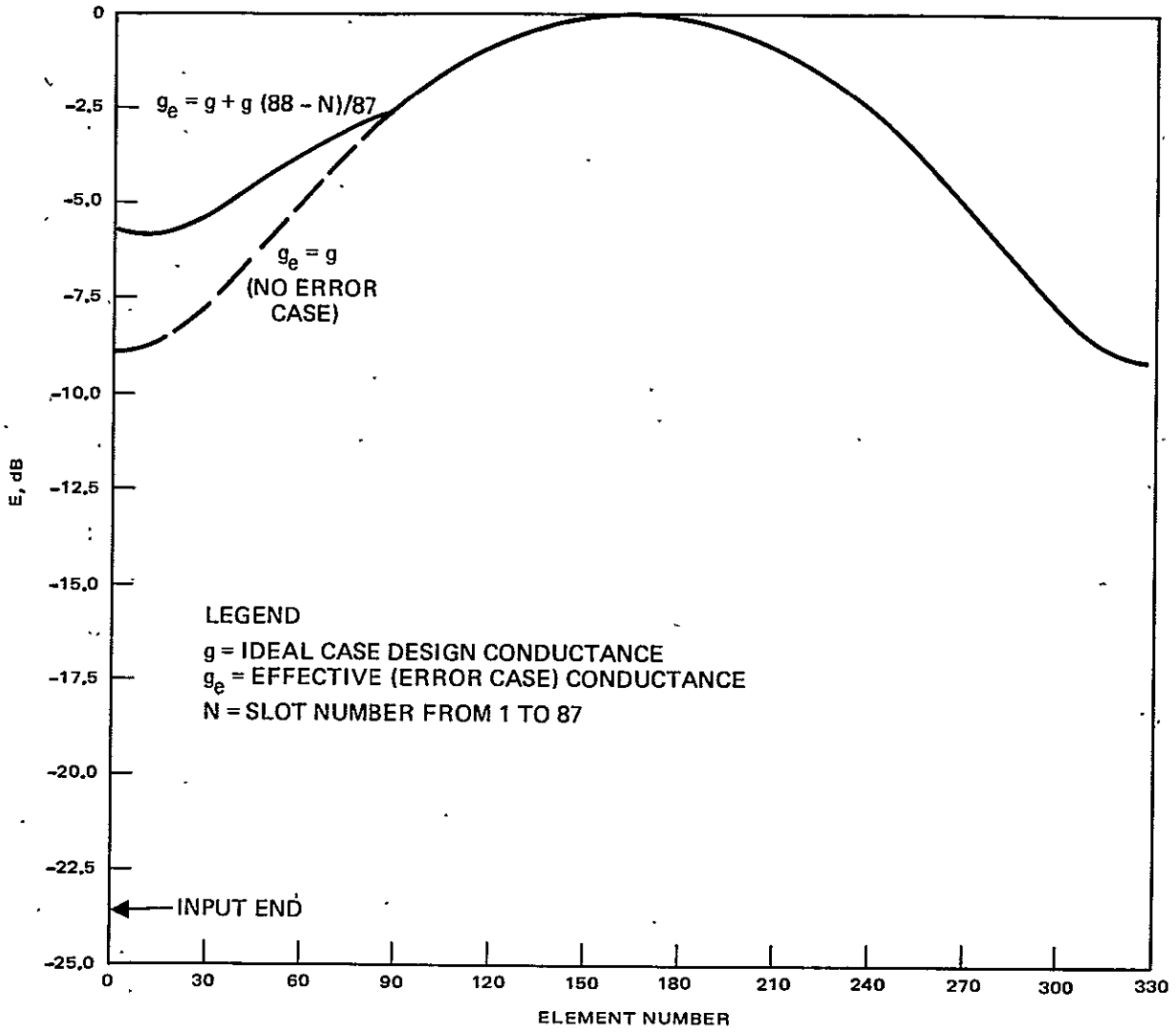

Figure 8. Aperture distribution for 5-meter linear traveling-wave array for no conductance error case and for linear conductance error case.

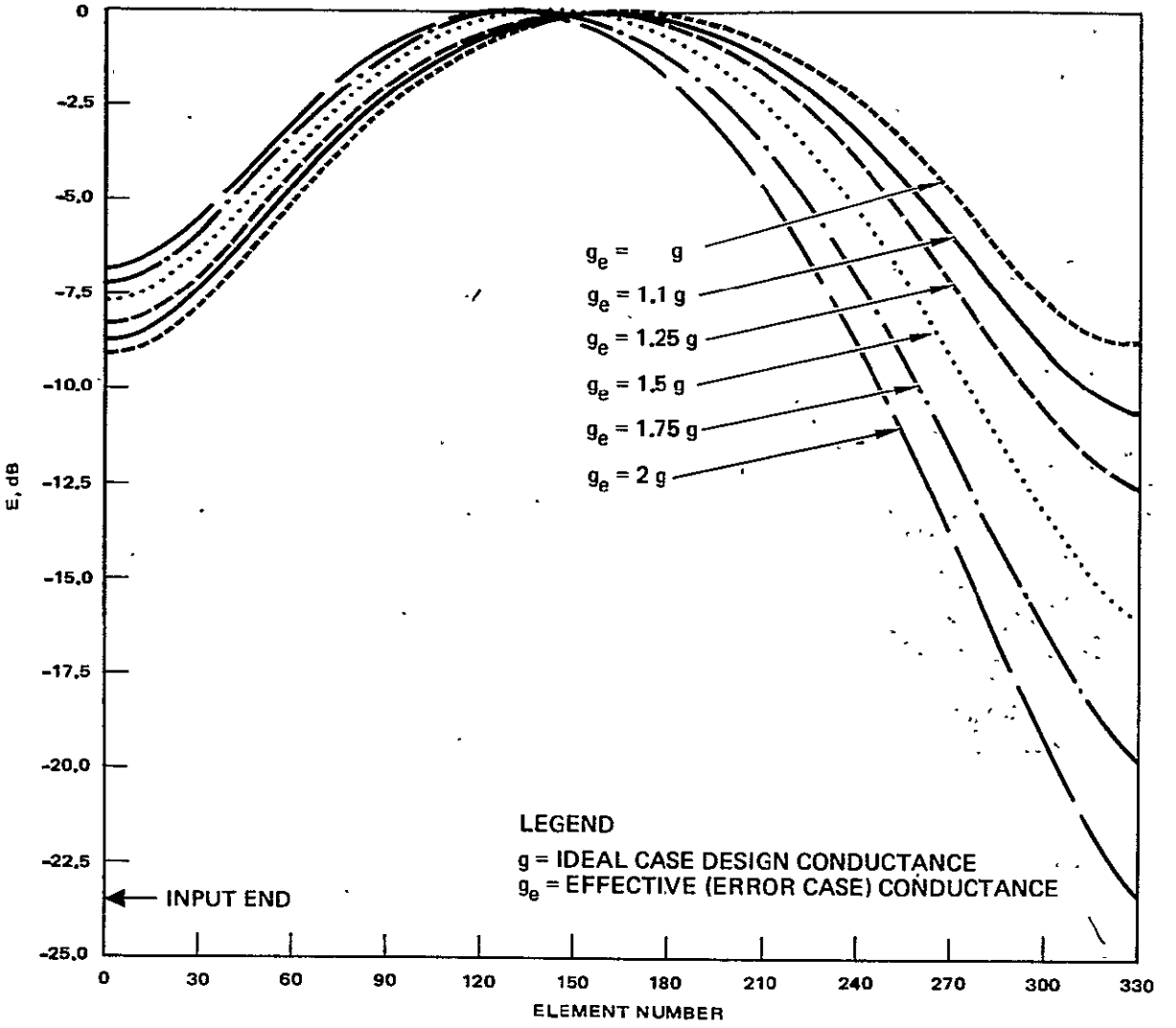

Figure 9. Aperture distributions for 5-meter linear traveling-wave array showing effects of increased slot conductances.

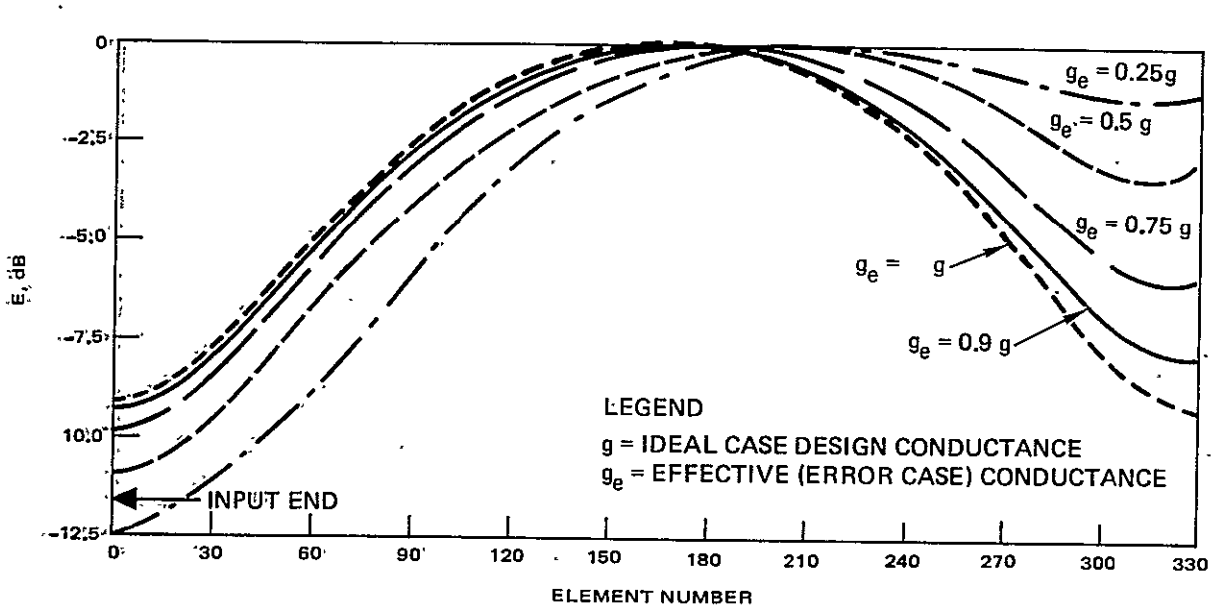

Figure 10. Aperture distributions for 5-meter linear traveling-wave array showing effects of decreased slot conductances.

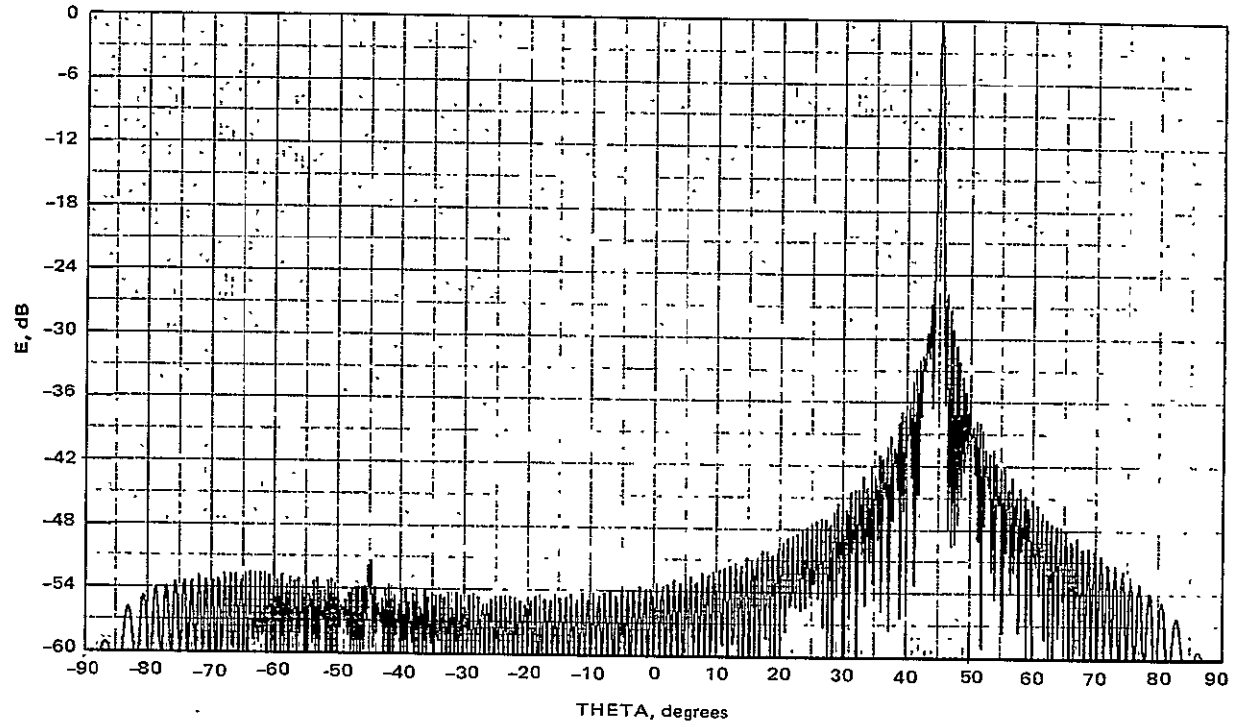

a. Effective conductance equals design conductance (no errors case)

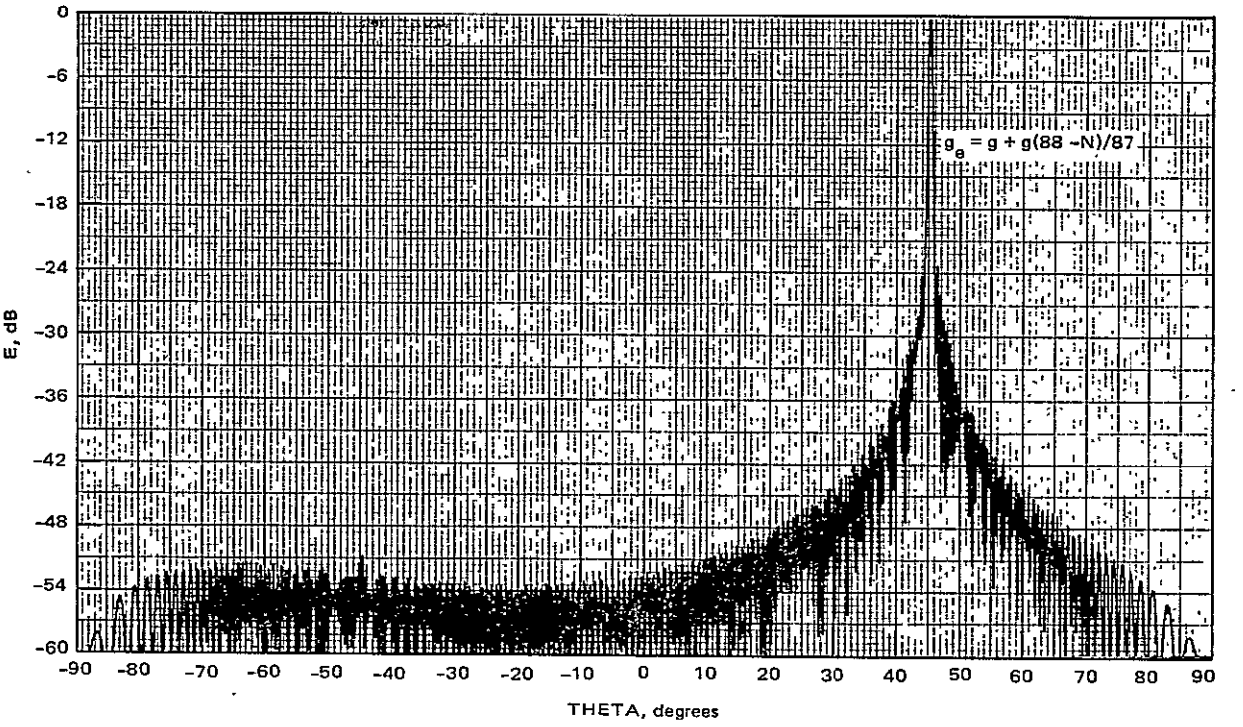

b. Effective conductance decreases linearly from two times design conductance at input end to design conductance beyond element 87

Figure 11. Elevation-plane patterns at 10 GHz for 5-meter linear traveling-wave array for no conductance errors case and linear conductance errors case.

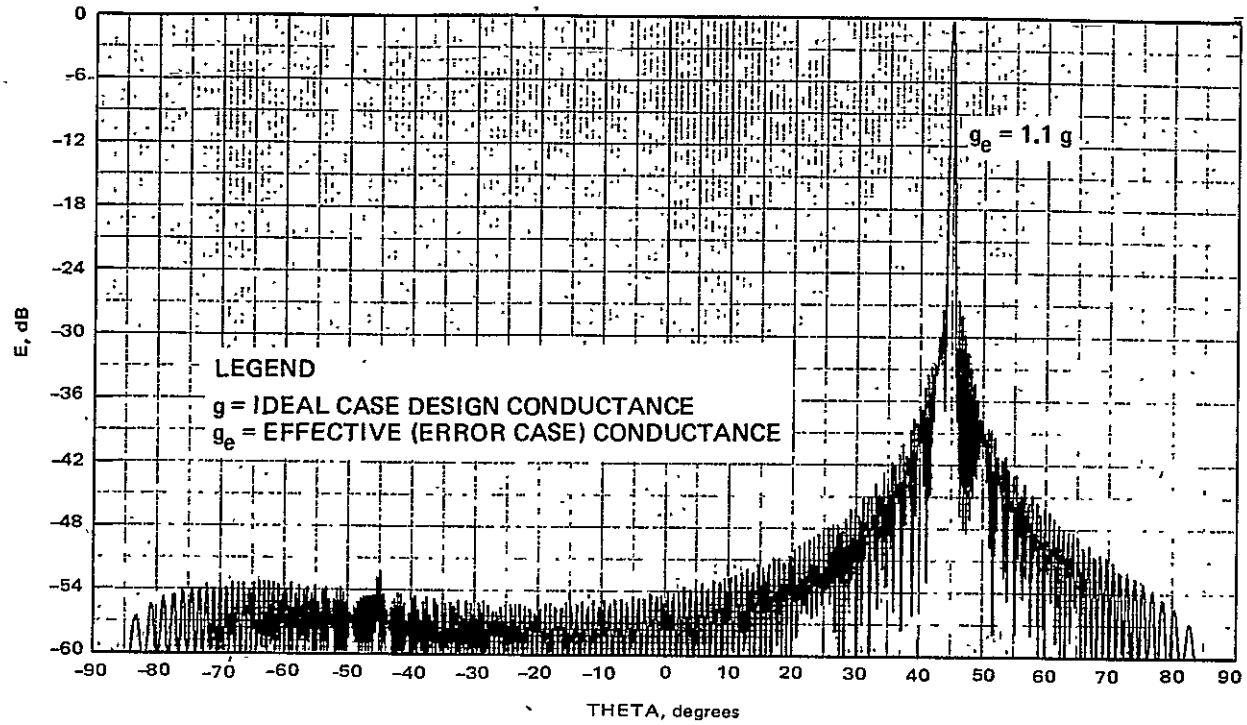

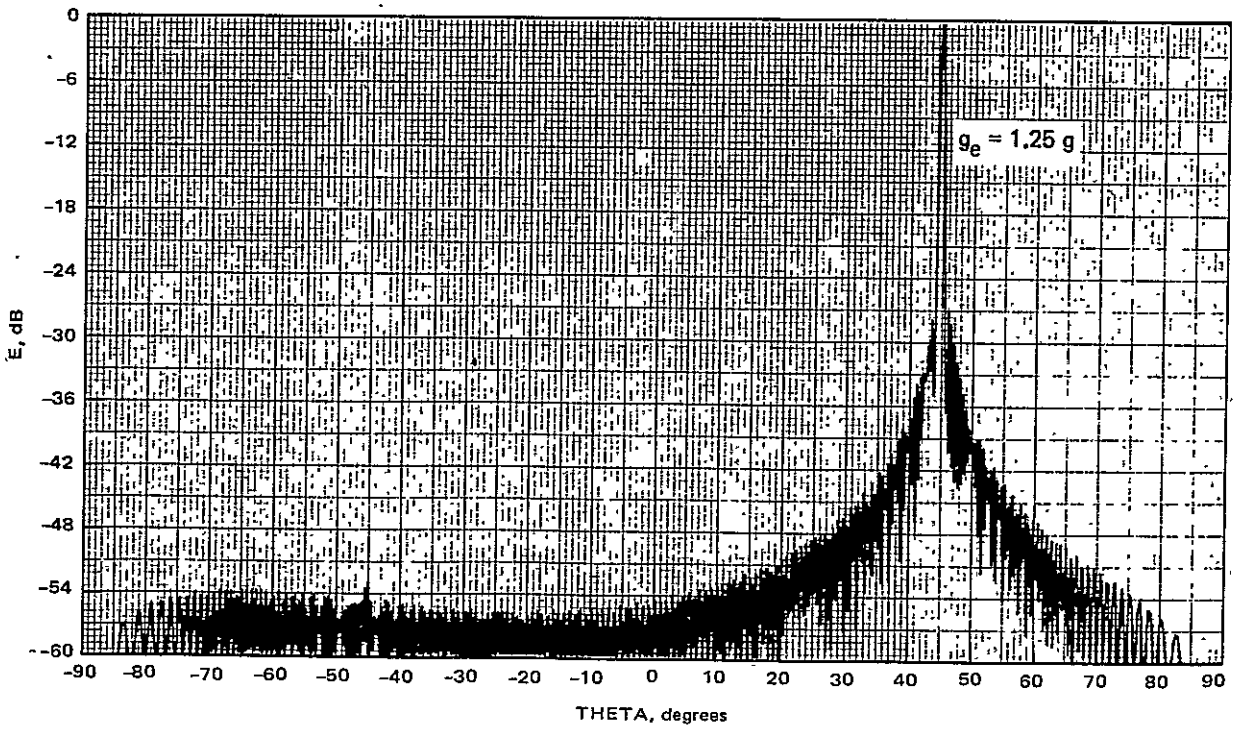

Figure 12. Elevation-plane patterns at 10 GHz for 5-meter linear traveling-wave array showing effects of increased slot conductances.

Figure 12 (continued)

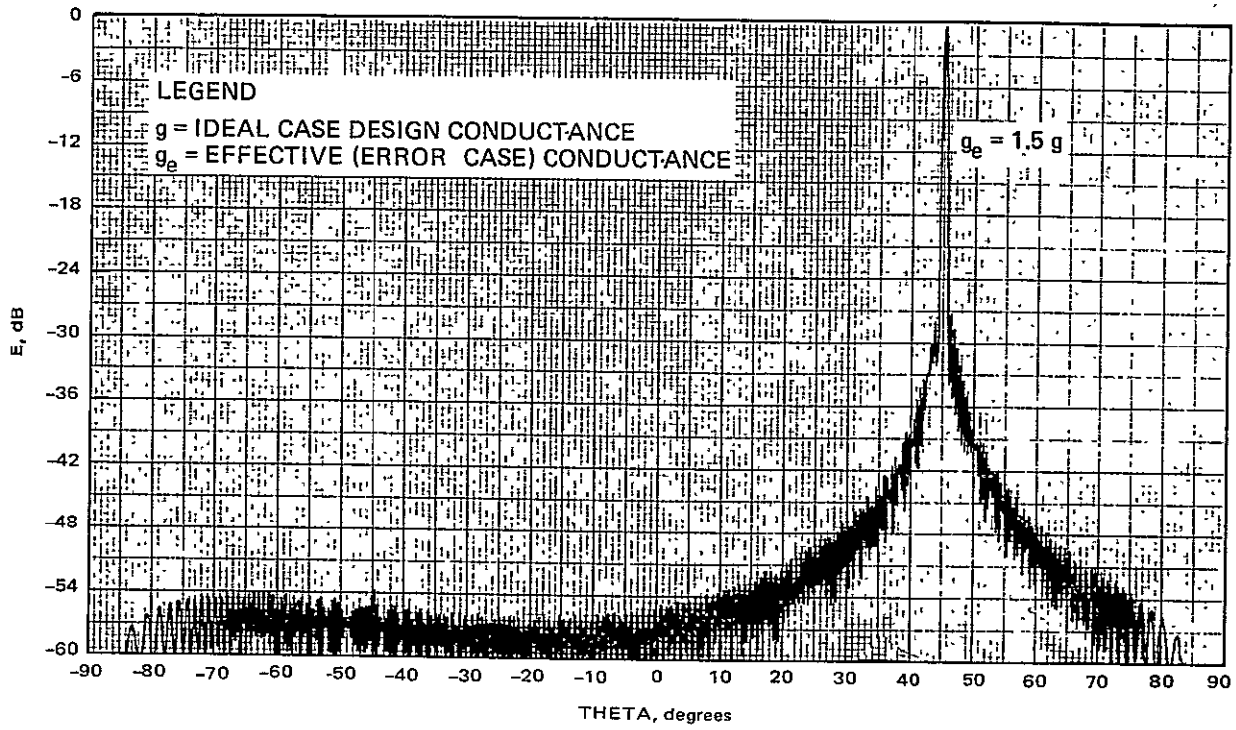

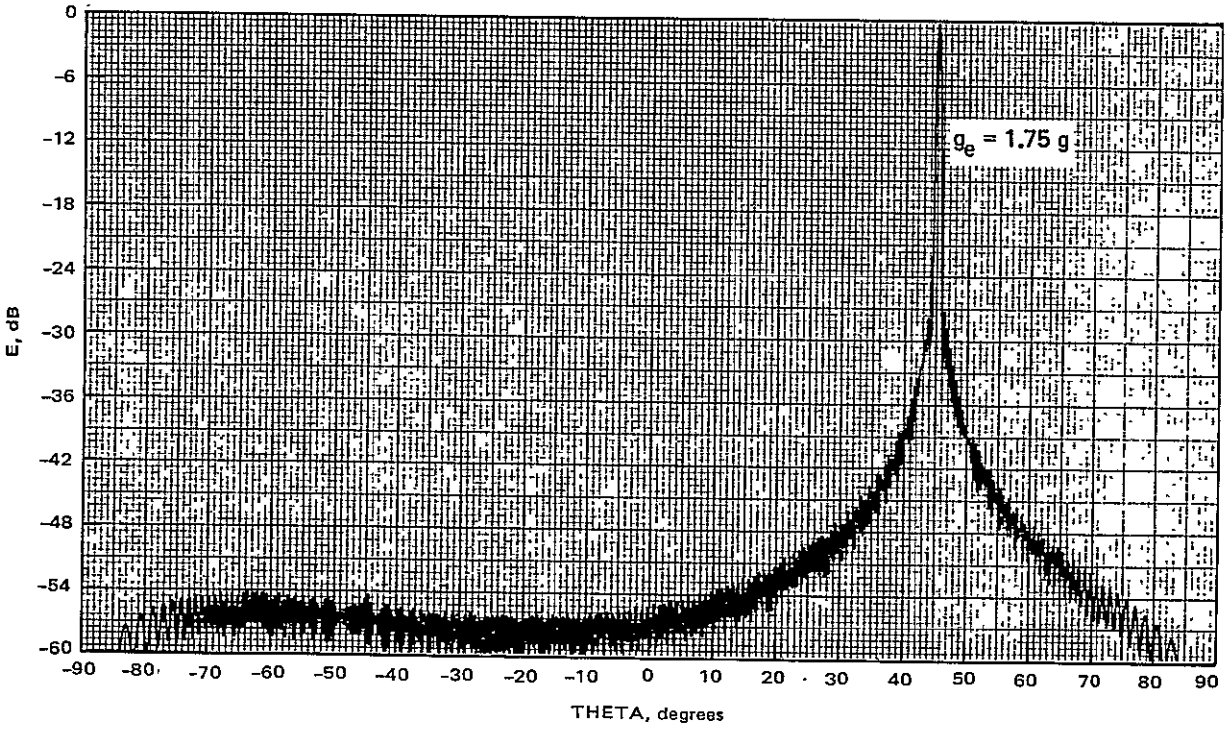

Figure 12 (concluded)

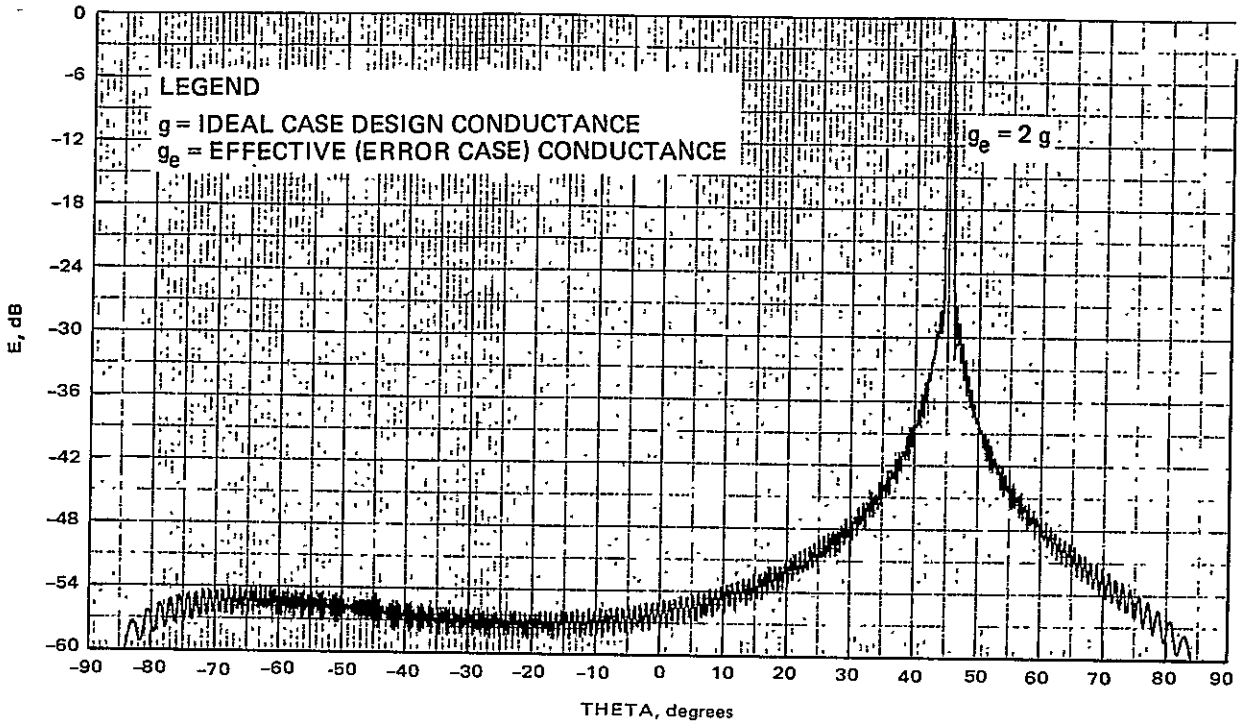

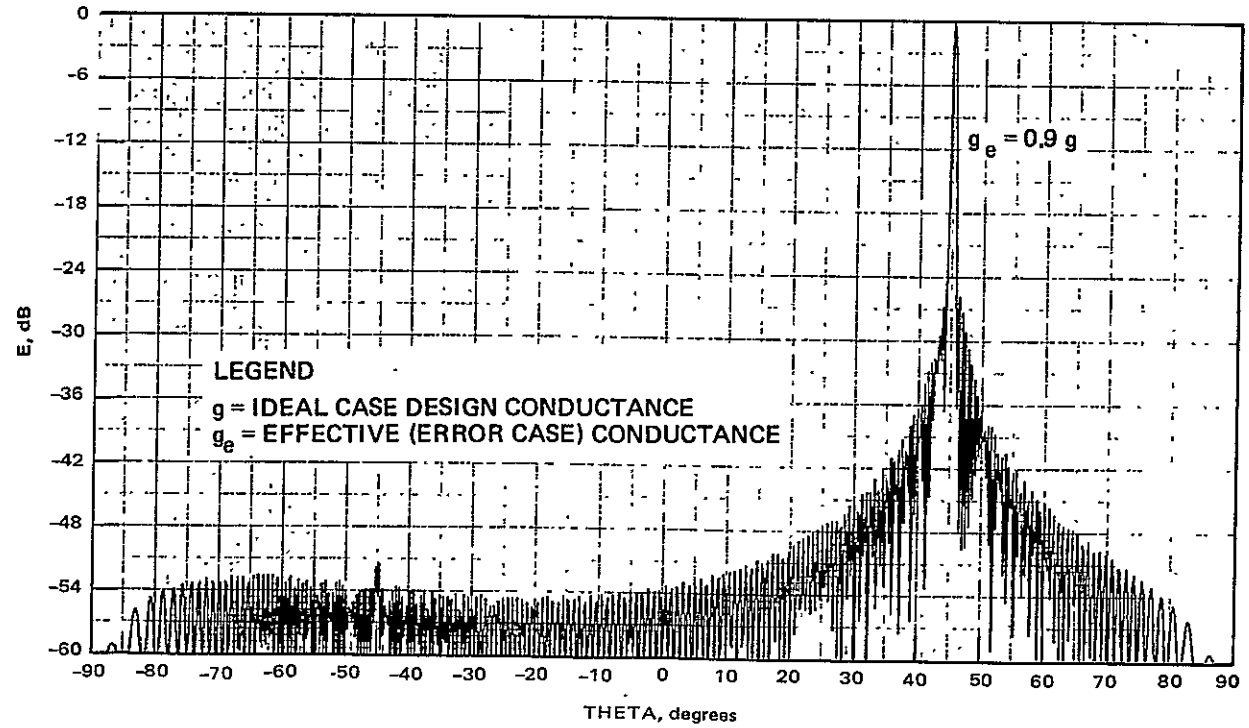

Figure 13. Elevation-plane patterns at 10 GHz for 5-meter linear traveling-wave array showing effects of decreased slot conductances.

Figure 13 (continued)

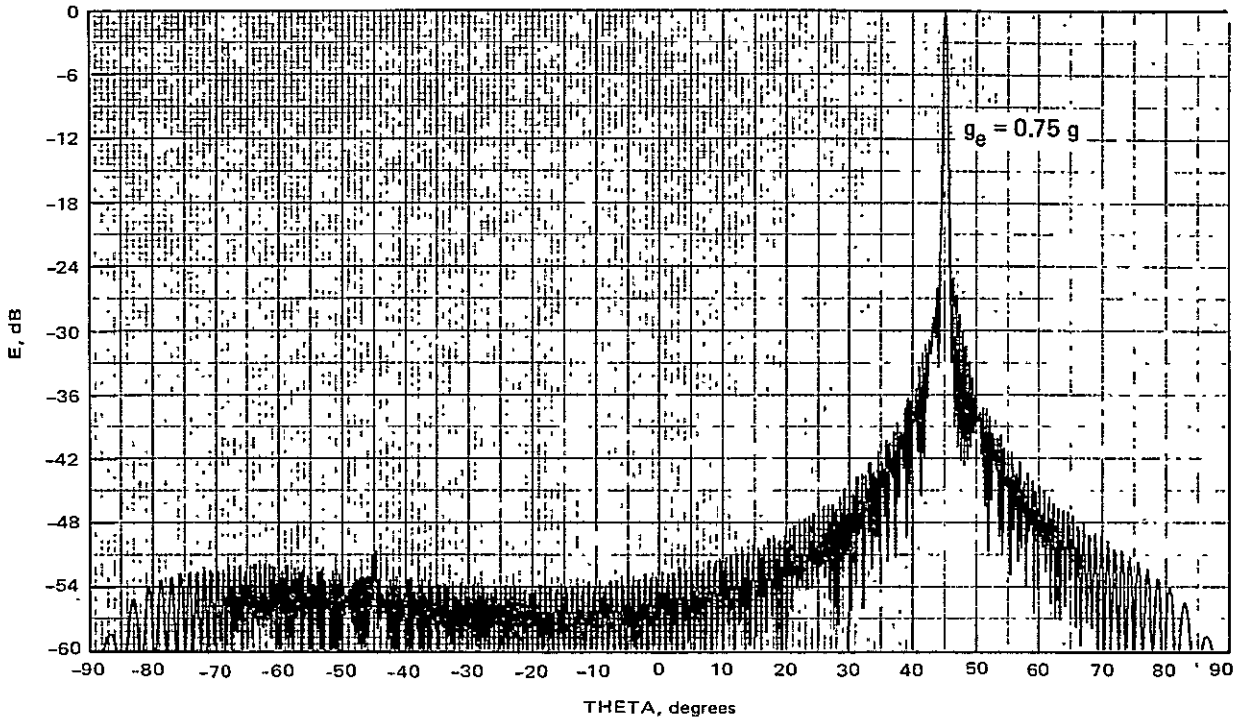

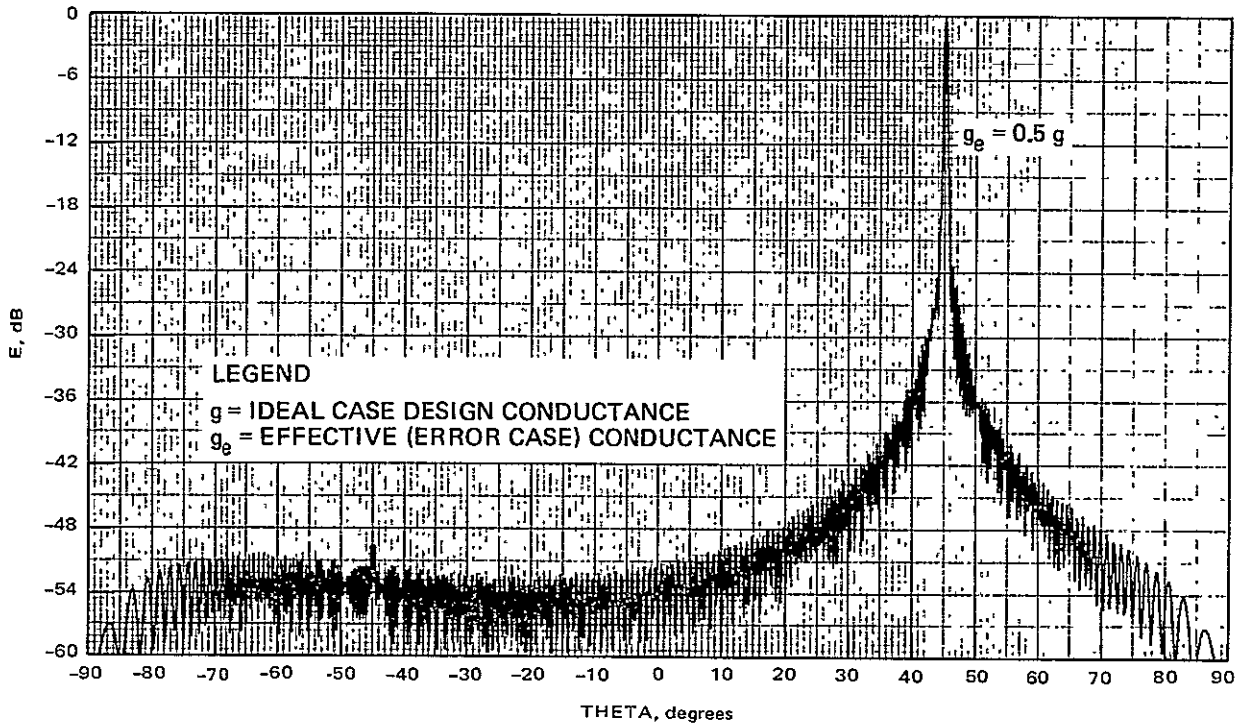

Figure 13 (concluded)

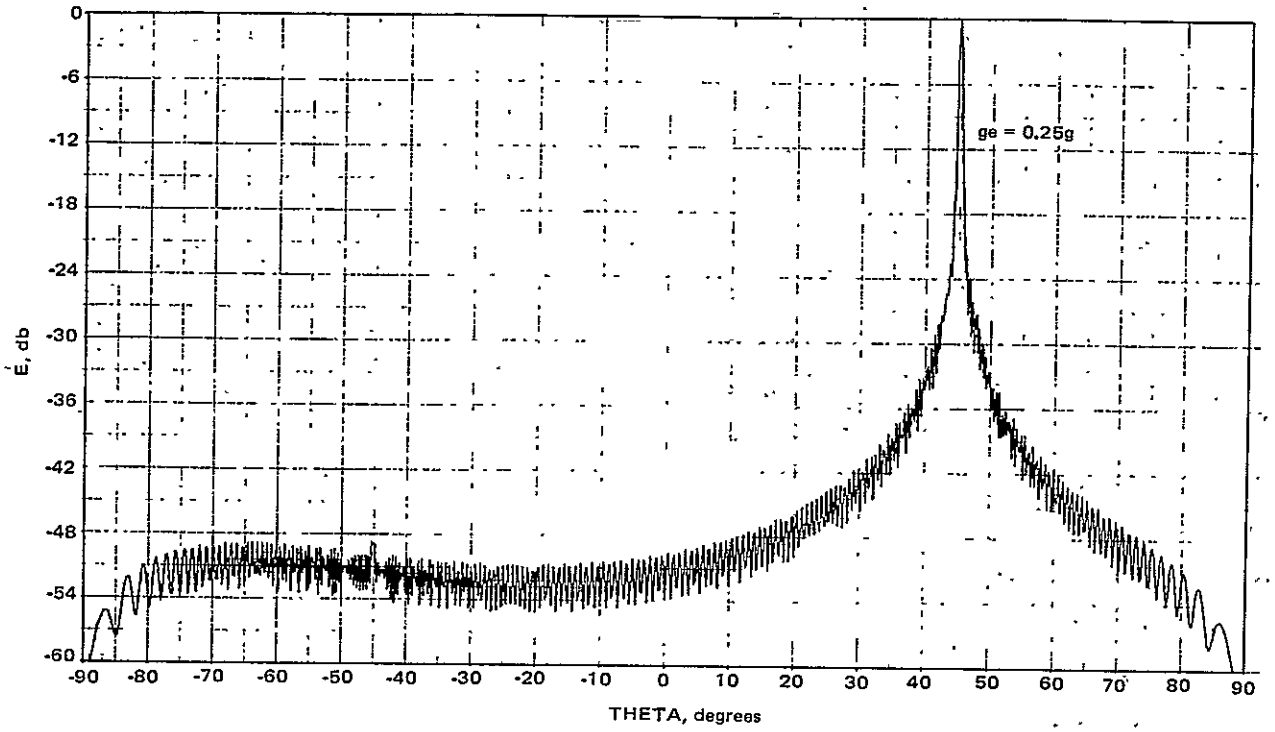

TABLE 2. SLOT-CONDUCTANCE DESIGN-ERROR EFFECTS ON BEAMWIDTH AND GAIN

Case	Error Type (see Table 1)	Percentage of Power to Load	Load Loss, dB	Elevation Plane Beamwidth	Relative Gain,[c] dB
1[a]	$g_e = 0.25g$	39.48	2.181	0.497°	-1.92
2	$g_e = 0.50g$	15.58	0.736	0.498°	-0.48
3	$g_e = 0.75g$	6.15	0.276	0.504°	-0.07
4	$g_e = 0.90g$	3.52	0.156	0.510°	-0.004
5	$g_e = g$ (no error)	2.50	0.110	0.515°	0 Ref.
6	$g_e = 1.1g$	1.67	0.073	0.520°	-0.005
7	$g_e = 1.25g$	0.96	0.042	0.530°	-0.05
8	$g_e = 1.50g$	0.38	0.016	0.548°	-0.18
9	$g_e = 1.75g$	0.15	0.006	0.565°	-0.30
10	$g_e = 2g$	0.06	0.003	0.583°	-0.43
11[b]	$g_e = g + g(88-N)/87$	2.3	0.101	0.498°	+0.16

a. g = ideal case design conductance, g_e = effective error case conductance

b. The case in which the conductance decreases linearly from two times the design conductance at the input end (N=1) to the design conductance beyond element 87.

c. Includes both load loss and beamwidth effects on gain.

3.4 SLOT DESIGN CONSIDERATIONS

3.4.1 Multiple Slots Per Element

Because of the very long length of the MRF, slotted, linear arrays, the slot-to-slot variation in radiation (and in the required conductance) is so small that it is practical to consider a group of identical slots as one element of the array. This approach presents two potential advantages: (1) the difficulty in maintaining very tight mechanical tolerances in the manufacturing process is alleviated, because it is then no longer necessary to fabricate to the very small mechanical differences occurring between adjacent slots, and (2) manufacturing costs are lowered, because cutting groups of identical slots is more economical than cutting many non-identical slots.

The feasibility and limits of this design approach are illustrated by the 5-meter linear array patterns shown in Figure 14. The reference pattern with one slot per element is shown in Figure 14a. Several design approaches using multiple slots per element result in the patterns shown in Figure 14b through 14d. Designs using 4 slots per element (Figure 14c) or 6 slots per element (Figure 14d) show low-level grating lobes; however, this lobing structure occurs above the main lobe (pointing either above the horizon or at long ranges towards the earth) so that it would probably be acceptable. With 8 or 10 slots per element (Figures 14e and 14f), low-level grating lobes (about -42 dB) occur that are below the mainlobe and at shorter ranges toward the earth; therefore, designs incorporating 8 or 10 slots per element would be less acceptable.

A somewhat more complex design approach using multiple slots per element results in the optimum pattern shown in Figure 14b. In this case, it is seen that any grating-lobe effects are essentially lost in the normal, low-level, side-lobe structure. In this design, the number of slots per element is variable, with one slot per element being used near the array center and the number being gradually increased to 11 slots per element at the array edge. The average number of slots per element is close to three. The number of slots per element is increased as the slope of the 25-dB Taylor distribution decreases across the array. In essence, the amplitude distribution

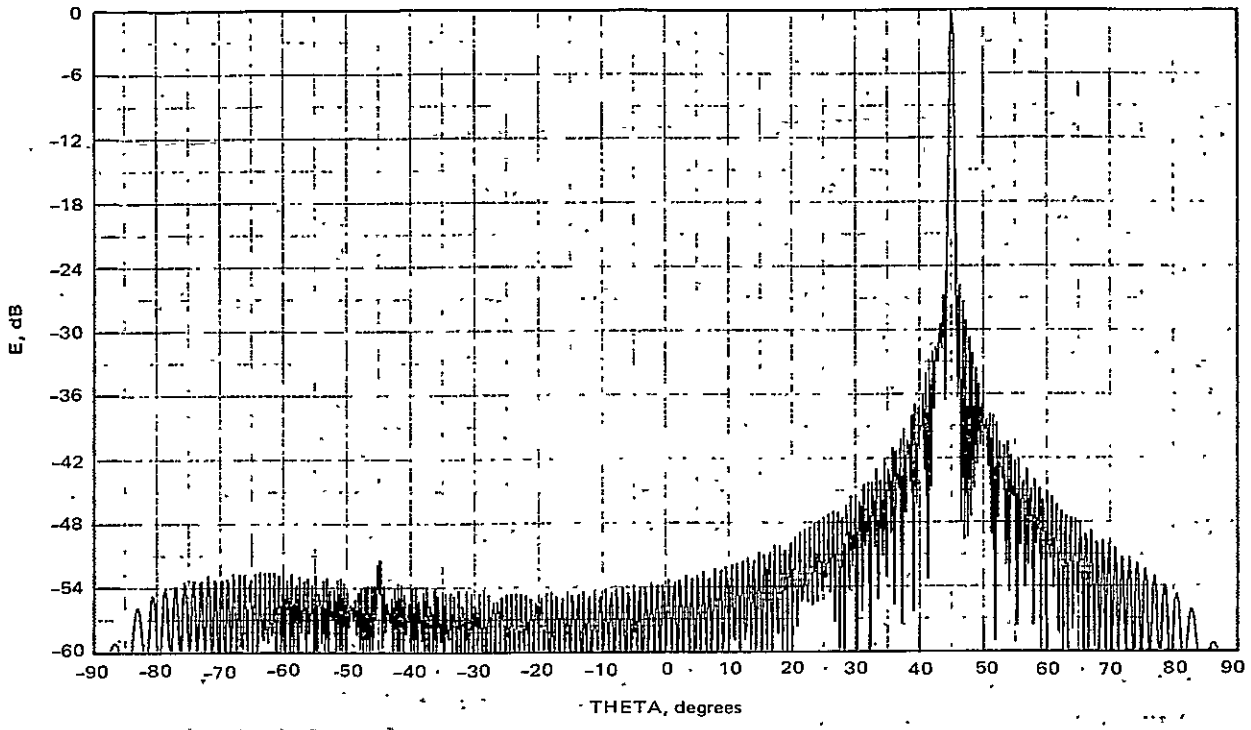

a. One slot per element with 0.6-inch slot separation

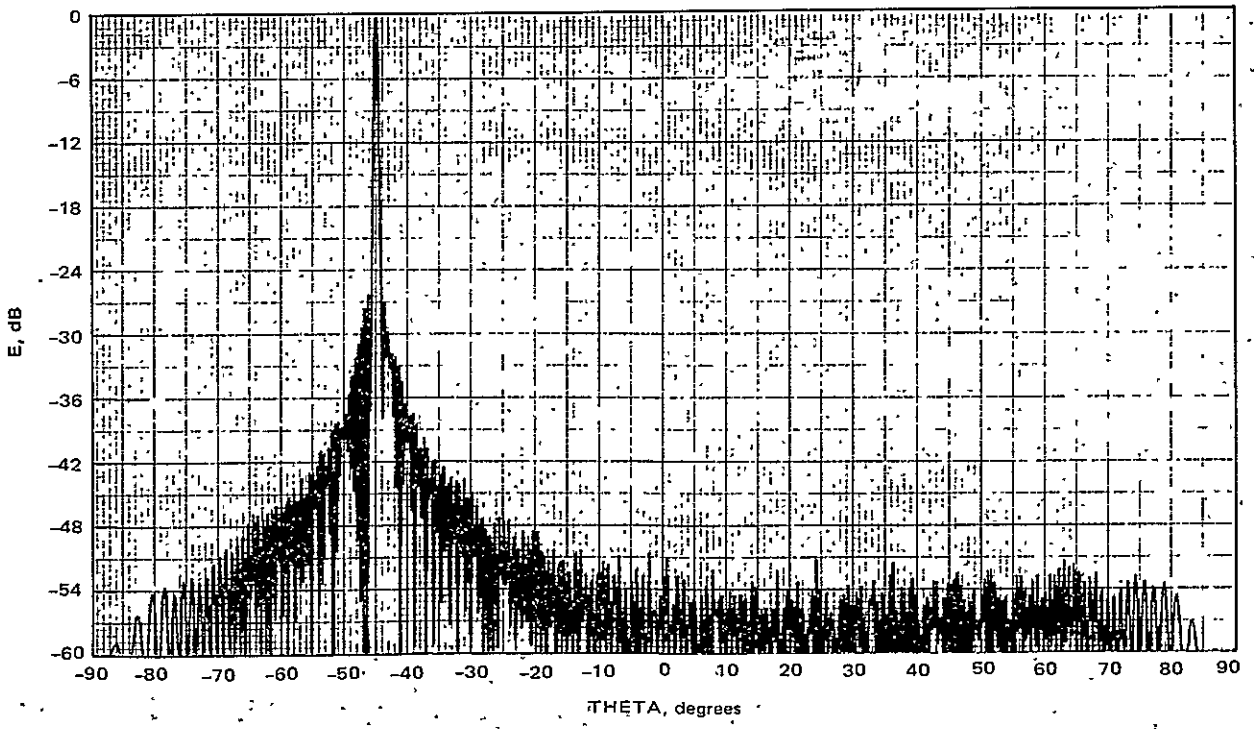

b. Varying slots per element: from 1 at center to 11 at edge with 0.6-inch slot separation

Figure 14. Elevation-plane patterns at 10 GHz for 5-meter linear traveling-wave array showing effect of multiple slots per element.

Figure 14 (continued)

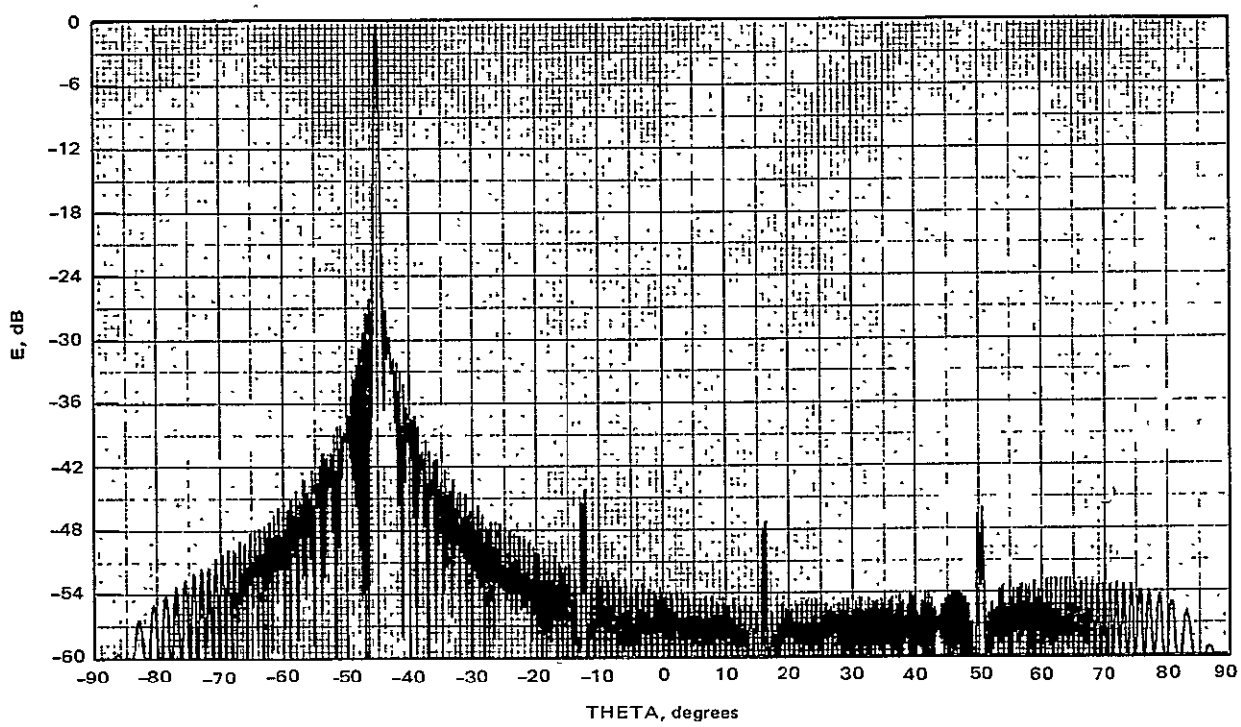

c. Four slots per element with 0.6-inch slot separation

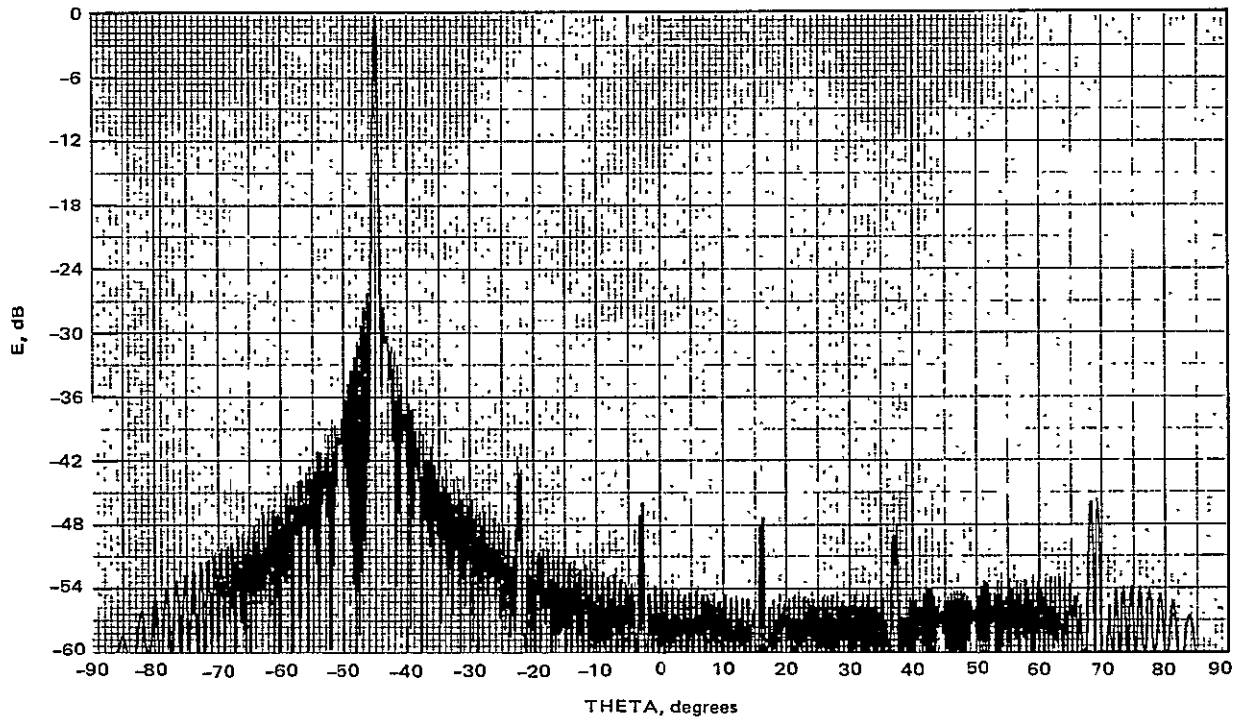

d. Six slots per element with 0.6-inch slot separation

Figure 14 (continued)

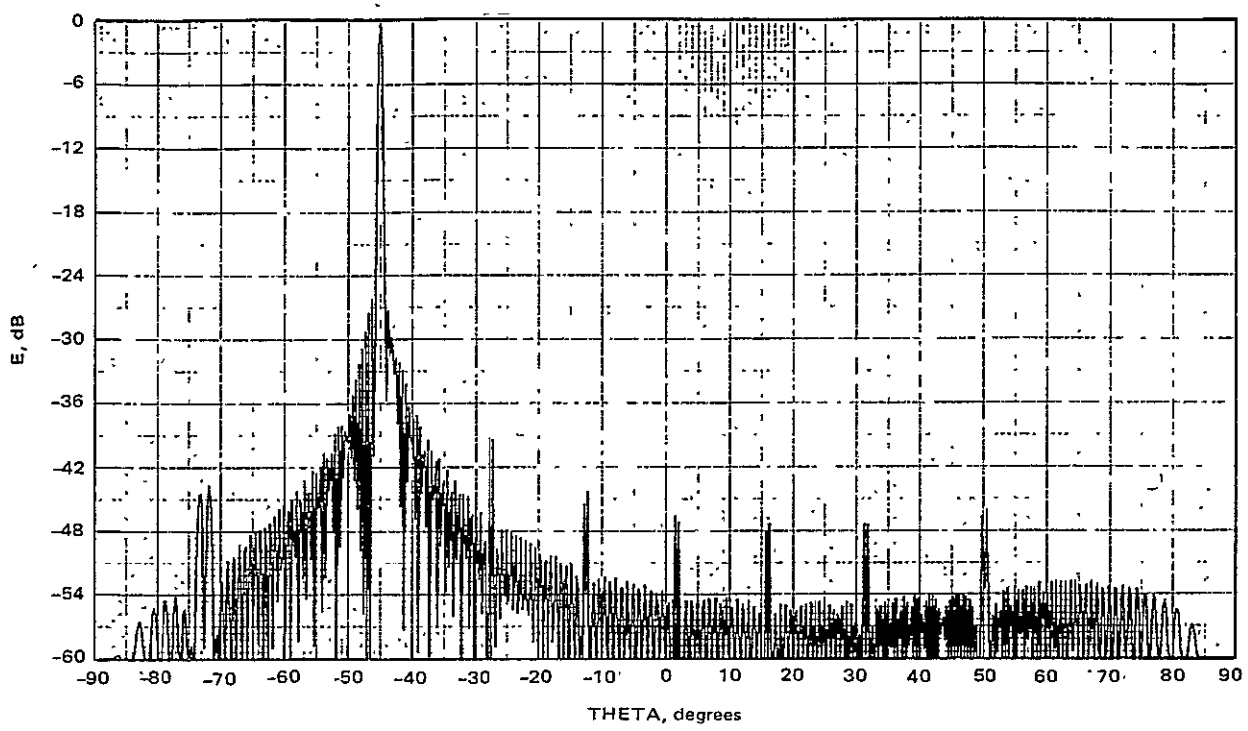

e. Eight slots per element with 0.6-inch slot separation

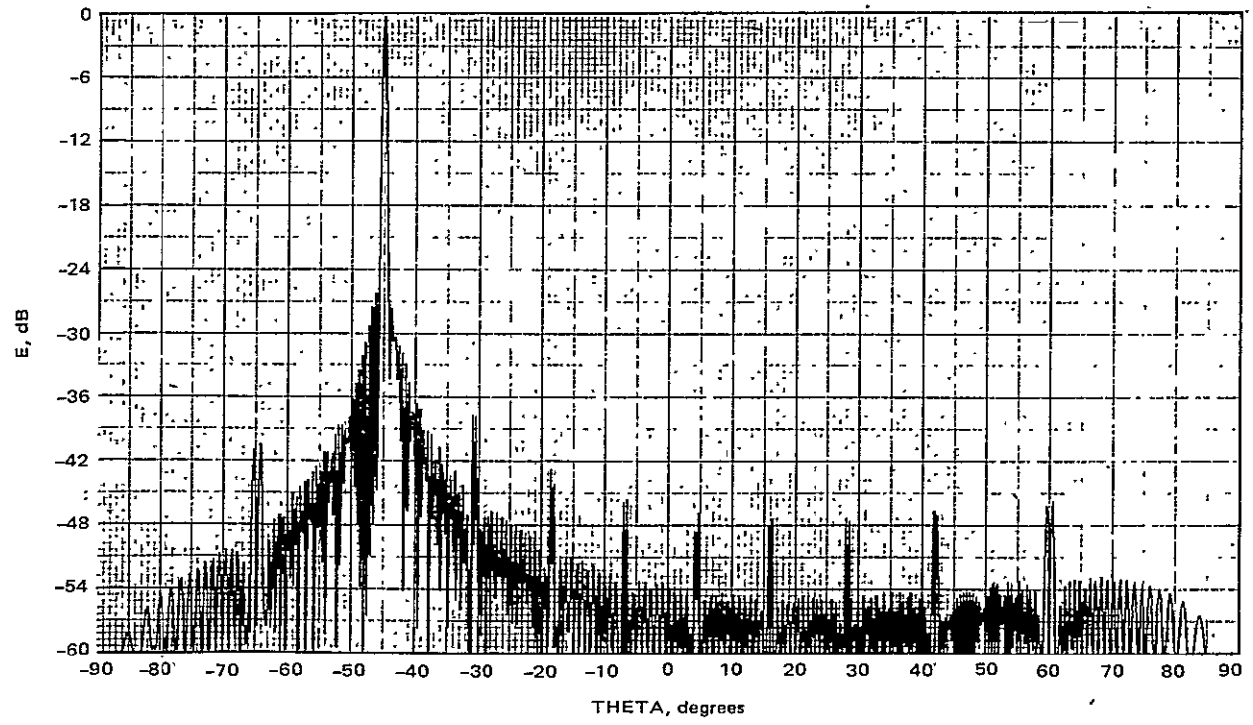

f. Ten slots per element with 0.6-inch slot separation

Figure 14 (concluded)

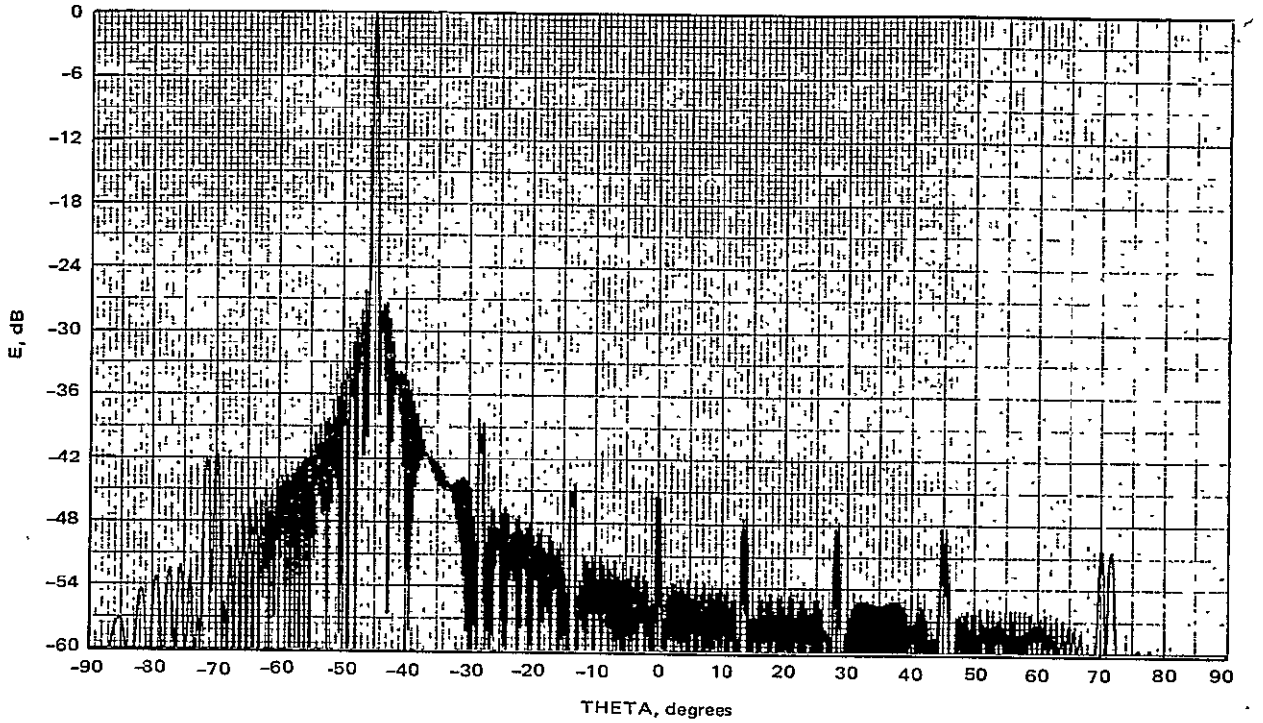

g. Ten slots per element with 0.5-inch slot separation

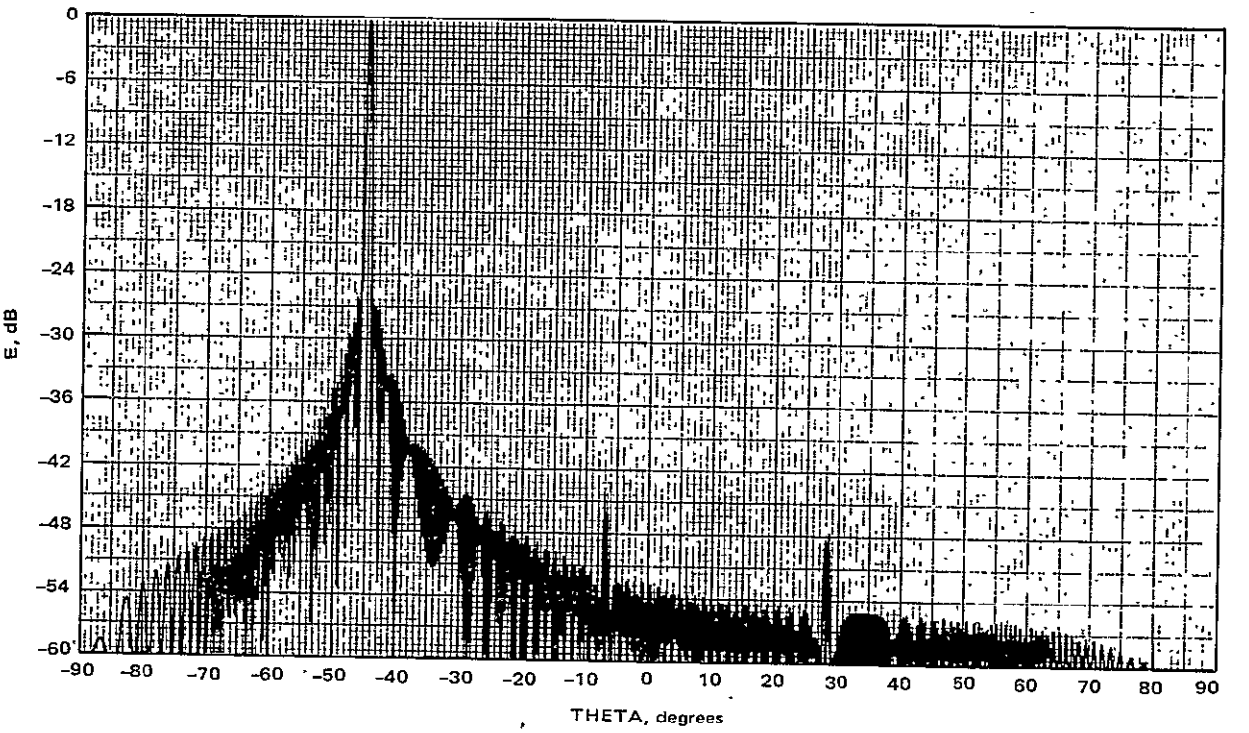

h. Four slots per element with 0.5-inch slot separation

is stepped with variable width steps. With some additional design effort, it is expected that the average number of slots per element could be increased above three while maintaining the grating-lobe structure close to the level of the normal sidelobe structure.

The patterns in Figures 14g and 14h illustrate the cases of 10 and 4 slots per element, respectively, with the slot spacing decreased from 0.60 to 0.50 inch. The grating-lobe levels are seen to be similar to their counterparts in Figures 14f and 14c, with 0.60-inch slot spacing. These patterns illustrate that, when multiple slots per element are used, grating lobe effects are relatively insensitive to slot spacing.

3.4.2 Slot Design Approach

In order that the experimental slot data be suitable for the MRF array design, it was necessary to anticipate the range of slot design parameters that were of interest before the actual test slot measurements were made. These slot design parameters were selected on the basis of the MRF traveling wave array conductance requirements given in Figures 4 and 5 and the theoretical slot conductance curves given in Figure 26. The conductance curves in Figure 26 are plots of conductance versus slot displacement for constant slot lengths. It was anticipated that, to minimize aperture phase errors, the first stage in the slot design would entail the selection of a fixed slot length and the selection of slot displacement according to one of the curves of Figure 26. The second stage design entails a variation in slot length; this will be discussed later in this section.

The slot parameters constituting the computed points on the graph in Figure 26 are summarized in Table 3. The more dense region of the matrix in Table 3 represents the slot parameters that would be similar to those needed for the 5-meter and 18-meter MRF array designs. The thinned portions of the matrix encompass the slot parameters that have been included for general completeness of the data. These slots were tested and found to agree sufficiently with the theoretical predictions; accordingly, the slot parameters next chosen for test are summarized in Table 4. The matrix in Table 4 is seen to be less thinned out than the matrix in Table 3; this is because the slot parameters in Table 4 were selected specifically for use in the MRF array design rather than for any general design information.

TABLE 3. MATRIX SUMMARY OF 43 TEST SLOTS IN STANDARD X-BAND WAVEGUIDE

L	S	S	S	S	S	S	S	S
0.240							0.280	0.340
0.280					0.160	0.220		0.340
0.320			0.080			0.220		0.340
0.360		0.060	0.080	0.120		0.220		0.340
0.400	0.040	0.060	0.080	0.120	0.160	0.220	0.280	0.340
0.440	0.040	0.060	0.080	0.120	0.160	0.220	0.280	0.340
0.480	0.040	0.060	0.080	0.120	0.160	0.220	0.280	0.340
0.520	0.040	0.060	0.080	0.120		0.220		0.340

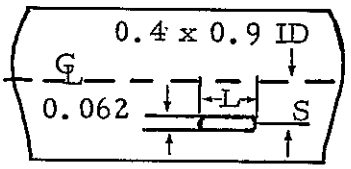

All dimensions in inches

TABLE 4. MATRIX SUMMARY OF 40 TEST SLOTS IN MRF DESIGN WAVEGUIDE

L	S	S	S	S	S	S	S	S
0.320	0.040	0.060	0.080	0.120	0.160	0.220	0.280	0.340
0.360	0.040	0.060	0.080	0.120	0.160	0.220	0.280	0.340
0.400	0.040	0.060	0.080	0.120	0.160	0.220	0.280	0.340
0.440	0.040	0.060	0.080	0.120	0.160	0.220	0.280	0.340
0.480	0.040	0.060	0.080	0.120	0.160	0.220	0.280	0.340

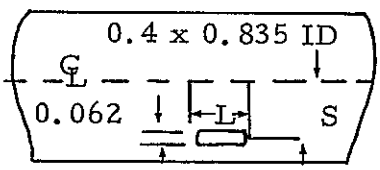

All dimensions in inches

The theoretical performance of the slots described in Tables 3 and 4 are presented in graphic form in Figures 24 through 35. Figures 24 and 30 show that the slot radiation phase is predicted to be constant as a function of slot displacement (for constant slot length); in contrast, the phase varies sinusoidally as a function of slot length, as seen in Figures 25 and 31. Both the absolute phase and the phase variation, as a function of slot length, are predicted to be independent of slot displacement. The implication is that, for phase errors to be kept to a minimum, the slot length should be kept constant and the conductance should be varied by variation of slot displacement. On this basis, the conductance curves in Figures 26 and 32 are the most applicable for the MRF slot array design, while the curves of Figures 28 and 34 should be sparingly used because radiation phase changes occur with slot length changes. For areas in the aperture design in which it is necessary to use different slot lengths, the consequent radiation phase errors would then be obtained from Figures 25 and 31. In order to avoid the rapid change in phase as slot length approaches the resonant length (approximately 0.590 inch at 10 GHz), any change in slot length necessary in the design should be limited to the shorter, low conductance, slots.

The above slot design approach applies, without reservation, to the case of a parallel type of feed system in which radiation phase errors occur, for an ideal parallel feed, only because of variations of the reactive slot radiation phase. Referring to Figure 15, this radiation phase is equivalent to the phase of the slot coupling coefficient phase, $< S_{31}$. For the case of a traveling-wave, series, feed system, such as will be used for the MRF design, the above slot design approach applies only in a limited way. This is because of the additional phase errors that accumulate when reactive slots are used in a traveling-wave series feeder. Referring again to Figure 15, these additional phase errors relate to the transmission coefficient phase, $< S_{21}$. Although the transmission coefficient phase is small (from 0 degree for a resonant slot and up to a maximum of about 4 degrees for the reactive slots used in the MRF array design), these phase errors accumulate down the slotted line and can add up to appreciable phase error between the input slots and the load-end slots if not accounted for in the slot design.

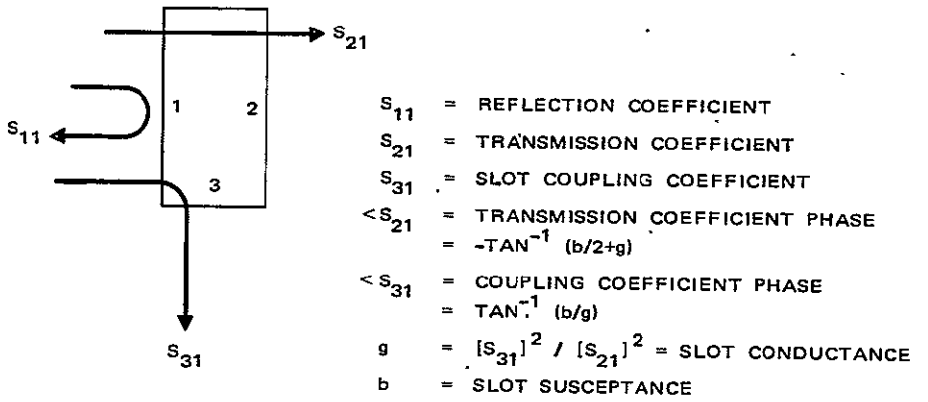

Figure 15. Coupled slot scattering parameter representation.

The aperture phase error, due to the accumulation of these transmission coefficient phases, is shown in Figure 16 for two design cases: (1) a constant slot displacement and a varying slot length, and (2) a constant slot length and a varying slot displacement. The first case results in the elevation-plane pattern shown in Figure 7b. When compared to the errorless pattern, Figure 7a, the pattern of Figure 7b is seen to have a broadened beamwidth (0.76 degrees compared to 0.52 degrees) and a larger tilt angle (46.2° compared to 45°). The gain loss associated with this broadened beamwidth is 1.7 dB. The increased tilt angle is associated with an average phase error per slot of 2.7°. This equivalent, linear, phase error of 2.7° per slot is shown superimposed on the actual aperture phase error in Figure 16, the remaining non-linear portion of this aperture phase error being responsible for the beam-broadening effect.

It is apparent that, to minimize the beam-broadening effect and attendant loss in gain, it is necessary in the slot design to both minimize and linearize the accumulated aperture phase error. The linearization results in a change of tilt angle, which can be corrected for by a change of waveguide width, without any beam broadening or gain loss. It is anticipated that this dual objective will require varying both slot length and slot displacement. As is shown in Figure 16, the case of the design using constant slot length results in a decrease of the accumulated phase error and is a first stage in the design process of minimizing and linearizing the accumulated phase error. The second stage would be to vary the slot length about the mean slot length established in the first stage design. A trial second stage design has verified that this linearization can be successfully implemented.

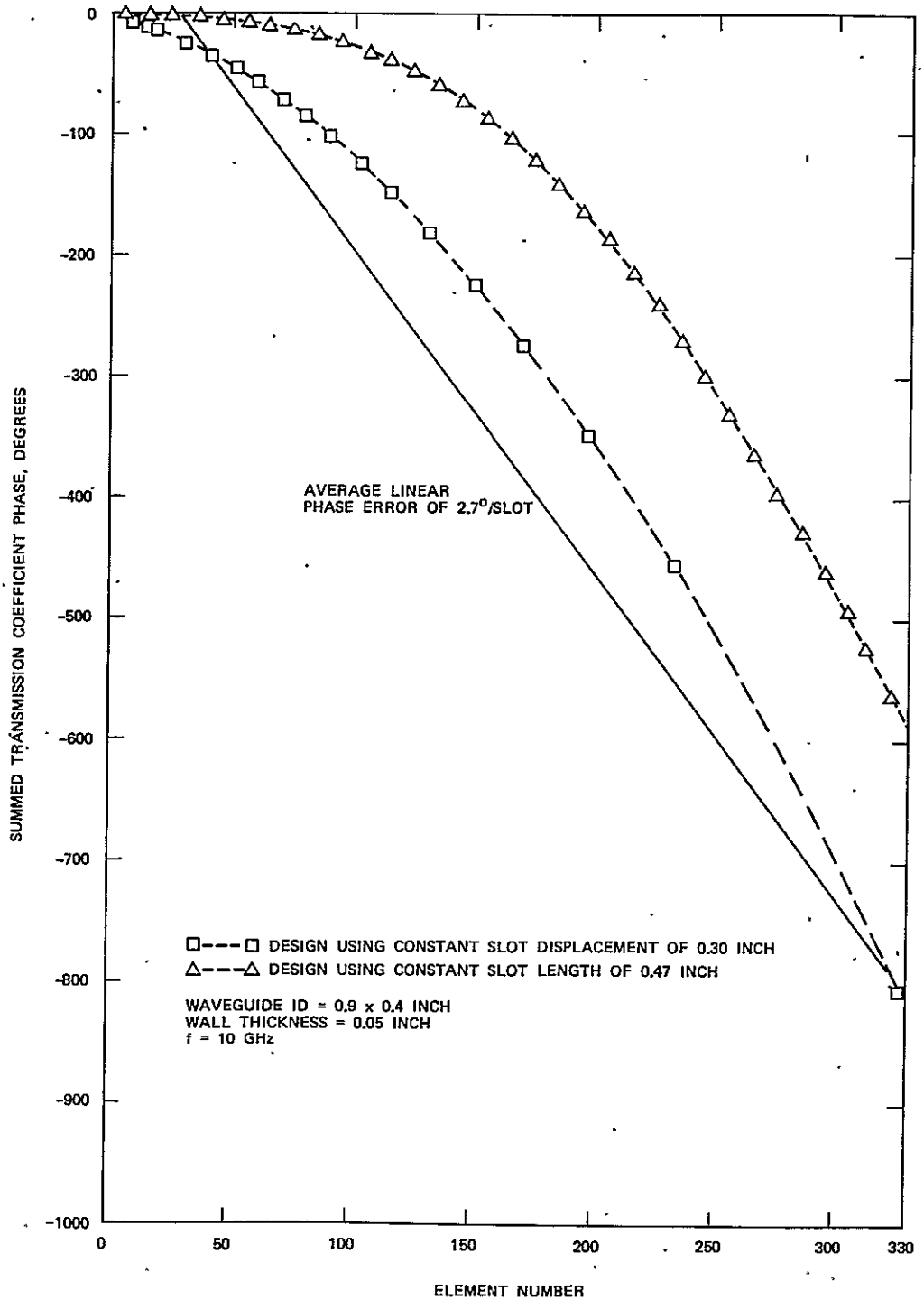

Figure 16. Transmission coefficient phase error accumulation over the aperture versus slot design approach.

4.0 EXPERIMENTAL INVESTIGATIONS

4.1 SLOT CONDUCTANCE MEASUREMENT TECHNIQUES

The principal techniques applicable to the measurement of slot conductance are impedance measurement,[8] interference radiation pattern measurement,[8][9] and probe comparison measurement.* The first method directly measures conductance while the other two methods are indirect in that they require comparison with a reference slot of known conductance. The most widely used method is the direct impedance measurement technique; however, this approach is practical only for conductances larger than 0.01. For example, a conductance of 0.01 presents a discontinuity VSWR of only 1.01:1; therefore, its effect can easily be obscured by another miscellaneous waveguide discontinuity. Because the 5-meter and 18-meter MRF arrays require the use of conductances in the approximate ranges of, respectively, 0.0007 to 0.028 and 0.0002 to 0.008, the impedance measurement technique is not appropriate for calibration of the slots to be used. However, the approach can be used indirectly, that is, the impedance method is used for calibration of a high conductance resonant slot (about 0.1), which, in turn, will be used as a standard reference for the interference pattern and the probe comparison measurement techniques.

4.1.1 Interference Pattern Measurement

In the interference pattern measurement, a known reference slot of comparatively large conductance is compared with an unknown slot of much lower conductance by measurement of the resultant radiation pattern of the two slots. From the angular locations and the magnitudes of the maximum and minimum of this interference pattern, the relative slot excitation amplitudes, transmission (or radiation) phases, and admittances of the slots can be derived by the following.

Two isotropic radiators whose radiated fields differ in phase by ϕ and whose magnitudes are proportional to A_1 and A_2 will have a power pattern proportional to

*The probe comparison technique, as far as published reports indicate, has not previously been used for the measurement of slot conductance; this technique is described in detail in Sections 4.1.2, 4.2, 4.3.3, and 4.4

$$P = \left| A_1 + A_2 e^{j(kd \sin \theta + \phi)} \right|^2$$

$$= A_1^2 + A_2^2 + 2A_1A_2 \cos (kd \sin \theta + \phi) \tag{2}$$

where d is the spacing between elements and θ is the angle measured from broadside. This power pattern is maximum (P_{max}) when the cosine term has a value of +1.0 (at the angle θ_{max}) and is minimum (P_{min}) when the cosine term has a value of -1.0 (at the angle θ_{min}). The ratio of the magnitudes of the excitation coefficients is

$$\frac{A_2}{A_1} = \frac{\left(\frac{P_{max}}{P_{min}}\right)^{1/2} - 1}{\left(\frac{P_{max}}{P_{min}}\right)^{1/2} + 1} \tag{3}$$

The relative phase between the element is

$$\phi = (2n - 1)\pi - kd \sin \theta_{min} \tag{4}$$

or

$$\phi = 2n\pi - kd \sin \theta_{max} \tag{5}$$

where n = 0, ±1, ±2, etc.

When the slot conductances are small and internal interactions, external mutual coupling, and guide attenuation are neglected, the power radiated by each slot is then proportional to its conductance and also proportional to the square of the magnitude of the excitation coefficients. It follows that, for shunt slots, the conductance of the test slot, G_2, is related to the conductance of the reference slot, G_1, by the equation

$$G_2 = G_1 \left(\frac{A_2}{A_1}\right)^2 \tag{6}$$

Because the phase of the radiated field of a shunt slot with respect to the field in the waveguide is equal to the phase of the slot admittance, the susceptance of the unknown slot compared to a known resonant slot is

$$B_2 = G_2 \tan \phi s \tag{7}$$

For traveling-wave feeding, ϕ, from Equations (4) and (5), and ϕ_s, from Equation (7), are related by

$$\phi = \frac{-2\pi d}{\lambda_g} + \phi_s \tag{8}$$

where λ_g is the waveguide length.

The slot conductance can be calculated from Equation (6) by use of the ratio A_2/A_1 from Equation (3). The susceptance can be calculated from Equation (7) by use of the angle ϕ from Equations (4) or (5) and the angle ϕ_s from Equation (8).

The sensitivity limitations of the interference pattern technique is illustrated by Table 5. For example, when the objective is measurement of conductance as low as 0.0001 and the reference resonant slot has a conductance of 0.1 (calibrated by impedance measurement), then an interference pattern maximum/minimum ratio of only 0.6 dB is obtained. If a maximum/minimum ratio of 1.5 dB or larger is necessary for acceptable test accuracy, then it is seen that, for a conductance as low as 0.0001 to be measured, either a reference conductance of about 0.01 is required, or three test slots, each of 0.0001 conductance, must be paralleled into a multi-slot element. In this latter case, 43 slot element tests per waveguide size (see Table 1) were planned, so 3 x 2 x 43 = 258 test slots would have to be cut. To avoid cutting too many slots, it was decided that the 0.1 reference resonant slot

TABLE 5. SUMMARY OF INTERFERENCE PATTERN MEASUREMENT SENSITIVITY

Case	Reference Slot Conductance	Test Slot Conductance	Number of Test Slots per Element	Interference Pattern Maximum/Minimum Ratio (dB)
1	0.1	0.01	1	5.7
2	0.1	0.0003	1	1.0
3	0.1	0.0001	1	0.6
4	0.1	0.0001	3	1.7
5	0.01	0.001	1	5.7
6	0.01	0.0003	1	3.0
7	0.01	0.0001	1	1.7

would be used for calibration, by interference pattern measurement, of a 0.01 reference resonant slot. The latter slot would then be used for most of the interference pattern measurements.

4.1.2 Probe Comparison Measurement

A technique that would provide the most sensitivity is that of direct measurement of the phase and amplitude of radiation from the reference resonant slot followed by a comparison measurement of the phase and amplitude of radiation from the test slots. The measurement sensitivity is simply a function of the coupling loss between the probe and slot radiator, line losses, transmitter power, and receiver sensitivity. With the use of such RF-to-IF receivers as the SA 1750 Phase/Amplitude Receiver, slot conductances as low as 0.0001 can be measured with little difficulty. It is the area of measurement accuracy, rather than measurement sensitivity, that needs close scrutiny where this probe measurement technique is used.

Equations (6), (7), and (8) apply to both the probe comparison measurement and the interference pattern measurement techniques. The interference Equations (2) through (5) do not apply, because, for the probe measurement case, the reference and test slot radiations are isolated from one another rather than combined into an interference pattern.

The following precautions are necessary, because the radiations from the reference and the test slots are measured separately.

1. Elimination of interference between reference and test slot radiations. The slot not being tested must be covered for interference to be prevented because reference and test slots are fed by the same traveling wave, but this covering process must present a minimum of change to the ground plane radiation environment.
2. Different interaction effects between the probe, and the slot and ground plane environment must be corrected for or avoided. The reactive and resonant slots will interact with the probe with different reflection phases, while the probe interaction with the ground plane is expected to be essentially unchanged whether the probe is over the reference or the test slot. The objective is measurement at a probe height above the ground plane at which interaction effects are either small or are almost equal.
3. Transmitter and receiver stability between reference and test slot measurements must be maintained.
4. Instrumentation accuracy must be achieved. The reference and test slot radiations may differ by as much as 30 dB and any instrumentation errors over this wide range will result directly in errors in the conductance measurements.

4.2 TEST FIXTURE DESCRIPTION

The principal test fixtures that were evaluated for the slot measurements, are illustrated in Figures 17 and 18. A block diagram for the complete experimental set up is presented in Figure 19. As can be seen, both slot measurement techniques utilize the same ground plane. For the radiation interference pattern measurements, the field monitoring horn is connected directly to the receiver. For the probe comparison measurements, the dipole probe is connected through a double stub tuner to a slotted line carriage that serves three functions: (1) to provide support for the coaxial line to the test dipole, (2) to allow for longitudinal, transverse, and vertical probe displacement; and guide the dipole between reference and test slots, and (3) to provide a movable microwave junction to connect the coaxial line from the test dipole to the slotted line, which in turn connects to the phase and amplitude measuring equipment. This movable microwave junction replaces the probe and detector that usually mount on the slotted line.

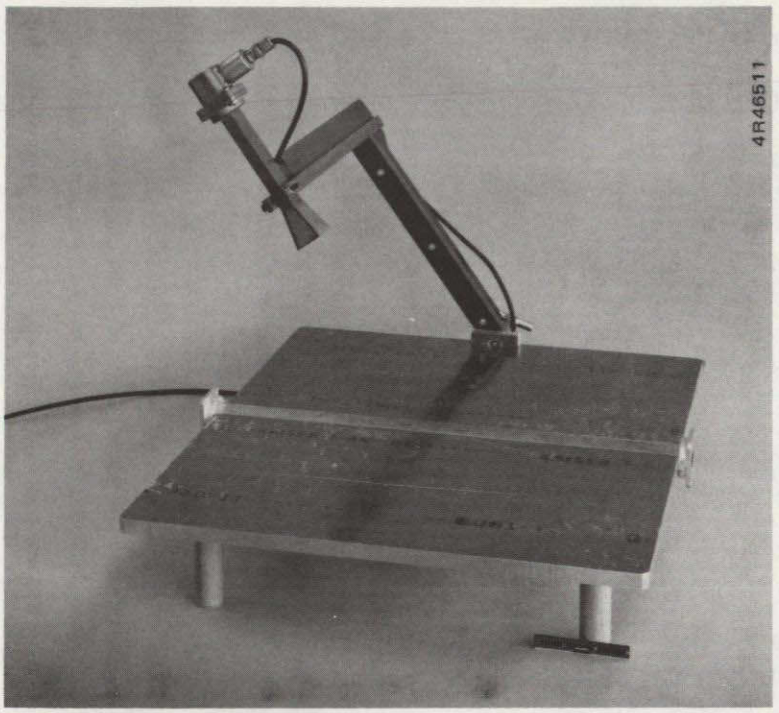

Figure 17. Fixture for slot interference pattern measurement.

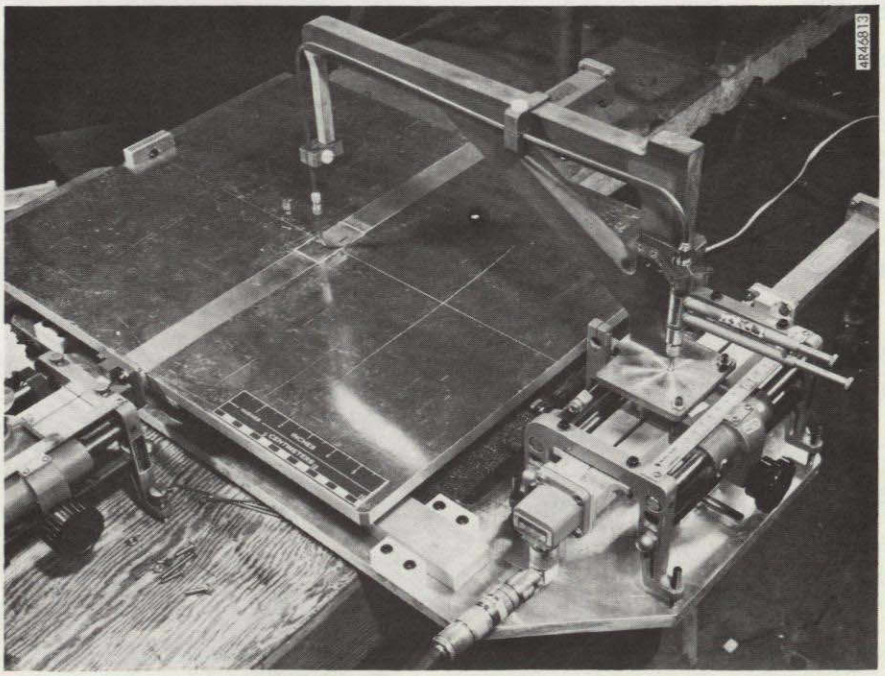

Figure 18. Fixture for probe comparison slot measurements.

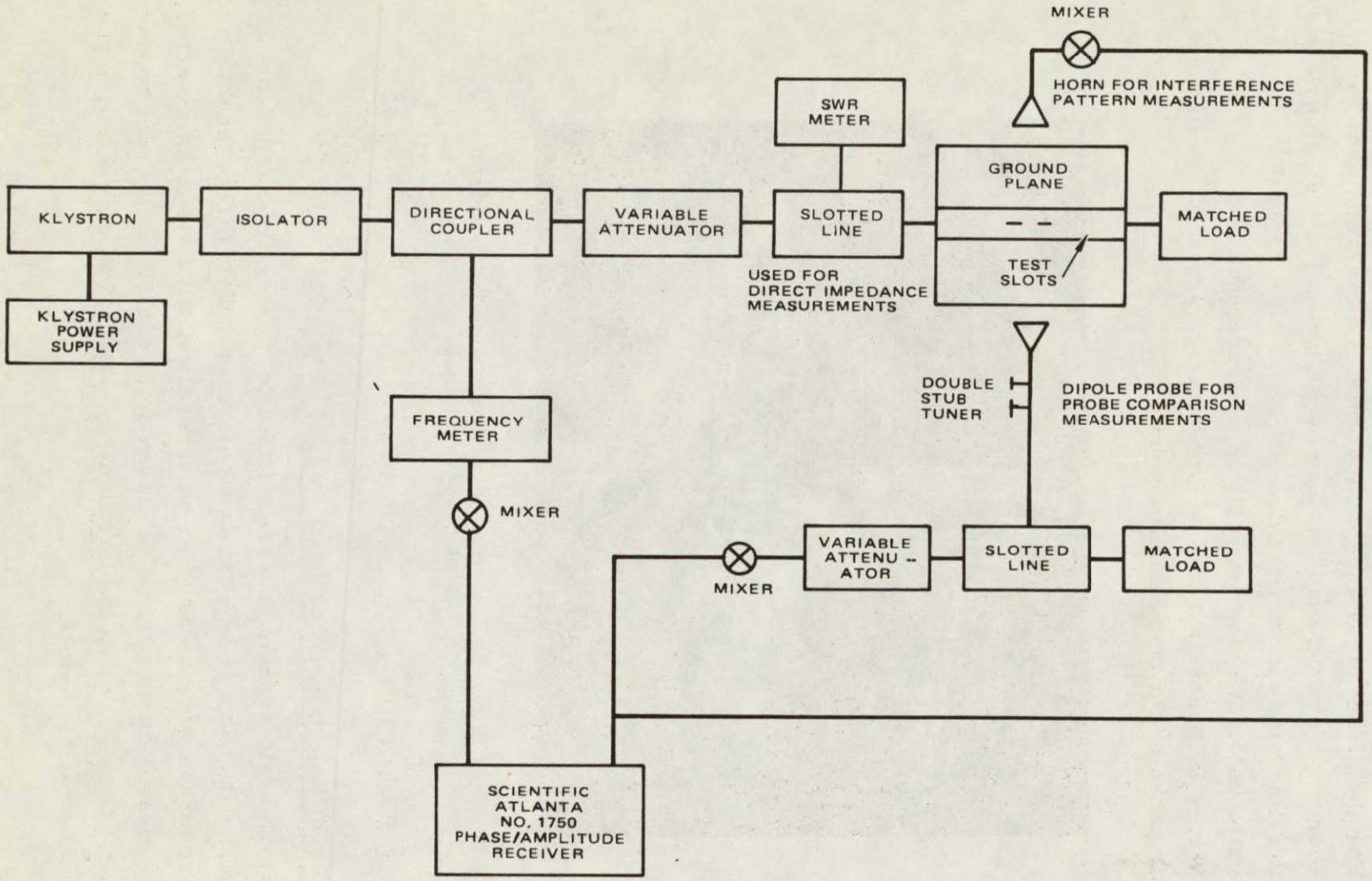

Figure 19. Block diagram of experimental setup.

For the direct impedance measurements a movable, non-contacting, type of short replaces the matched load at the end of the test-slot waveguide. The slotted line with a bolometer detector, the standing wave meter, and the variable attenuator are also used in this measurement.

Figure 20 presents a close-up of the test slots with two of them positioned for probe comparison measurement.

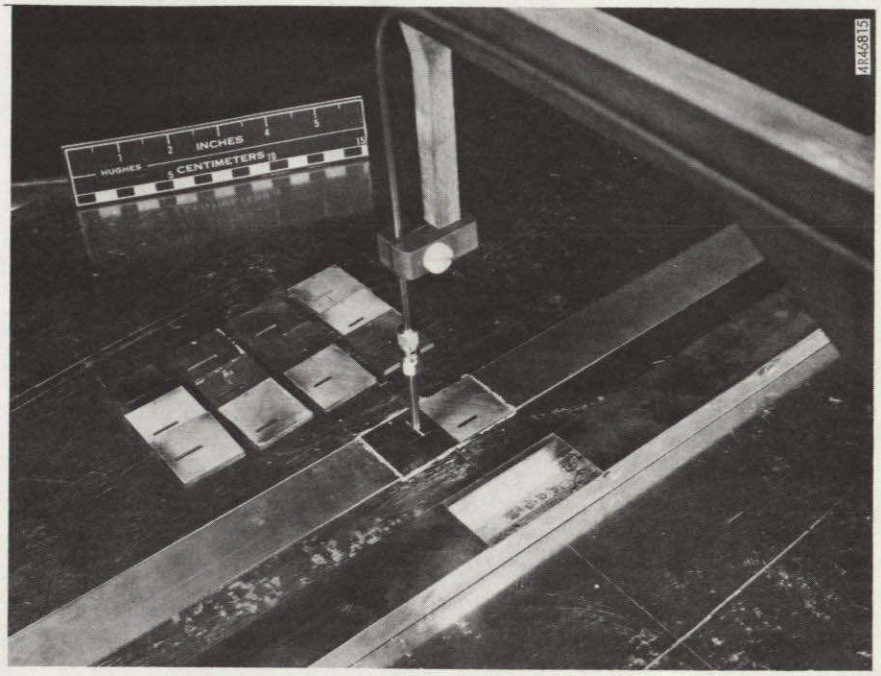

Figure 20. Components for probe comparison slot measurements.

4.3 TEST TECHNIQUE EVALUATION

4.3.1 Direct Impedance Measurement

Slotted line techniques were utilized to measure the impedance of the resonant slot that was to be used as a reference. This direct technique of impedance measurement was tried on several reactive slots; as expected, however, measurement errors increased quite rapidly as the slot conductance decreased. Consequently, the technique was applied to only a few, higher conductance, reactive slots.

4.3.2 Interference Pattern Method

The interference pattern method was tested extensively, and it presented several problems. When a horn, one-inch square, was used as the receiving element, its interaction with the ground plane strongly affected the slot radiation patterns. Also, an edge effect probably occurred due to the finite extent of the ground plane. An interference pattern from two slots of equal conductance ($g = 0.1$), with the horn positioned at a distance of 6 inches from the test slots, is shown in Figure 21. It can be seen that it is very difficult to accurately determine the angle of maximum field strength because of the large pattern ripple. Increasing the distance from the horn to the test slot decreases the pattern ripple to some extent but not sufficiently to eliminate the problem. For example, the predicted ratio of the maximum to the minimum of the interference pattern, Table 3, is less than one dB for the shorter test slots, whereas the interference patterns obtained using the horn, Figure 21, showed a peak-to-peak ripple of approximately 2 dB. The 2 dB test-fixture ripple would then obviously obscure the interference pattern of the test slots. An open-ended waveguide was next tested as the pickup element. It gave a smoother interference pattern, but the level of the received signal dropped considerably, resulting in poor data repeatability. Another point of concern was the differences in gains and beamwidths between slots. Patterns of individual elements were taken, Figure 22, and it was found that the element beamwidths and, consequently, the element gains varied from one test slot to the next. Also, slots of the same lengths displayed different beamwidths, and patterns were not repeatable when the slots were moved to different positions. This was especially the case for the weaker slots. The radiation interference pattern measurement method was not used because of the aforementioned problems.

4.3.3 Probe Comparison Measurement

The probe comparison technique was found to be the most sensitive and repeatable method. The interaction of the dipole probe with the test slot presented a problem at first, but it was corrected by tuning out or minimizing all possible sources of mismatch. Repeatability of the measured data was

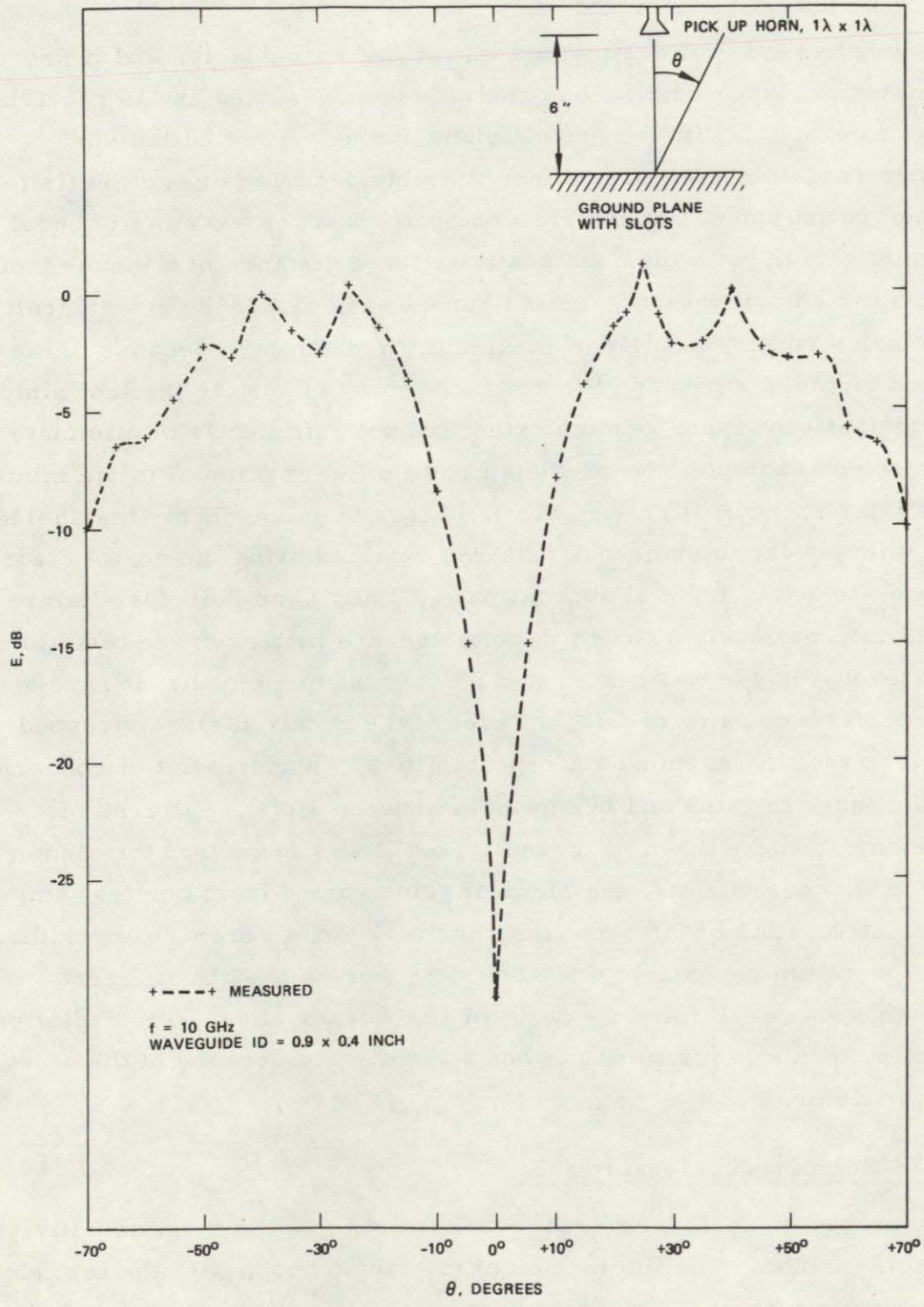

Figure 21. Interference pattern for two resonant slots separated by a half guide wavelength.

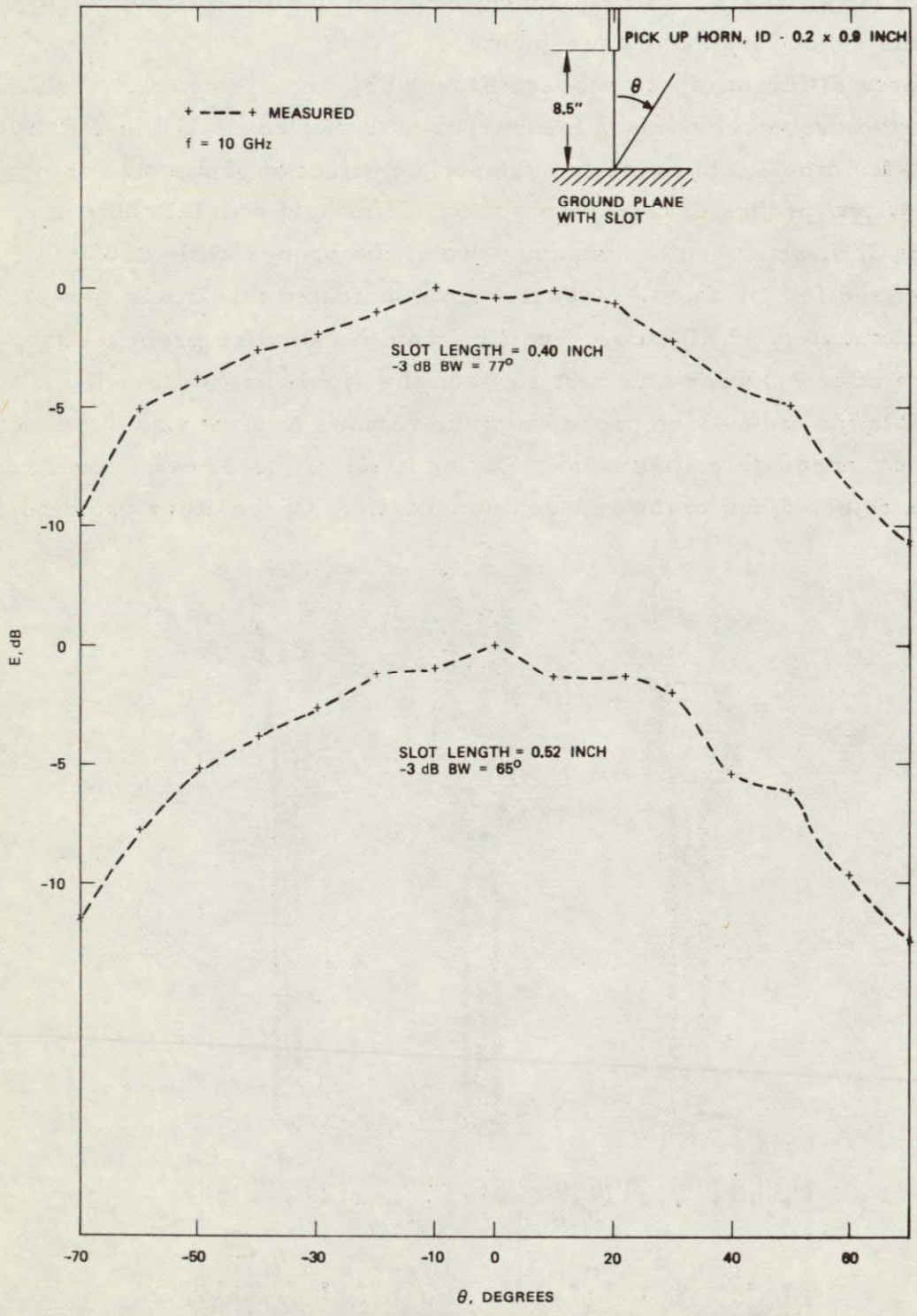

Figure 22. H-plane patterns of reactive slots.

found to be very good (±0.3 dB). Therefore, this method was chosen to be used for the reactive-slot measurements.

Three different dipole probes, Figure 23, were tested and evaluated for use in the probe comparison measurements: two coaxial-line-fed dipoles and a slot-fed dipole. In order to evaluate the effect of probe size on probe sensitivity, and probe-test slot interaction, semirigid coaxial cable of 0.141 inch O.D. was used to construct two of the probes while 0.080 O.D. cable was used for the third. Measurements indicated that the larger probes were approximately 11 dB more sensitive than the smaller probe. Also, interaction effects between the test slot and the dipole probe were found to be negligible for either size probe when the various mismatches were either tuned out or adequately attenuated. On the basis of these tests, the smaller probe was rejected due to the reduced sensitivity. Of the other two dipoles,

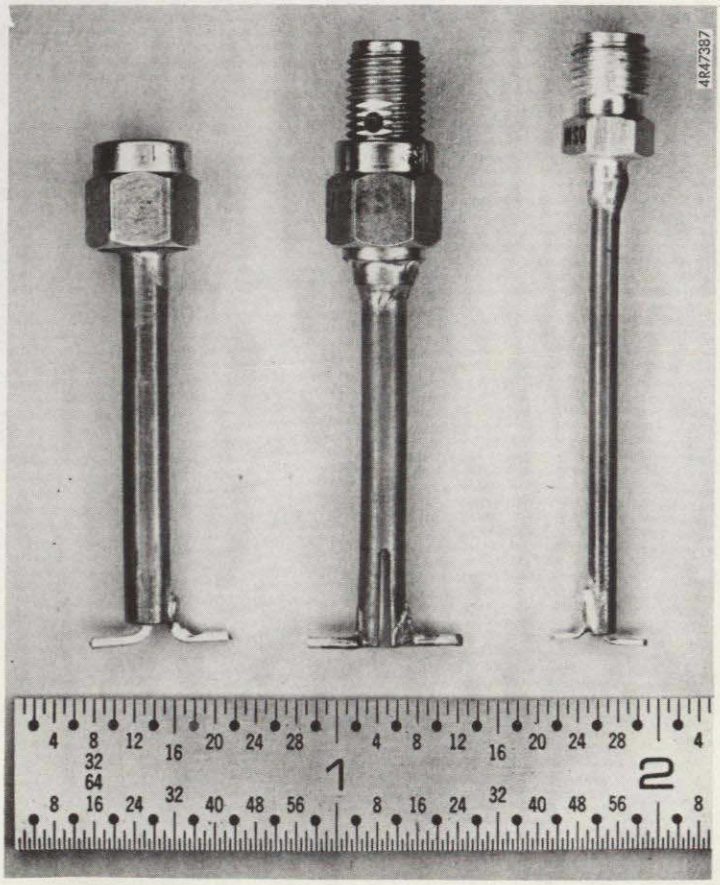

Figure 23. Probe types for probe comparison measurement.

the optimum height above the slot was 0.3 inch. For heights smaller than 0.3 inches the sinusoidal field distribution along with slot was being perturbed; and for heights greater than 0.3 inches probe-slot interactions became insignificant, but probe signal levels were low.

Another point of attention is to assure adequate sealing at the junctions between the waveguide walls and the removable slotted plates. Conductive paint and copper tape with conductive adhesive were used during the measurements to prevent any radiation leakage that might interfere with the radiation fields of the slots under test.

Finally, since differences in radiation amplitude between the reference and test slots can be as much as 30 dB, equipment accuracy is essential; thus, a precision variable attenuator should be used to calibrate the amplitude measuring equipment.

5.0 THEORETICAL AND EXPERIMENTAL RESULTS

5.1 THEORETICAL PERFORMANCE

The theoretical* performance of the slots described in Tables 3 and 4 are presented in graphic form in Figures 24 through 35. The data is plotted as a function of both slot displacement for constant slot length and slot length for constant displacement. Inspection of the data in Figure 24 reveals that the phase of the slot radiation is predicted to be constant versus slot displacement while inspection of the data in Figure 25 shows that the phase of the slot radiation is predicted to vary sinusoidally versus slot length. Since the radiation phase is derived from the relation: $\theta = \tan^{-1}(b/g)$, constant radiation phase versus slot displacement means that as the conductance, g, changes with slot displacement (Figure 26) the susceptance, b, changes proportionally (Figure 27). Conversely the data in Figures 28 and 29 shows that, as slot length is varied, the conductance changes more rapidly than the susceptance; hence the rapid phase change, versus slot length, is attributable mostly to the rapid conductance change. Comparison of Figures 26 and 27 with 32 and 33 show that in going from the 0.9 by 0.4 ID waveguide, with 0.05 wall thickness, to 0.835 by 0.4 ID waveguide, with 0.02 wall thickness, the slot conductance increase by an average of approximately 5 dB while the susceptance increase by an average of only about 3 dB. This smaller ratio, b/g, of slot susceptance to slot conductance is reflected in the curve of radiation phase for the 0.835 x 0.4 ID waveguide (Figure 31) displaying a smaller phase with decreasing slot length in comparison to the phase curve for the 0.9 x 0.4 ID waveguide (Figure 25).

5.2 EXPERIMENTAL DATA

The experimental data for the slots described in Tables 3 and 4 are presented in graphic form in Figures 24, 25, 30, 31, and 36 through 43. As for the theoretical case, the data are plotted as a function of both slot

*Arthur A. Oliner, "The Impedance Properties of Narrow Radiating Slots in the Broad Face of Rectangular Waveguide," IRE Trans. on Antennas and Propagation, Vol. AP-5, No. 1, pp. 4-20, January 1957.

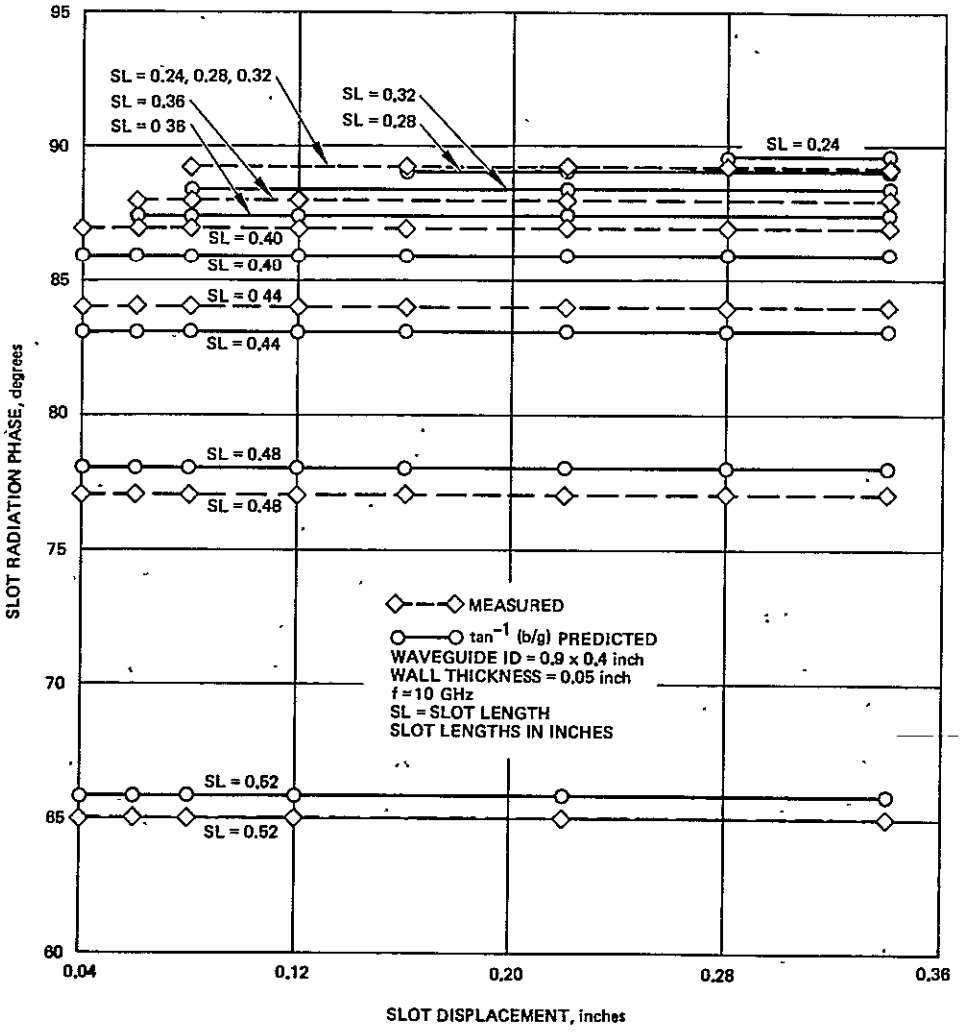

Figure 24. Radiation phase of longitudinal shunt slot as a function of slot displacement (referenced to a resonant slot).

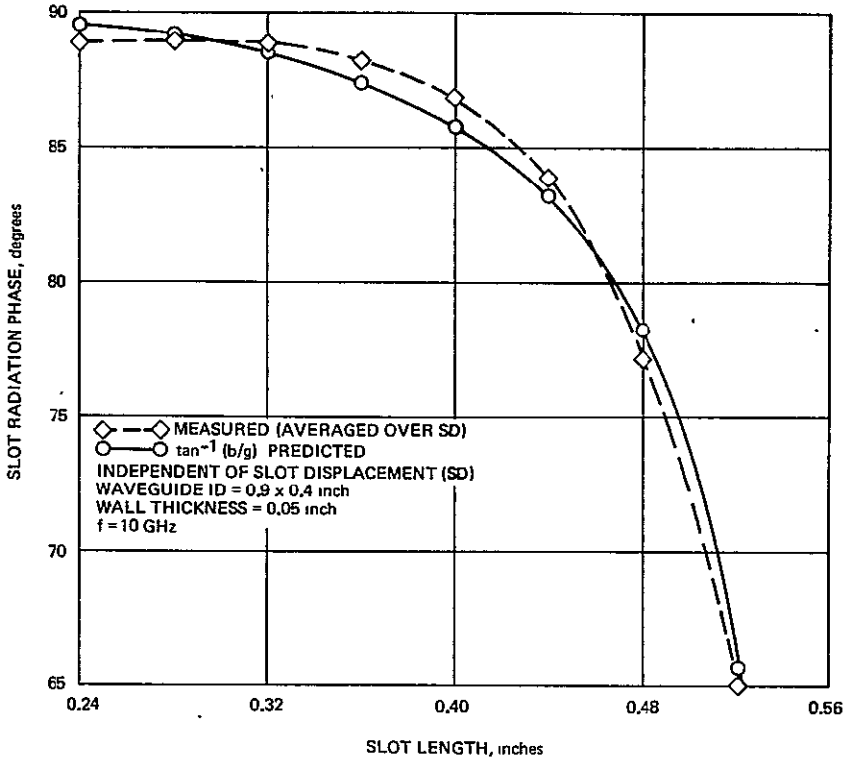

Figure 25. Radiation phase of longitudinal shunt slot as a function of slot length (referenced to a resonant slot).

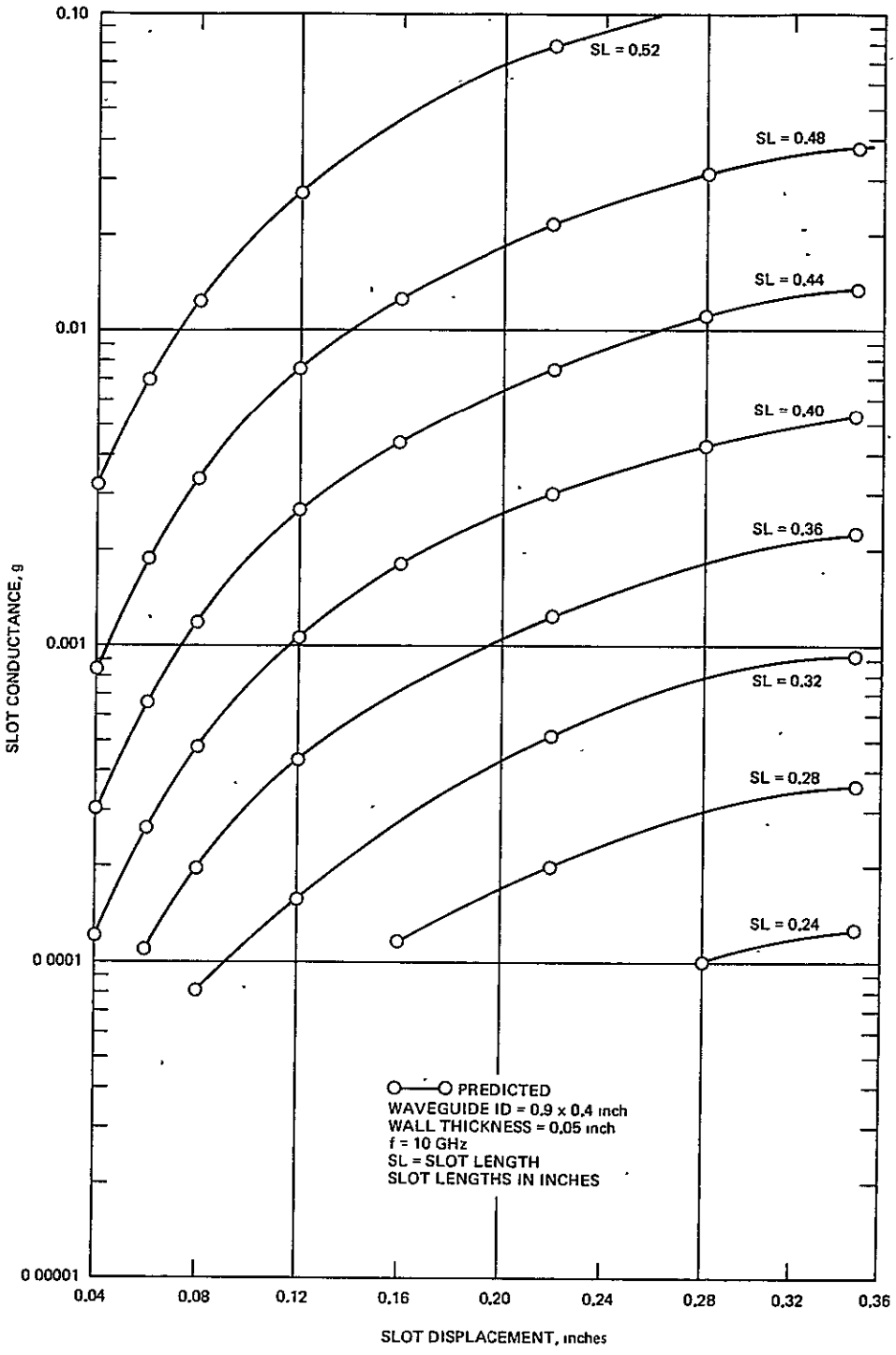

Figure 26. Conductance of longitudinal shunt slot as a function of slot displacement.

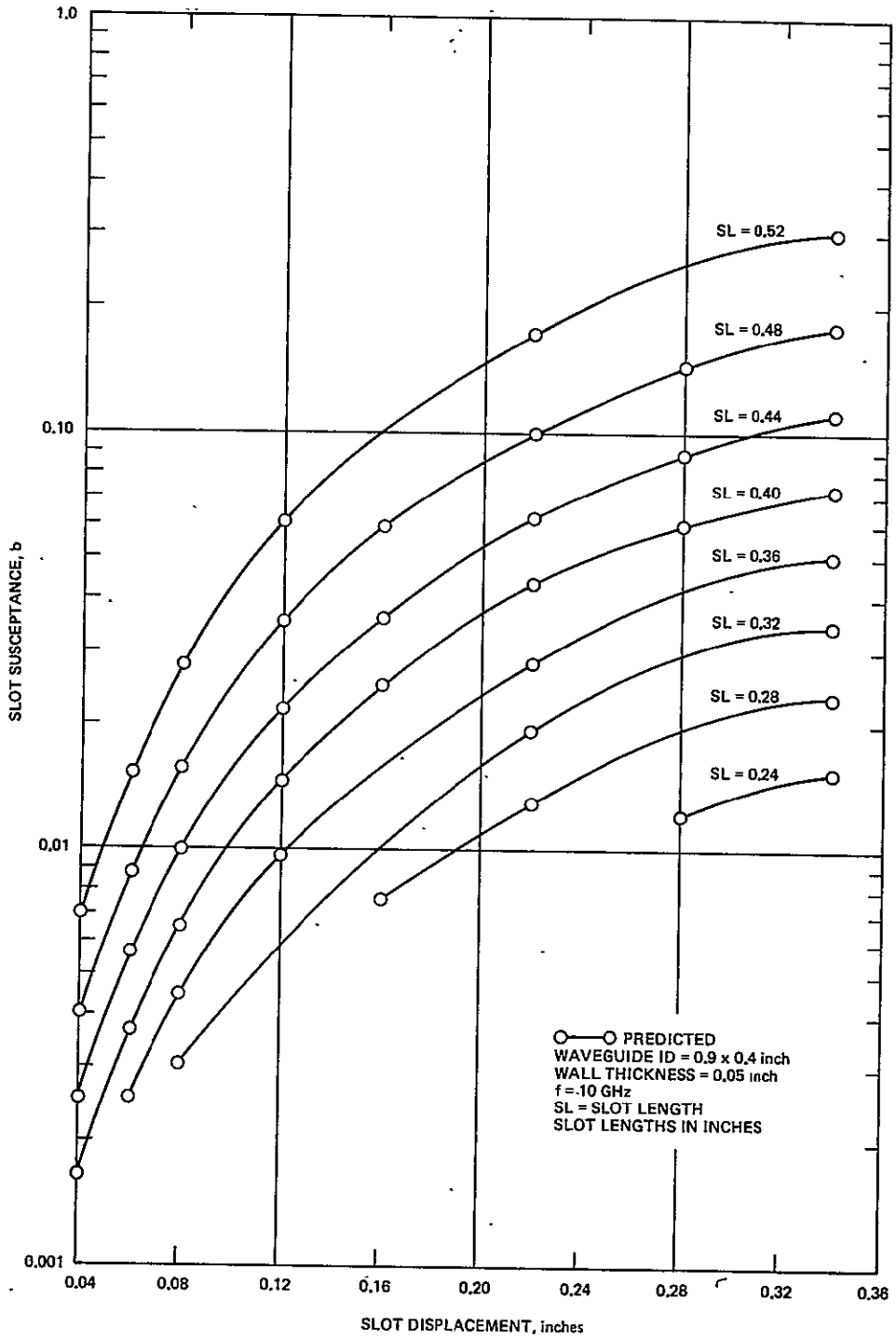

Figure 27. Susceptance of longitudinal shunt slot as a function of slot displacement.

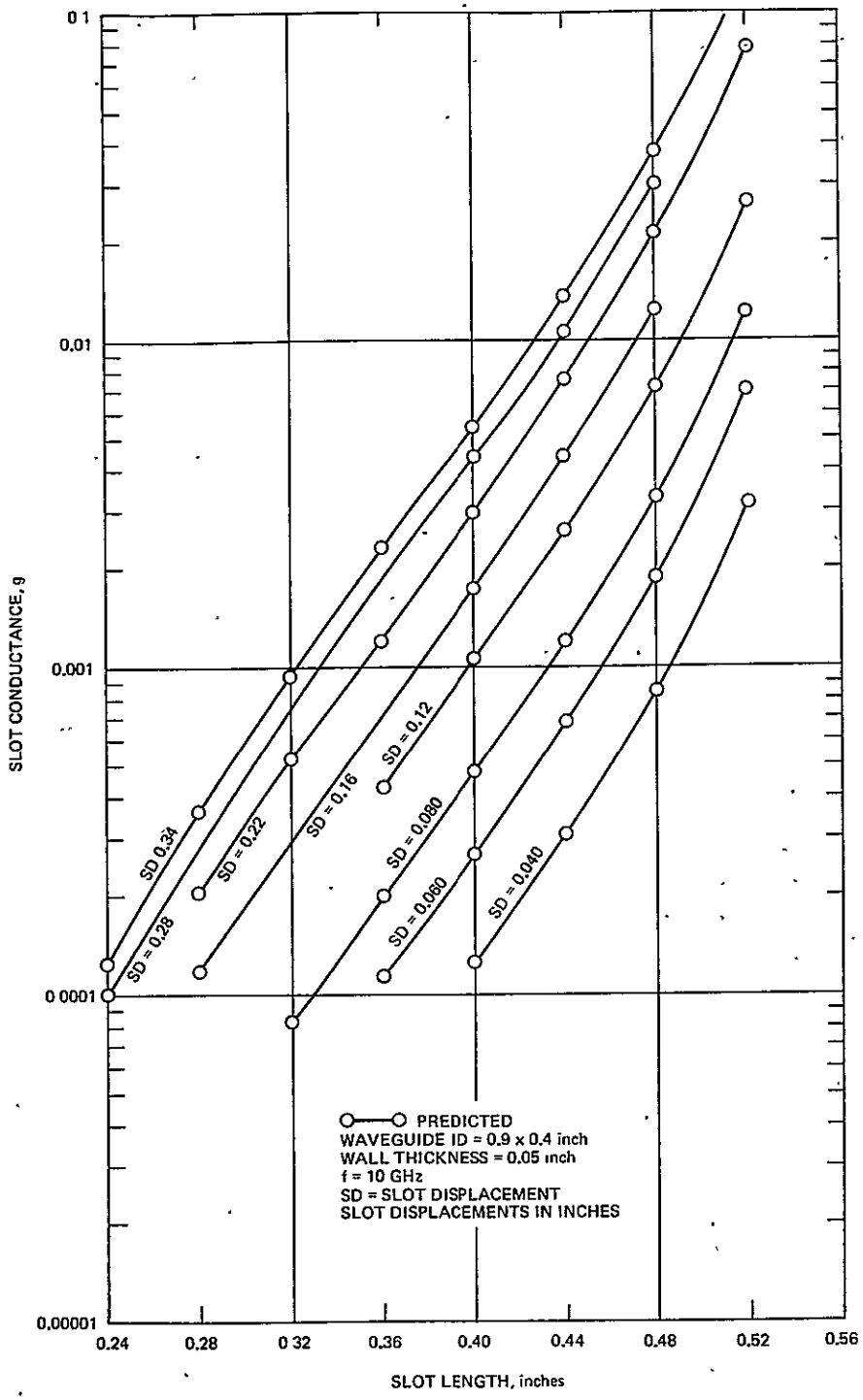

Figure 28. . Conductance of longitudinal shunt slot as a function of slot length.

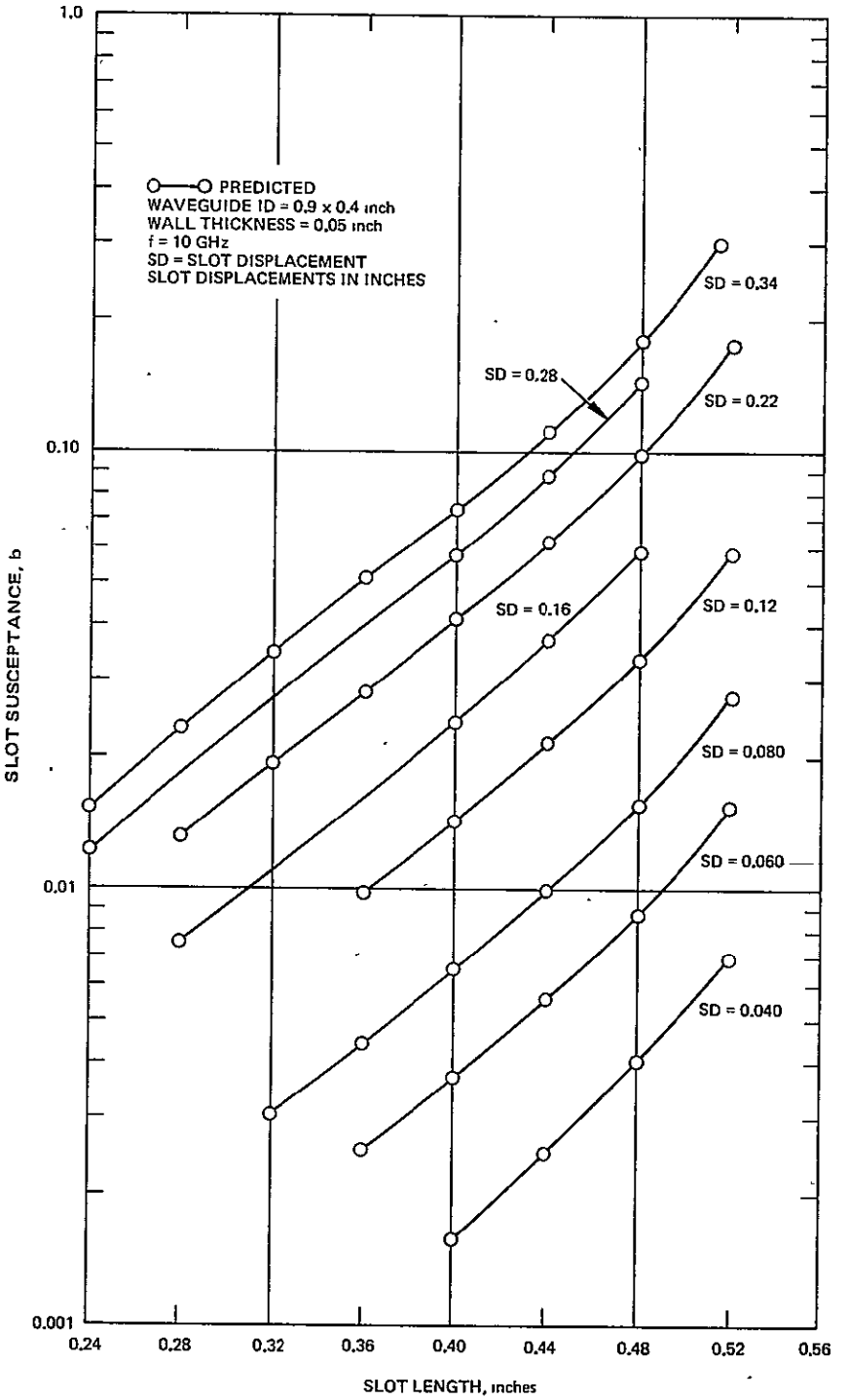

Figure 29. Susceptance of longitudinal shunt slot as a function of slot length.

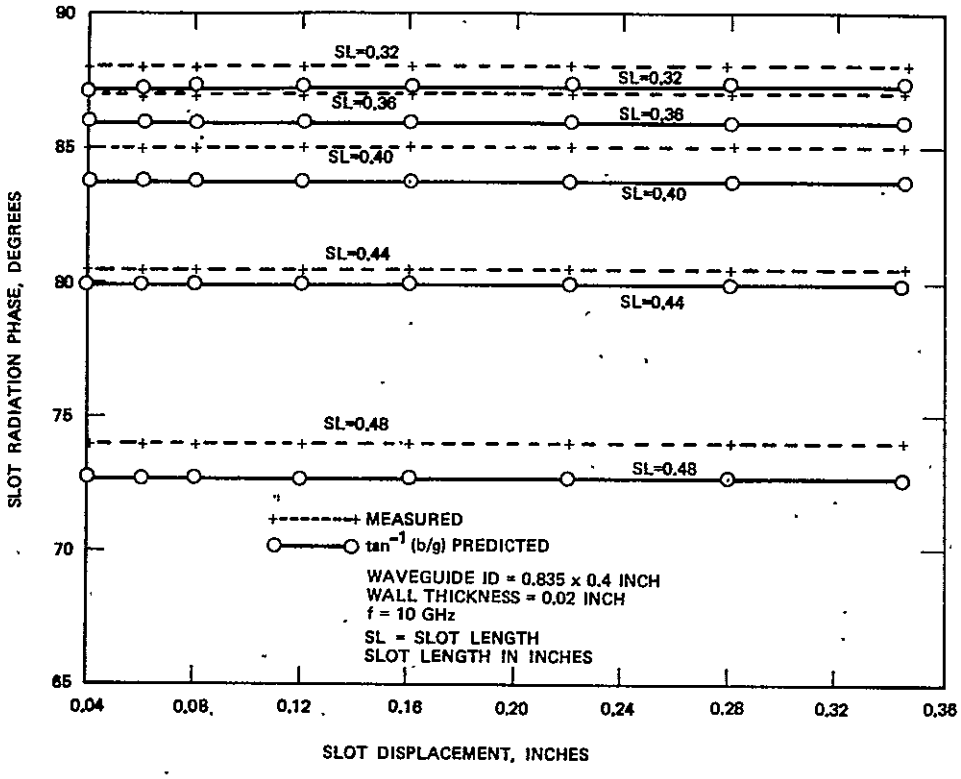

Figure 30. Radiation phase of longitudinal shunt slot as a function of slot displacement (referenced to a resonant slot).

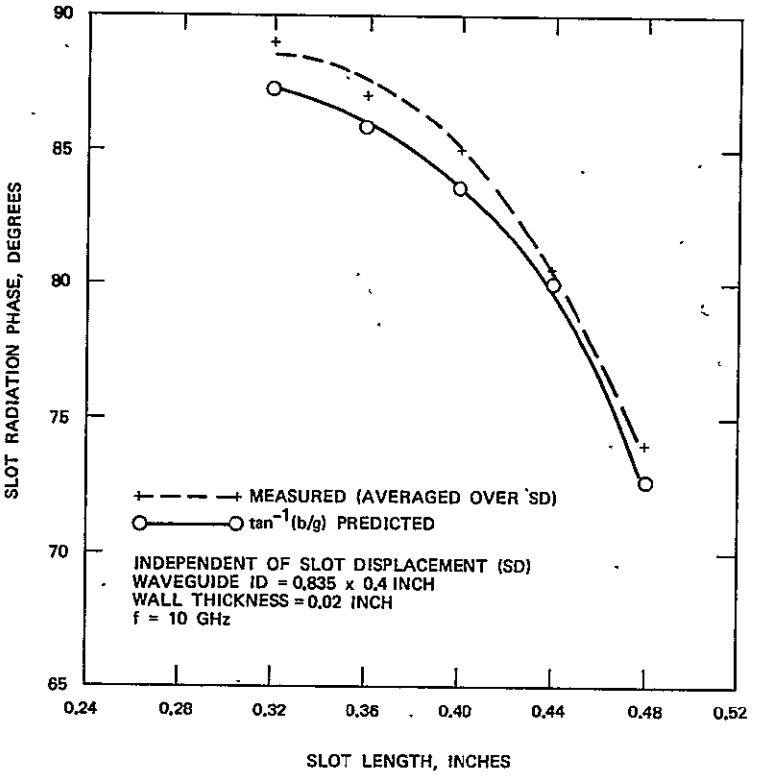

Figure 31. Radiation phase of longitudinal shunt slot as a function of slot length (referenced to a resonant slot).

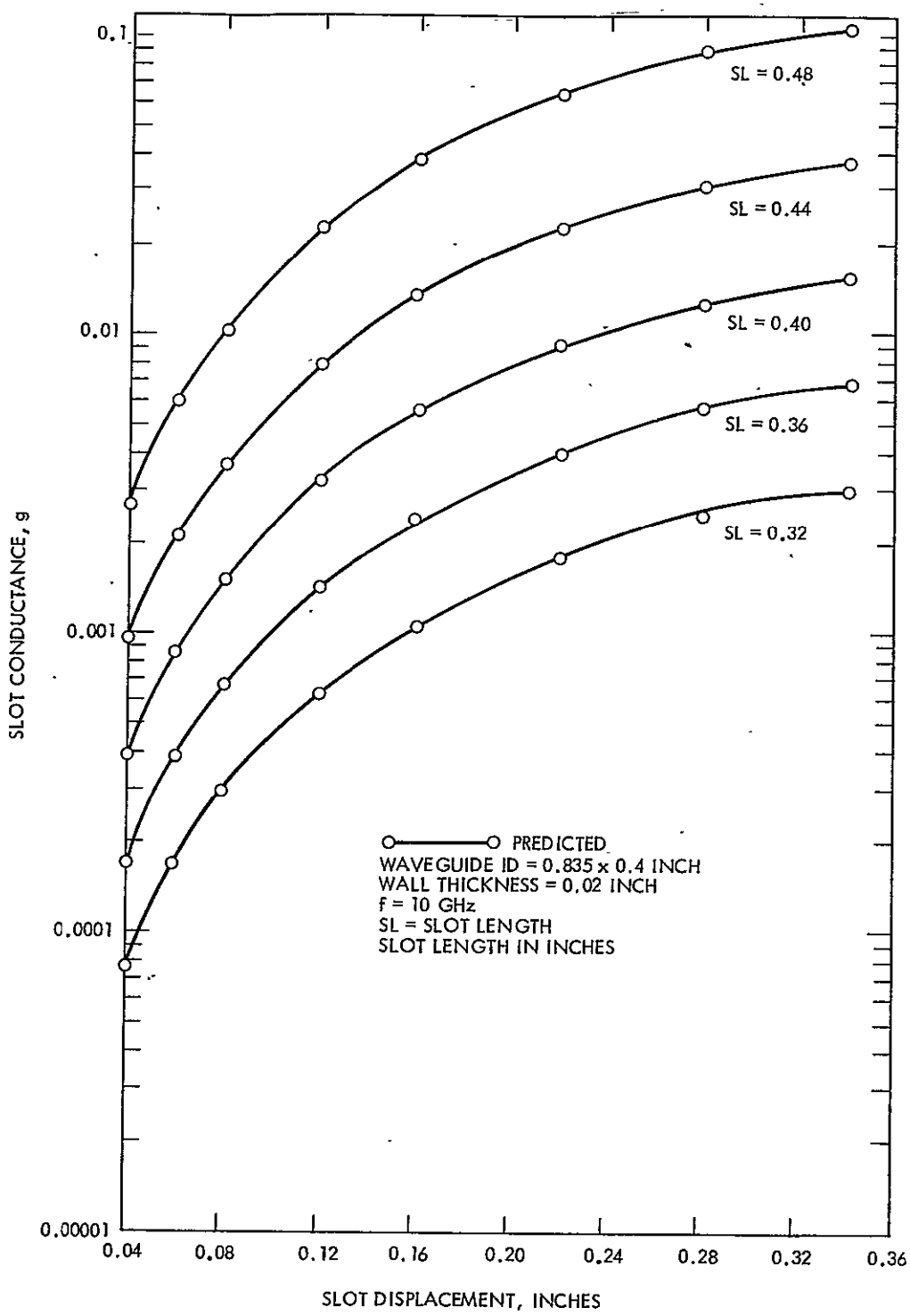

Figure 32. Conductance of longitudinal shunt slot as a function of slot displacement.

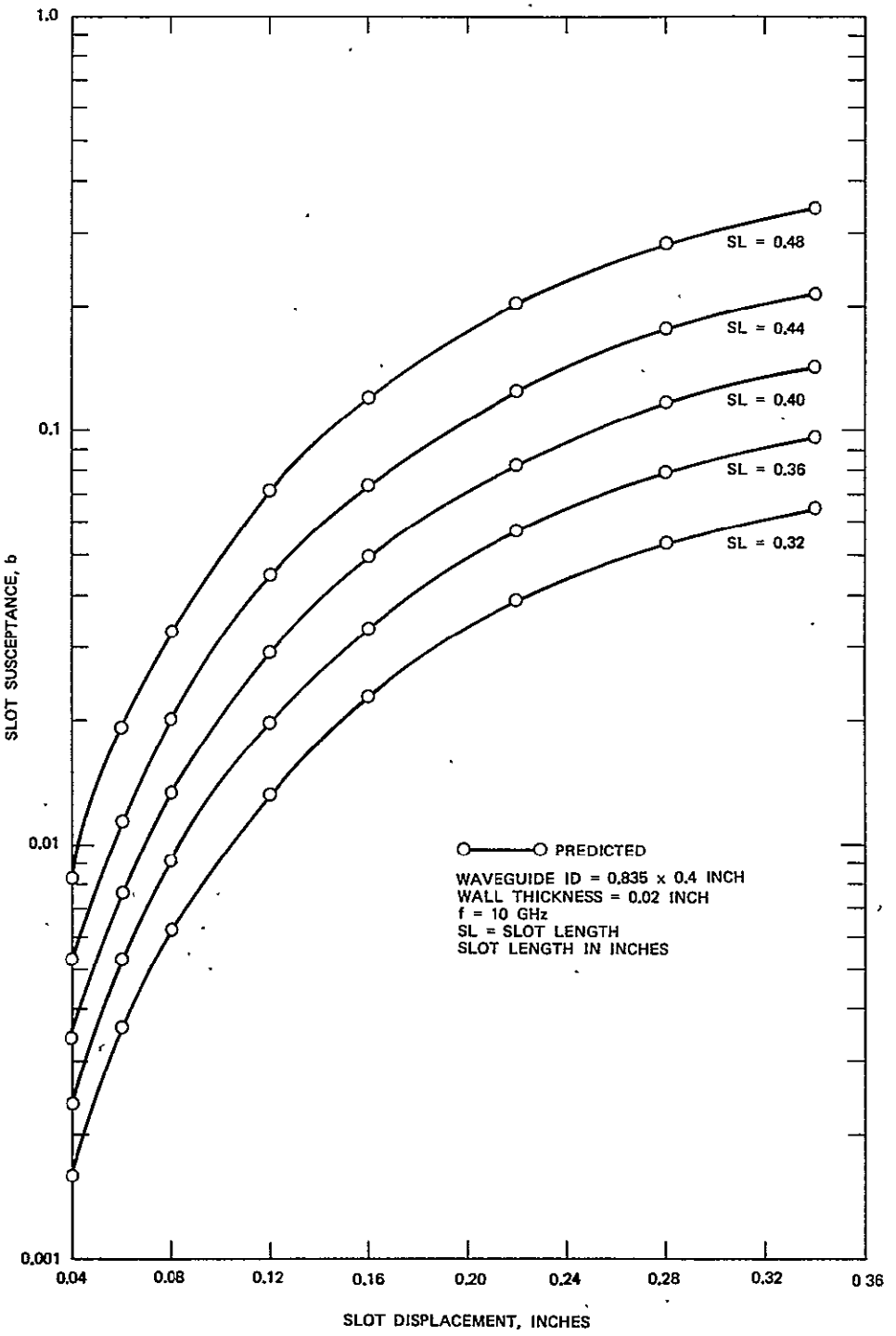

Figure 33. Susceptance of longitudinal shunt slot as a function of slot displacement.

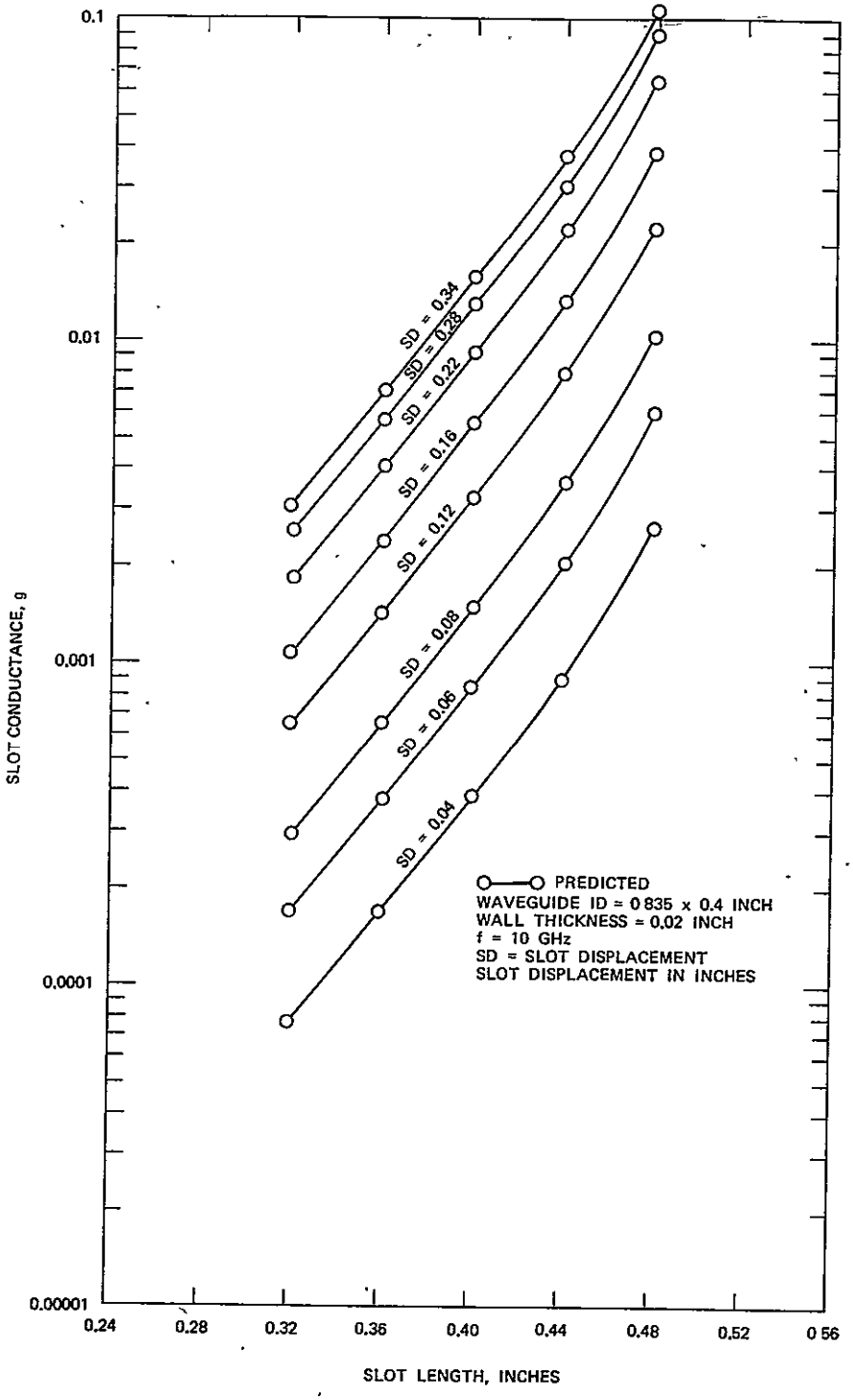

Figure 34. Conductance of longitudinal shunt slot as a function of slot length.

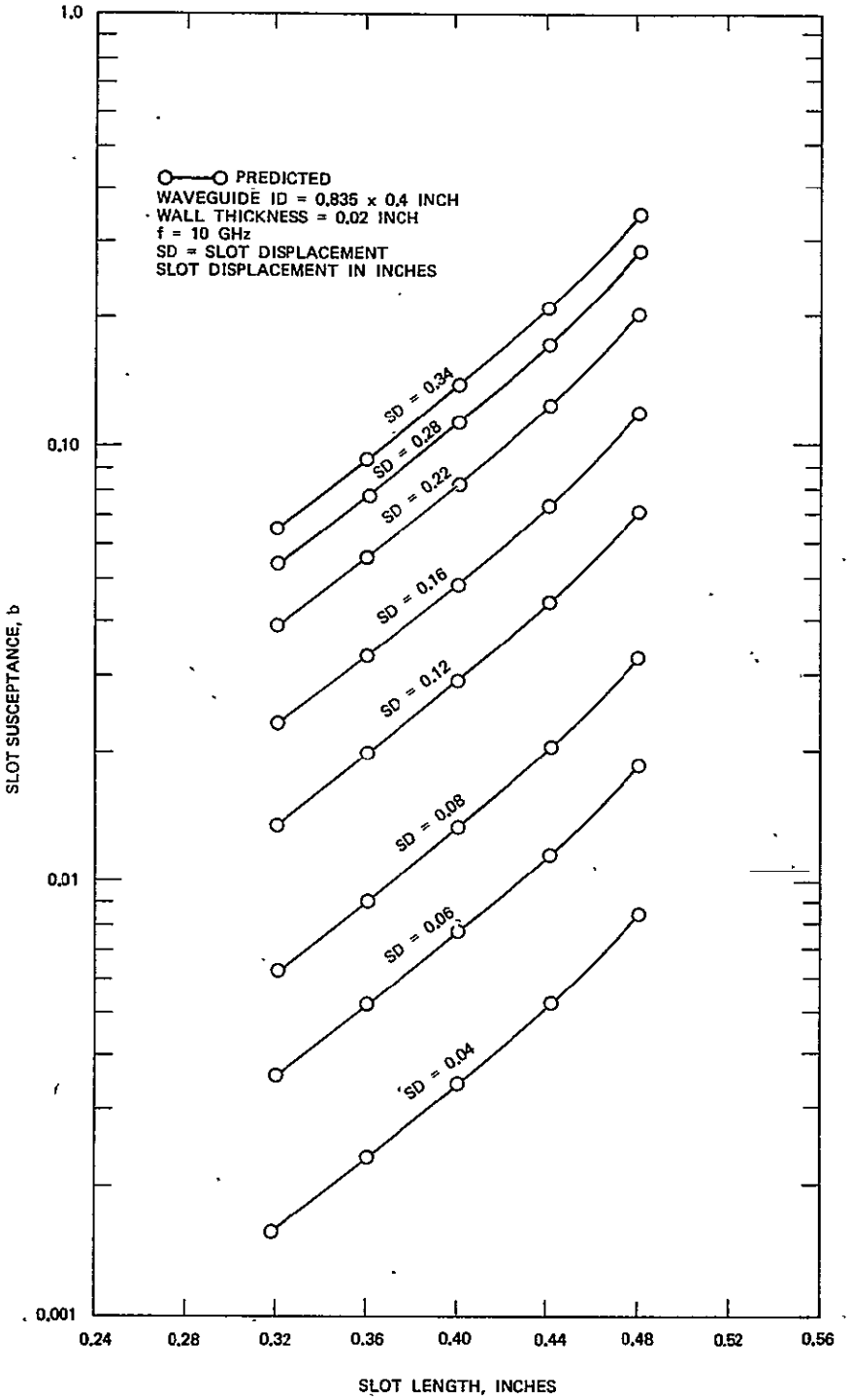

Figure 35. Susceptance of longitudinal shunt slot as a function of slot length.

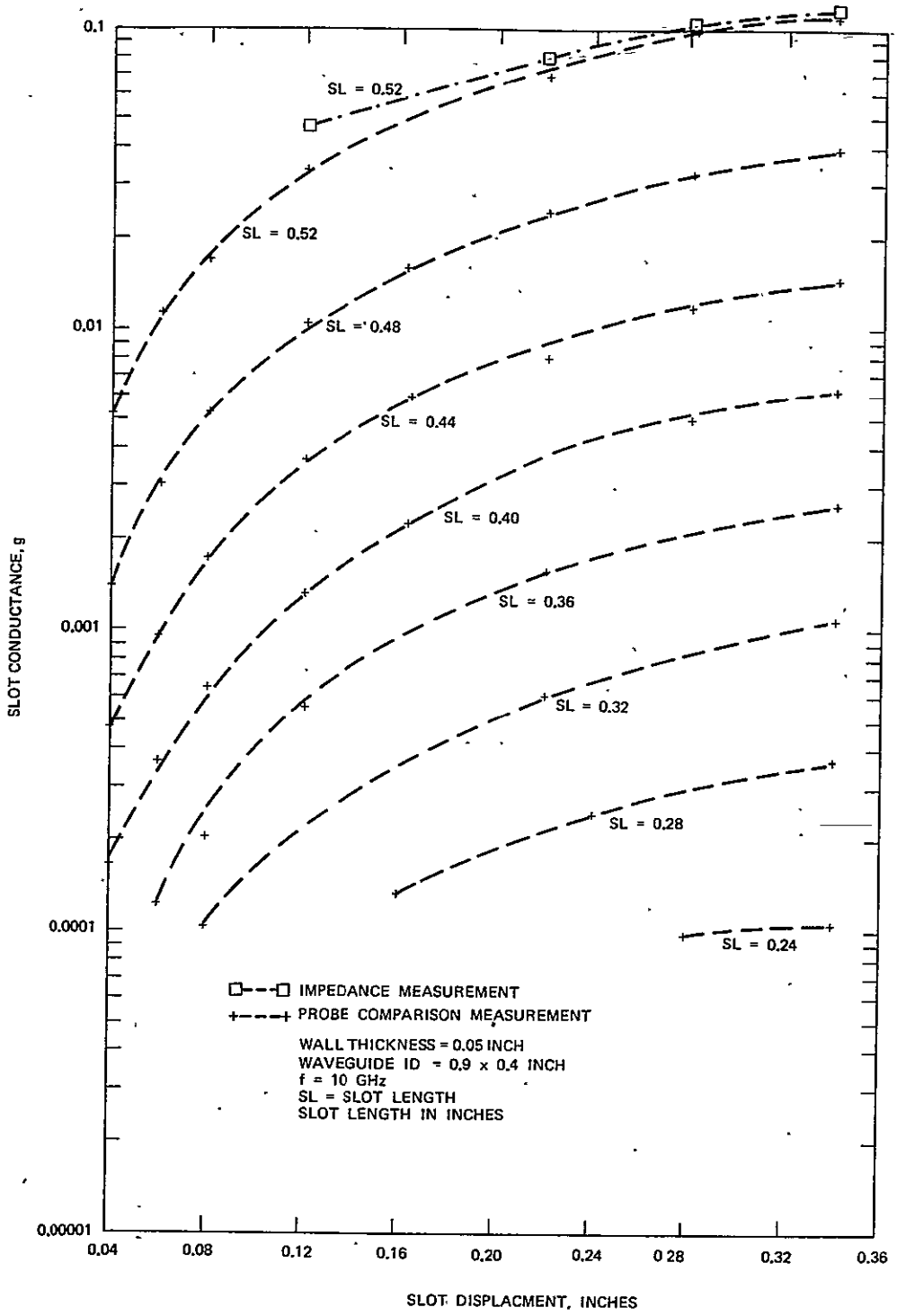

Figure 36. Conductance of longitudinal shunt slot as a function of slot displacement.

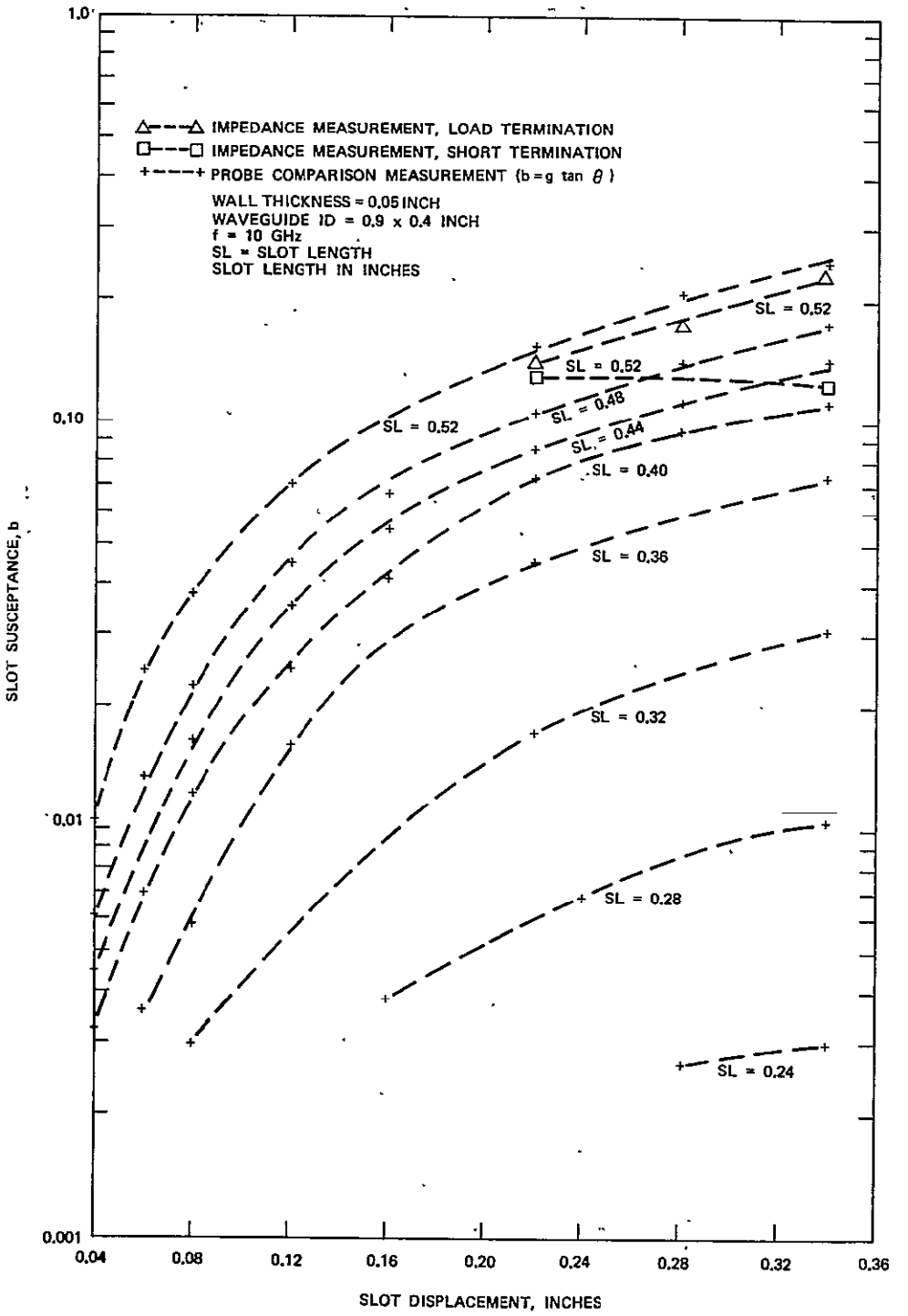

Figure 37. Susceptance of longitudinal shunt slot as a function of slot displacement.

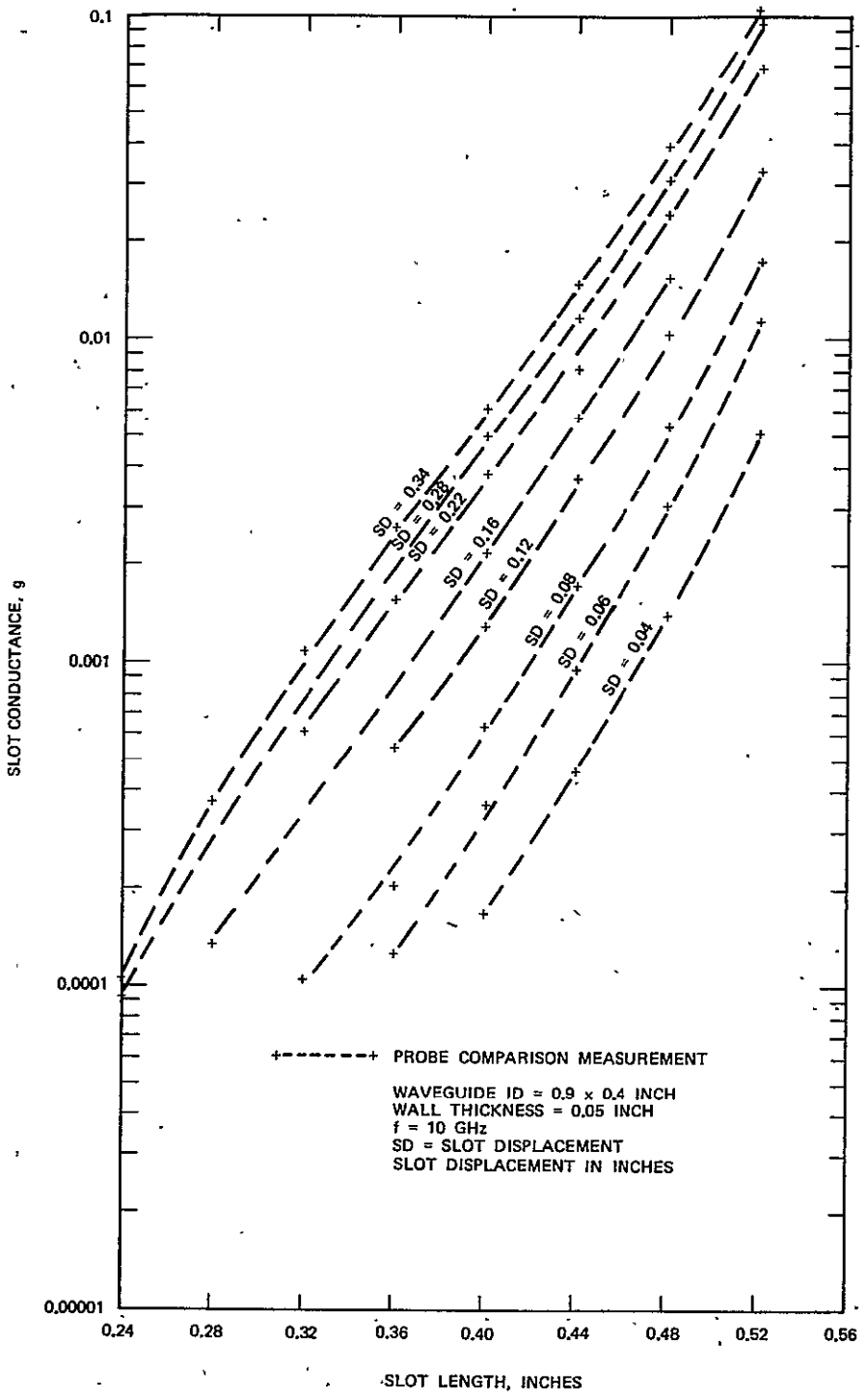

Figure 38. Conductance of longitudinal shunt slot as a function of slot length.

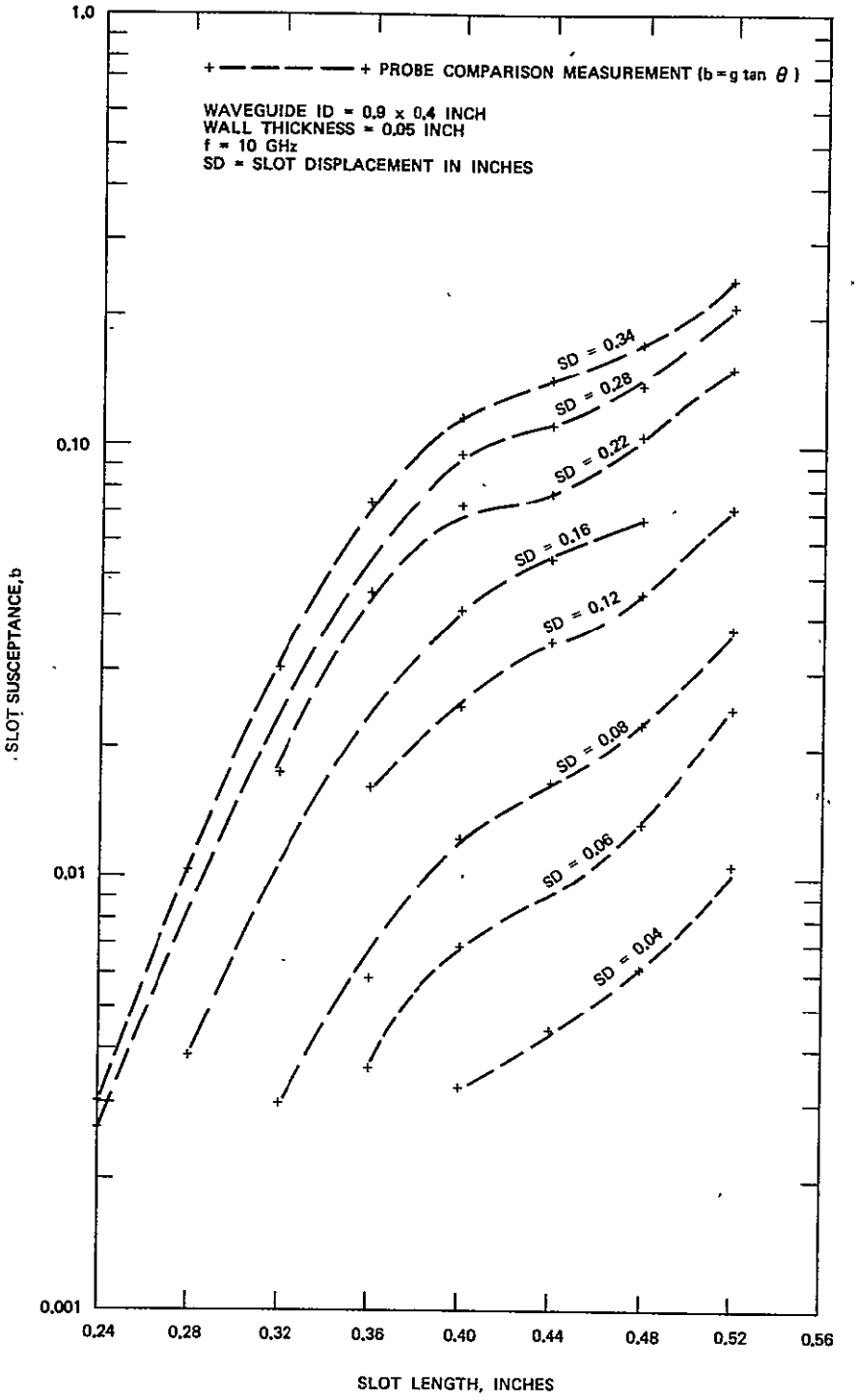

Figure 39. Susceptance of longitudinal shunt slot as a function of slot length.

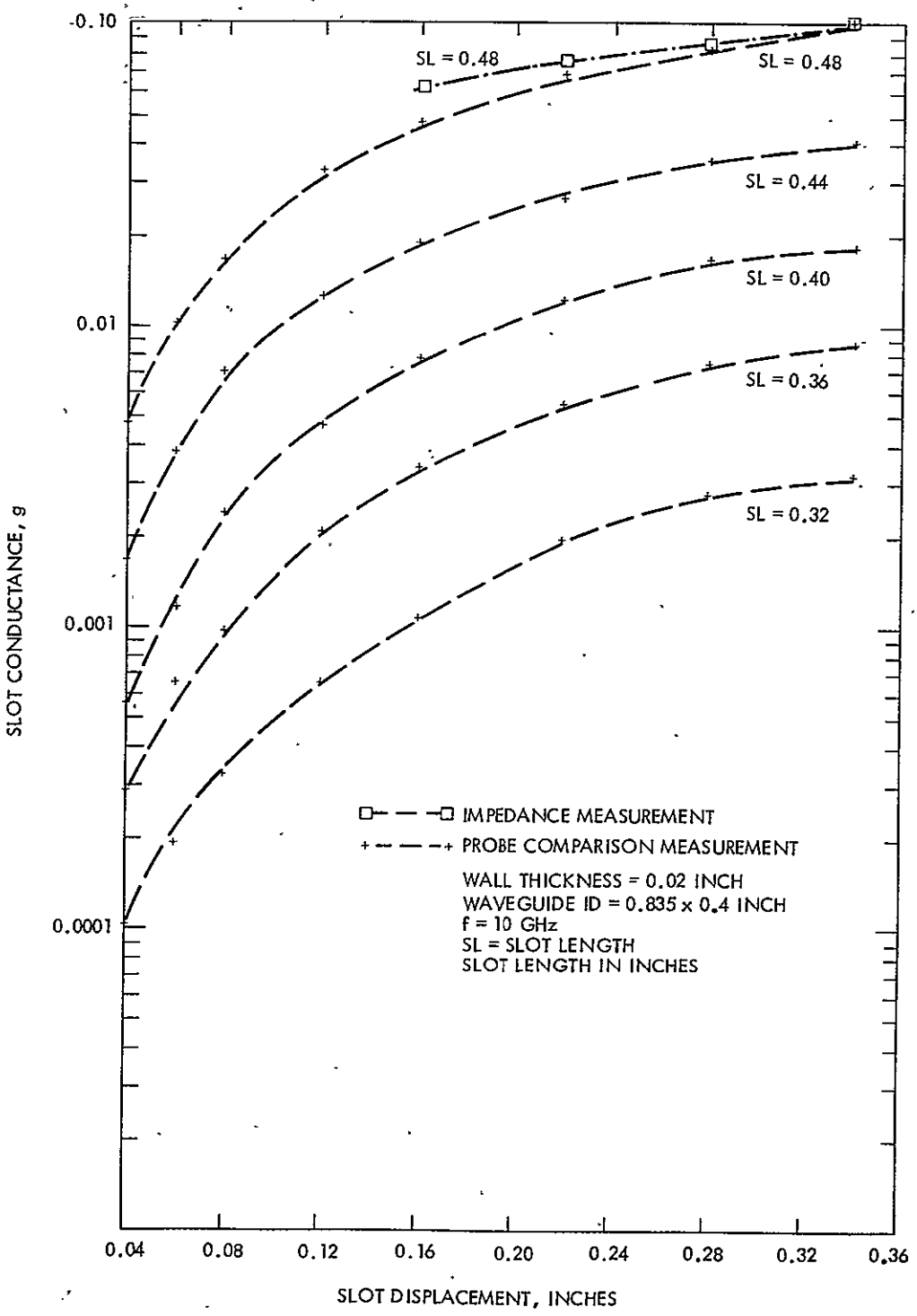

Figure 40. Conductance of longitudinal shunt slot as a function of slot displacement.

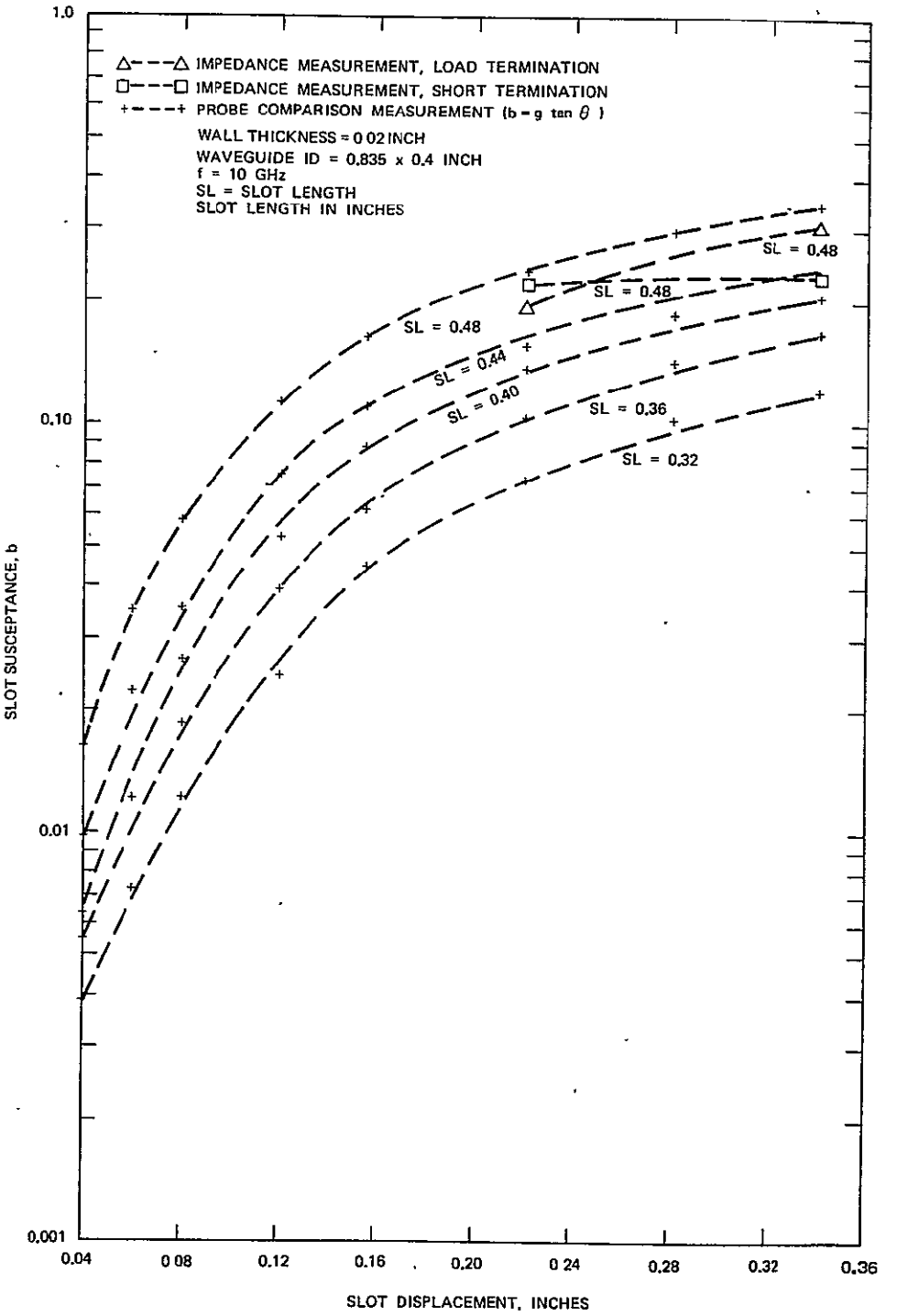

Figure 41. Susceptance of longitudinal shunt slot as a function of slot displacement.

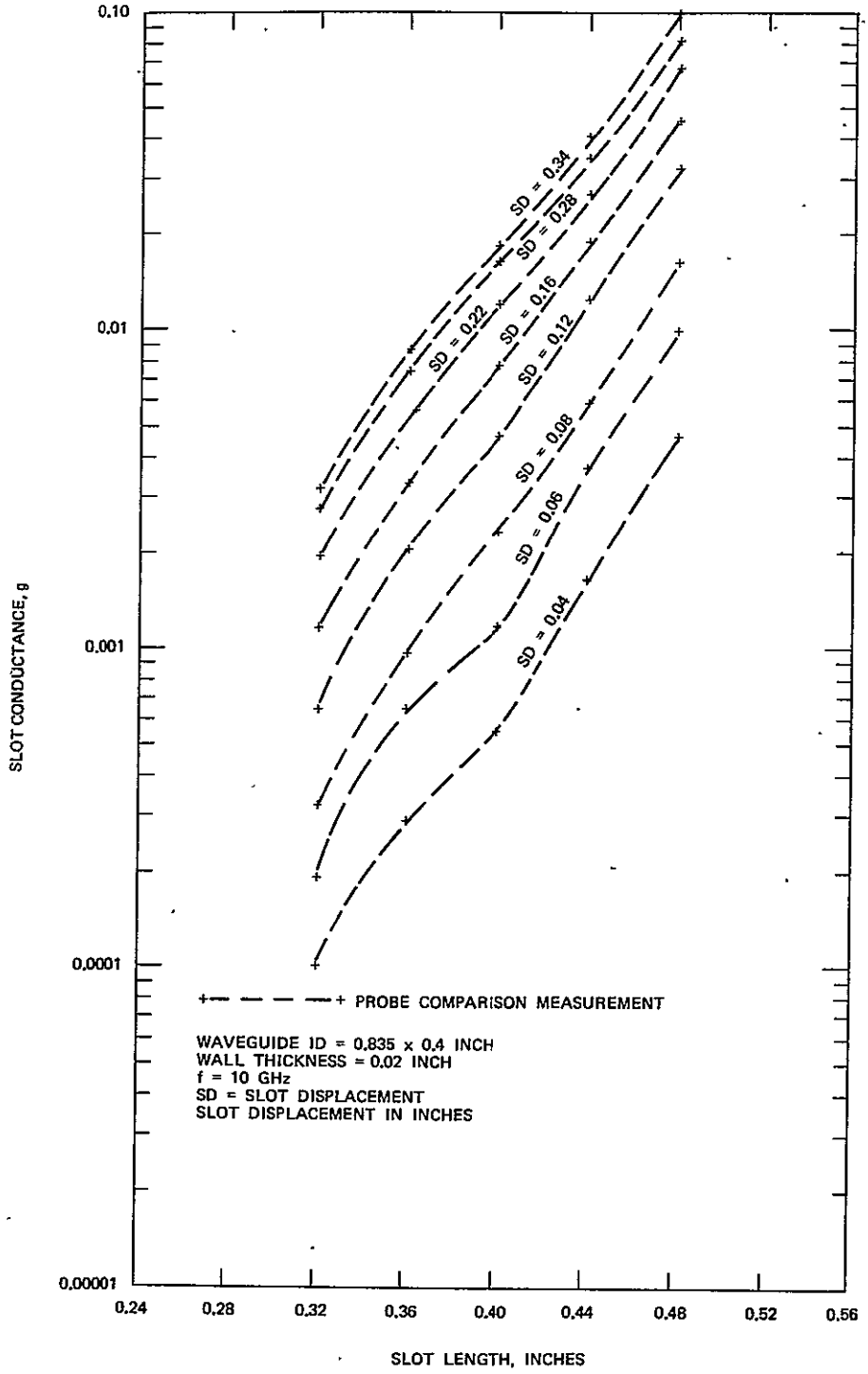

Figure 42. Conductance of longitudinal shunt slot as a function of slot length.

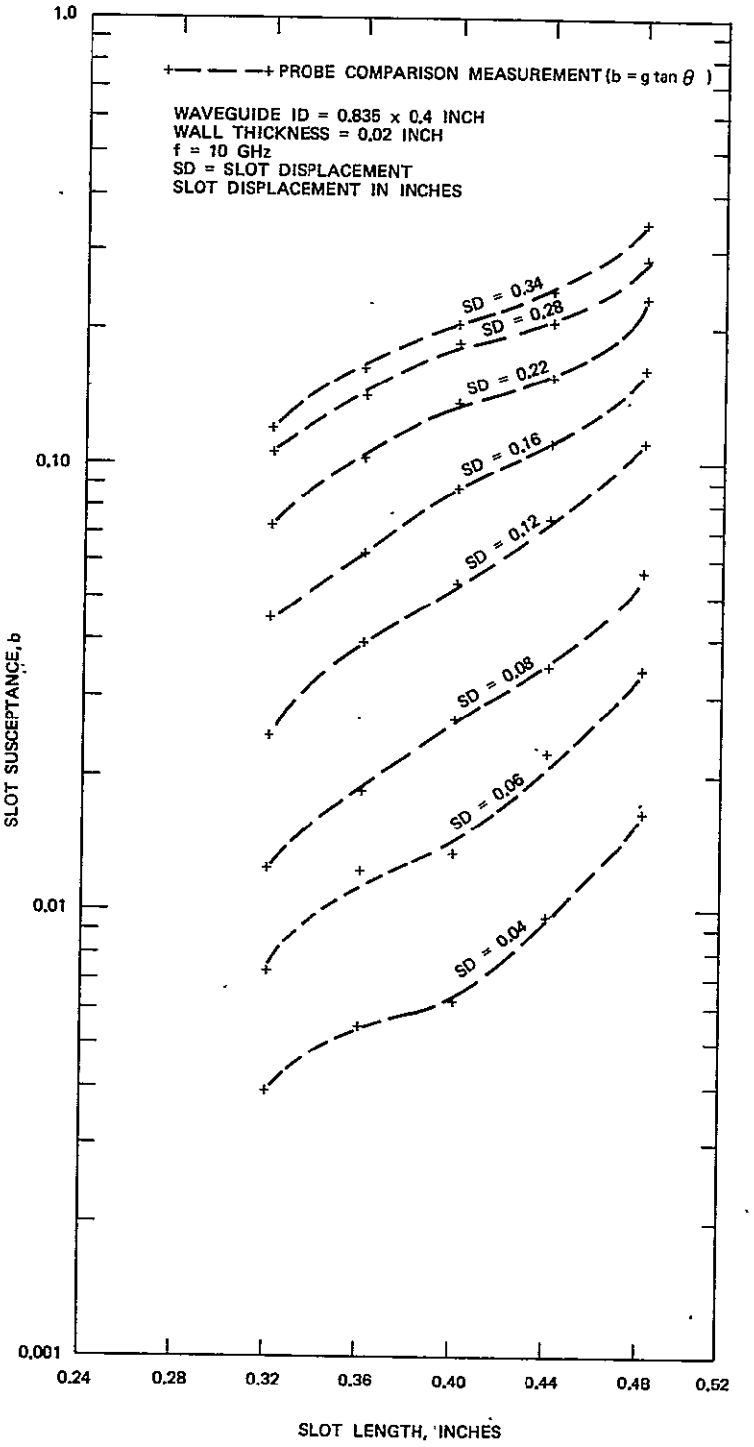

Figure 43. Susceptance of longitudinal shunt slot as a function of of slot length.

displacement for constant slot length and slot length for constant displacement. Since all the measurements were made by the probe comparison technique, except for a few impedance measurement cases which were used for reference purposes, the measured data was radiation amplitude and phase compared to that of a reference resonant slot whose theoretical conductance had been confirmed by impedance measurement. On this basis, the radiation phase and conductance plots are essentially directly measured data (conductance and radiation amplitude are simply related by Equation (6), Section 4.1.1) while the susceptance plots are derived from the measured conductances and radiation phases by the relation: $b = g \tan \theta$. It is this derivation which, in large part, probably accounts for the wavy nature of the experimental susceptance plots (Figures 39 and 43) in contrast to the smooth theoretical susceptance plots shown in Figures 29 and 35. Because of the large radiation phase angles being measured, and because the susceptance is derived from the tangent of these phase angles, small phase angle measurements errors can lead to large errors in the values of the calculated susceptances. For example, a 1.5-degree measurement error at 83° will result in a 1.1-dB error in the calculated susceptance; and a 1.5-degree measurement error at 87 degrees will result in a 3-dB error in the calculated susceptance.

In order to verify the accuracy of the probe comparison technique, comparative impedance measurements were made of some of the higher conductance slots. It is seen in Figures 36 and 40 that the slot conductances, as measured by the impedance and probe comparison techniques, agree well at the higher conductance values where agreement is within 0.3 dB or better for conductances of 0.08 or higher. Some divergence occurs at the lower conductance values. At these lower values, the conductances from the impedance measurements are seen to be higher; this is expected with the impedance technique because waveguide losses, especially the losses at the silver painted boundary of the slotted plates, will result in the measurement of a higher apparent conductance. The slot susceptances (Figures 37 and 41) measured by the impedance and probe comparison techniques, are also seen to agree well at the higher conductance values, when the impedance measurement is made with a load terminating the slotted waveguide. Agreement is

poorer when the impedance measurement is made with a short terminating the slotted waveguide. This is because, with a short termination, the real part of the slot reflection coefficient is the much larger term and tends to obscure the reactive part; while, with a load termination, the reactive (or imaginary) part of the slot reflection coefficient is the larger term, so it can be determined more accurately. The agreement between the probe comparison and impedance measurement (with load termination) techniques is seen to be 0.6 dB or better for the 0.4-inch x 0.9-inch waveguide and 0.9 dB or better for 0.835-inch x 0.4-inch waveguide.

Since the general shapes of the experimental conductance and susceptance curves follow the theoretical curves, it can be inferred that (1) the theory presented by Oliner has neither left out nor introduced major factors that obscure the basic slot behavior and (2) the probe comparison method is a reliable technique and does not introduce any major source of error. A more absolute comparison of theory and experiment requires the inspection of the superimposed graphs presented in the following section.

5.3 THEORETICAL VERSUS EXPERIMENTAL PERFORMANCE

The theoretical and experimental performance of the slots described in Tables 3 and 4 are presented in graphic form in Figures 24, 25, 30, 31, and 44 through 47. The comparative data is given for both waveguide sizes and in terms of radiation phase versus slot displacement, Figures 24 and 30, radiation phase versus slot length, Figures 25 and 31, conductance versus slot displacement, Figures 44 and 45, and susceptance versus slot displacement, Figures 46 and 47.

The theoretical and experimental radiation phase are seen to agree to within 1.5° or better, while the conductance values agrees to within 2.5 dB or better for the 0.835- x 0.4-ID waveguide and to within 1.8 dB or better for the 0.9- x 0.4-ID waveguide. The experimental conductances are generally higher than the theoretical conductances. The conductance agreement is generally best at the larger slot displacements and the disagreement gradually increases to a maximum as the slots approach the waveguide centerline. At the smallest slot displacement tested, 0.04 inch, the edge of the

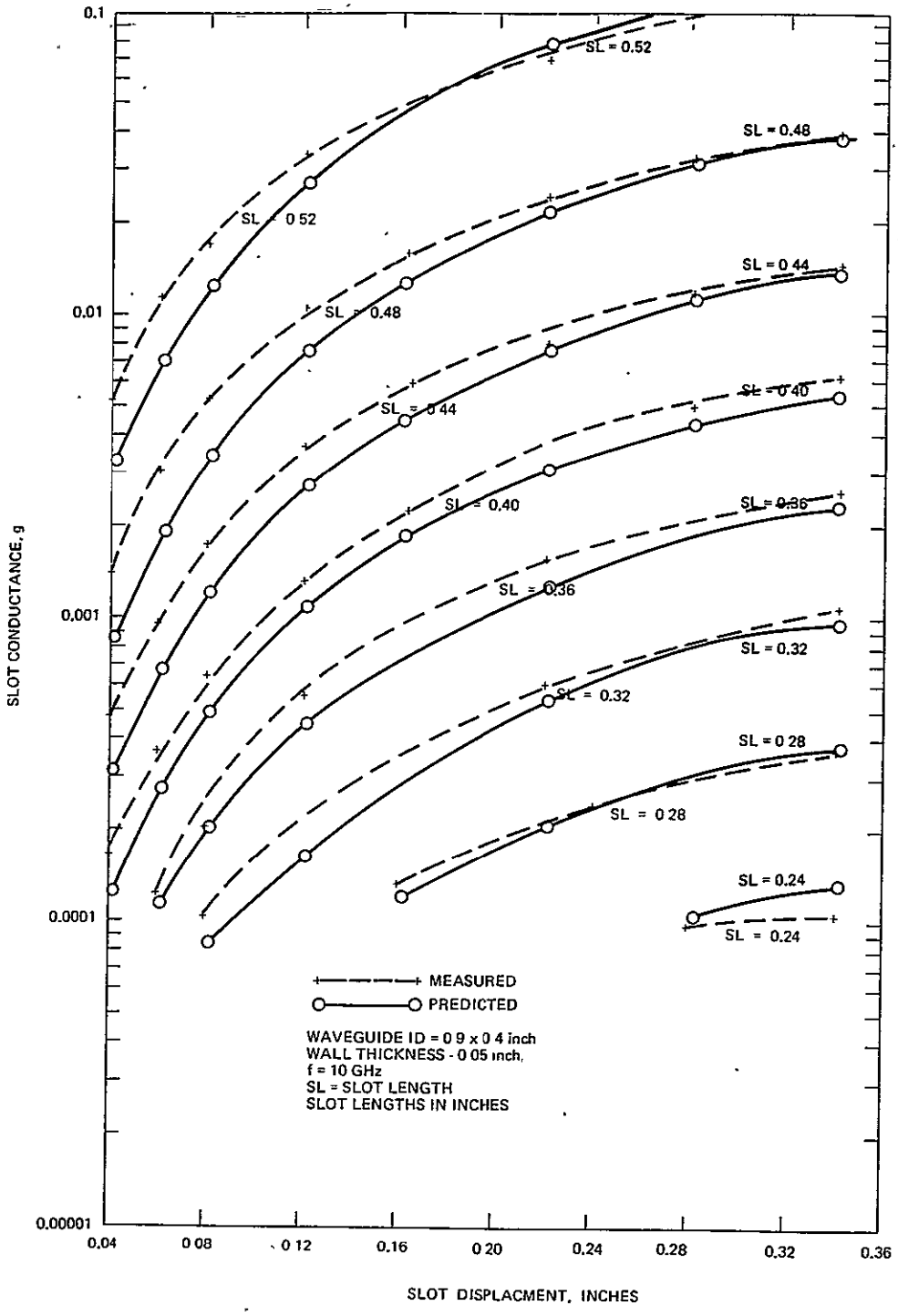

Figure 44. Predicted versus measured conductance of longitudinal shunt slot as a function of slot displacement.

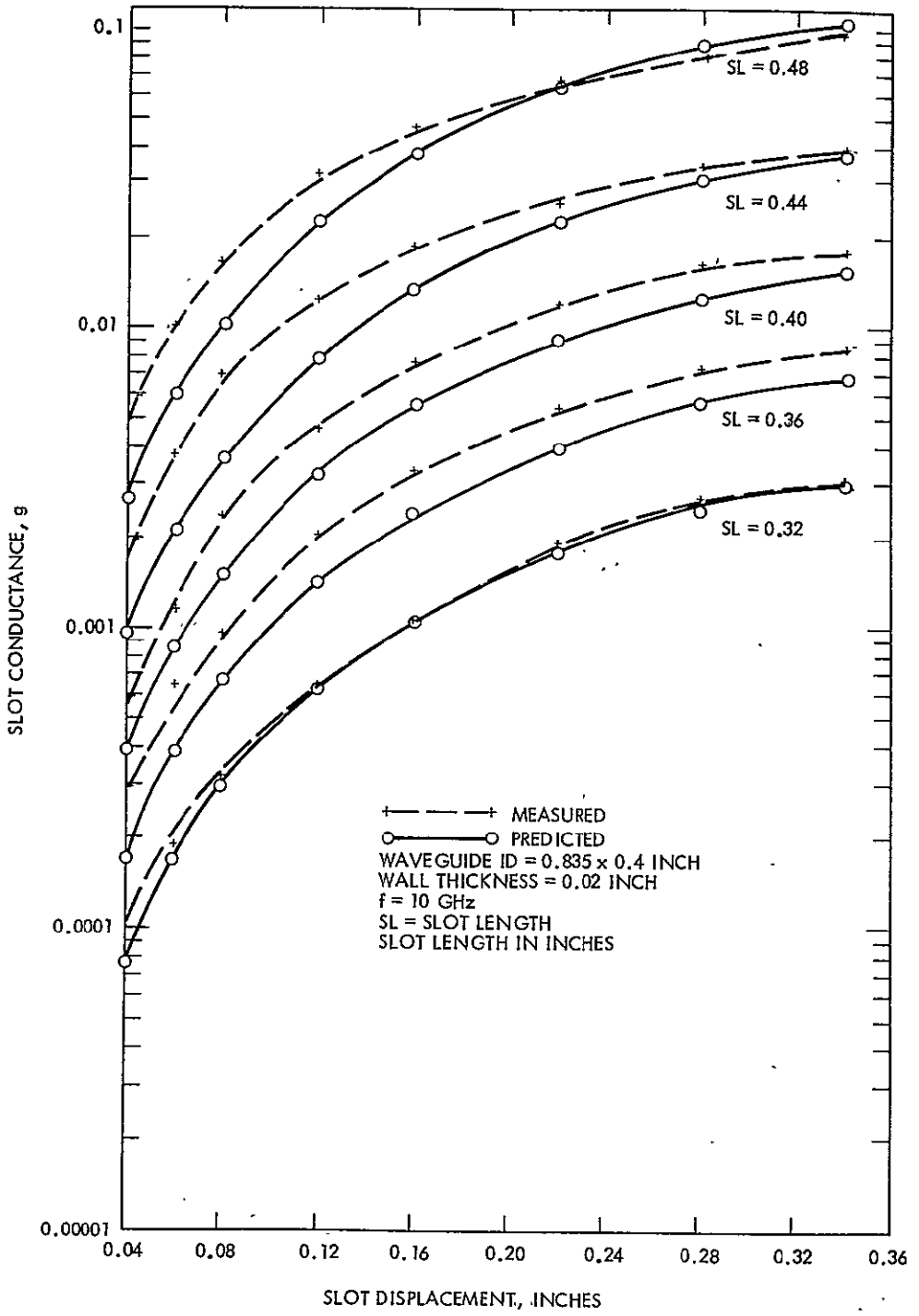

Figure 45. Predicted versus measured conductance of longitudinal shunt slot as a function of slot displacement.

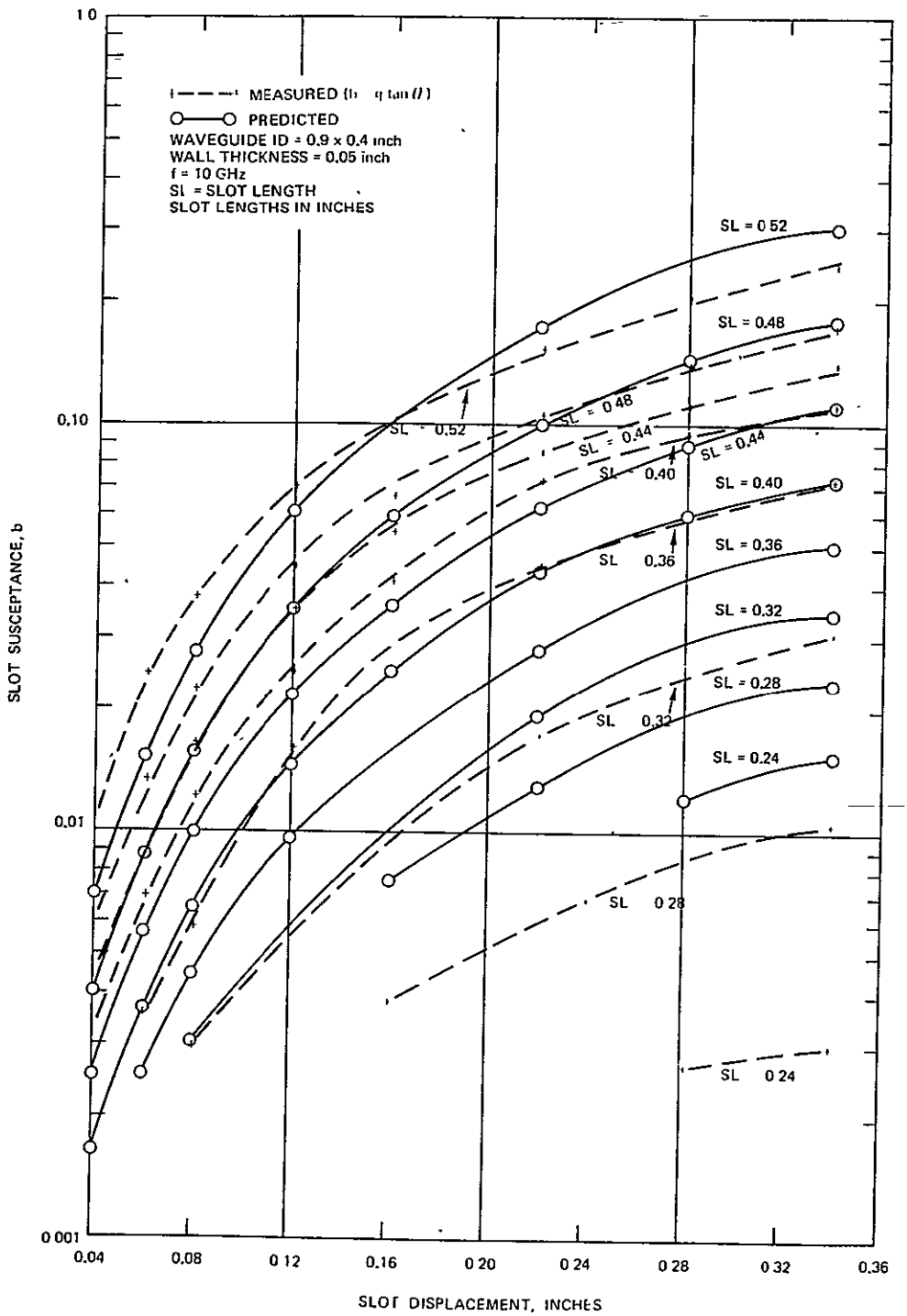

Figure 46. Predicted versus measured susceptance of longitudinal shunt slot as a function of slot displacement.

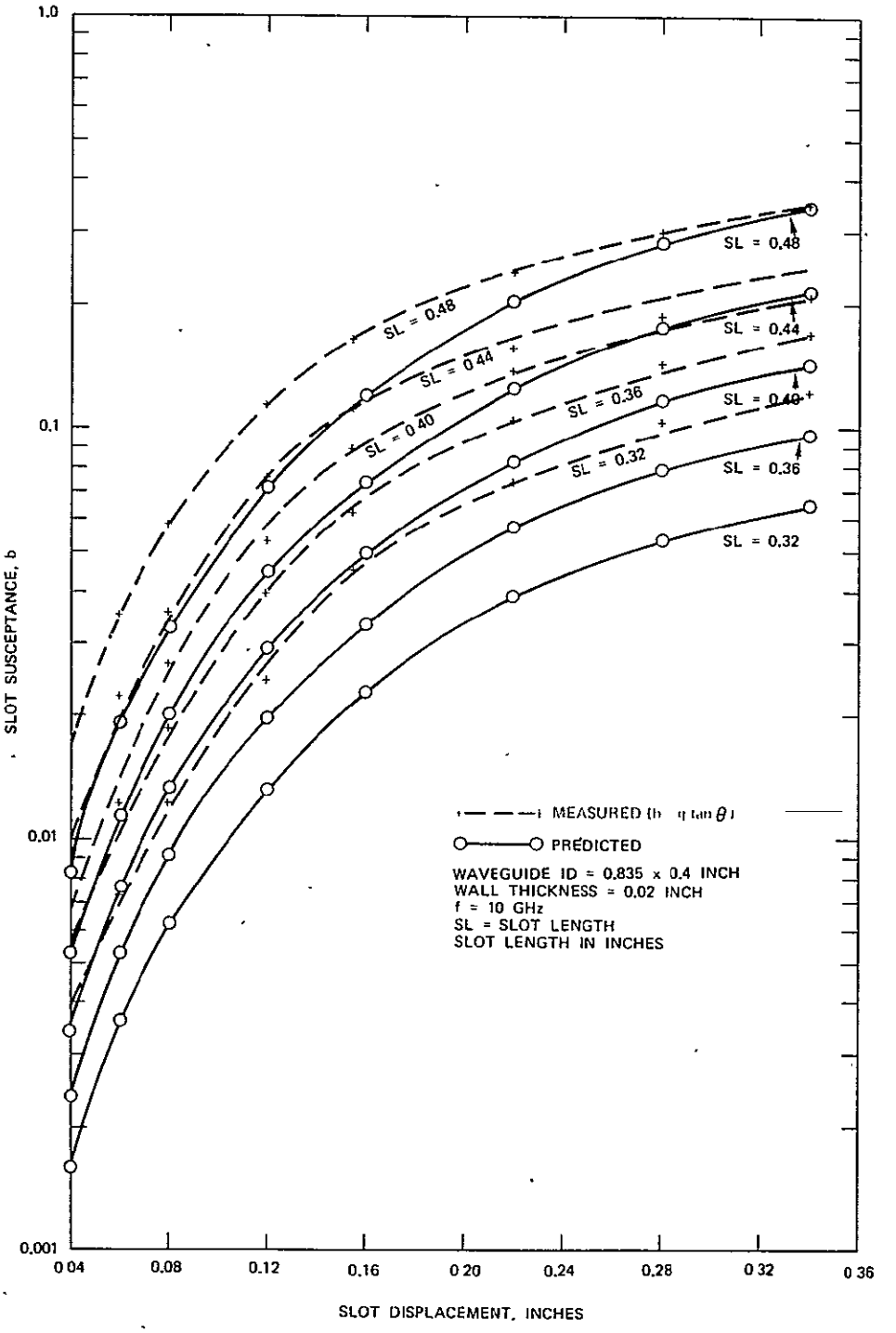

Figure 47. Predicted versus measured susceptance of longitudinal shunt slot as a function of slot displacement.

0.062-inch-wide slot is only 0.008 inch from the waveguide centerline. Because the transverse wall currents, which excite the longitudinal shunt slots, go thru zero and reverse direction at the waveguide centerline, it is to be expected that the prediction of slot conductance would be most subject to error in this region. The experimental conductance curves are seen to fall off less rapidly than the theoretical curves in this centerline region. The implication here is that, although theory predicts zero conductance when the slot is on the centerline, the finite width of the slot will result in a finite conductance.

In general, the poorest agreement between the theoretical and experimental results is seen to occur for the slot susceptance performance, Figures 46 and 47. Also, similarly to the slot conductance curves, the experimental susceptance curves are seen to fall off less rapidly than the theoretical curves as the slots approach the waveguide centerline. As previously discussed in Section 5.2, the susceptance plots are derived from the measured conductances and radiation phases by the relation $b = g \tan \theta$. Since the radiation phase angle, θ, is in the range of 65 to 89.5 degrees for the slot parameters tested (see Figures 25 and 31), small errors in the measurement of the radiation phase can result in large errors in the derived susceptance. For example, referring to Figure 31 for the case of a slot length of 0.32 inches, the measured and theoretical phases are, respectively 89 degrees and 87.3 degrees. This 1.7 degree phase difference is small, however it gives an experimental susceptance that is 2.7 times (4.3 dB) larger than the theoretical susceptance. Similarly, referring to Figure 25 for the 0.24 inch slot length, the 0.5 degree phase difference (measured phase = 89 degrees, theoretical phase = 89.5 degrees) gives an experimental susceptance that is 2 times (3 dB) smaller than the theoretical susceptance. The significance of these errors is discussed in Section 6.

5.4 EXPERIMENTAL SLOT PERFORMANCE WITH BAFFLES

Baffles, or image planes, serve the purpose of simulating the presence of similar slots which, together with the slot under consideration, form an infinite linear array in the direction transverse to the baffles. Referring to the experimental arrangement illustrated in Figure 48, the

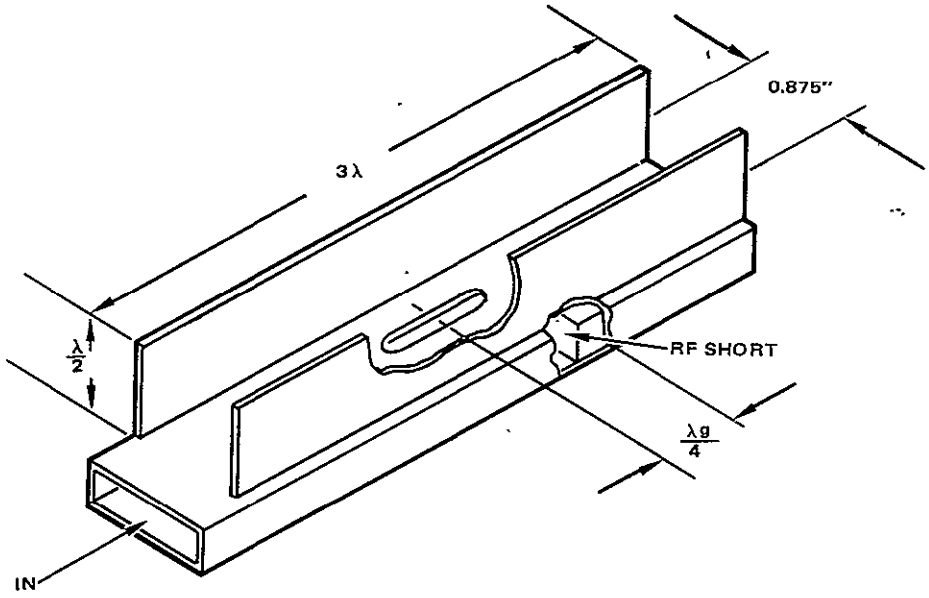

Figure 48. Broadwall longitudinal shunt slot with baffles.

simulated, infinite, linear array is in the direction parallel to the electric-field polarization of the slot. The objective of measuring the slot performance with baffles is to arrive at an estimate of slot conductance and susceptance under conditions of mutual coupling from other slots in the environment. Since a single slot with baffles simulates only an infinite linear array, some measurements were also made with an arrangement of 10 broadwall longitudinal shunt slots with baffles. In this case the simulation would be of 10 infinite linear arrays which more realistically represents the MRF planar array configuration.

The baffle arrangement is represented in Figure 48. The baffles were located symmetrically about the centerline of the slot and spaced a distance 0.875 inch apart, where 0.875 inch is the spacing between the vertically running linear arrays making up the MRF planar array. To obtain more complete and meaningful data, it was later decided to vary this spacing. The height of the baffles was one-half free-space wavelength, and for the single slot, their length was three wavelengths. For the ten-slot case, the slots were spaced by a half guide wavelength (0.782 inch), and the baffles were extended 1.5 free-space wavelengths beyond the center of the end slots.

The experimental performance of some sample slots with baffles are graphically presented in Figures 49 and 50. All the test data was taken by impedance measurement with short terminations spaced a quarter of a guide wavelength from the slot, or from the last slot in the 10-slot case. For reference purposes, the conductance and susceptance values of these slots in the absence of the baffles are also given in Figures 49 and 50.

Inspection of the conductance data, Figure 49, reveals that the conductances of single reactive slot and of the 10 reactive slots are affected similarly by the baffles. In both cases, the effect of the added baffles is to strongly decrease the conductances. At the MRF array baffle spacing, the conductances of the single reactive and 10 reactive slots decreased by 2.5 dB and 3 dB, respectively. In contrast, the susceptance data of Figure 50 shows that the susceptance of the reactive slots increases slightly when the baffles are added. At the MRF array baffle spacing, the addition of baffles increased the slot susceptance of the single reactive and of the 10 reactive slots by 1.31 dB and 0.9 dB, respectively. The change in reactive-slot conductances and susceptances is small with change in baffle spacing. For a baffle spacing change from 0.5 to 0.9 free-space wavelengths, the slot conductances and susceptance change by a maximum of 1.2 dB.

Although the MRF array will not use resonant slots in the design, resonant slot data is presented in Figures 49 and 50 both for comparison purposes and as a guide for interpolation for slot lengths that fall between the 0.59-inch resonant slot length and the 0.48-inch reactive slot length that was selected for test. What stands out most clearly for the resonant slot data, Figure 49, is the rapid change in conductance, versus baffle spacing, for both the single and 10 slot cases. For a baffle spacing change from 0.5 to 0.9 wavelengths, the single slot and 10 slot conductances change, respectively, by 4.4 and 4.3 dB. As seen in Figure 49, the addition of baffles generally increases the resonant conductances but, with baffles spaced widely (about 0.8 wavelengths and greater) the conductances will decrease.

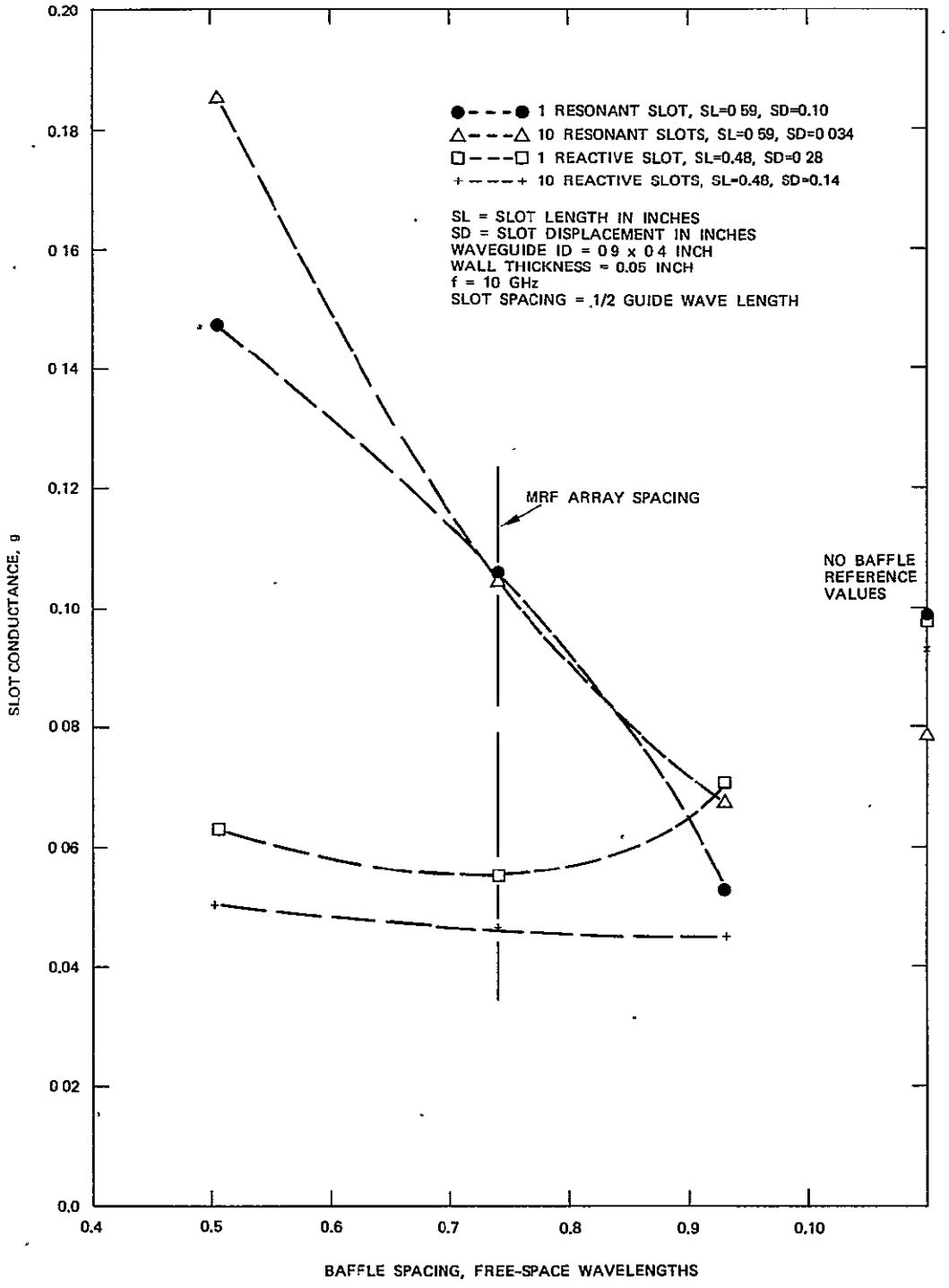

Figure 49. Conductance of longitudinal shunt slot as a function of baffle spacing.

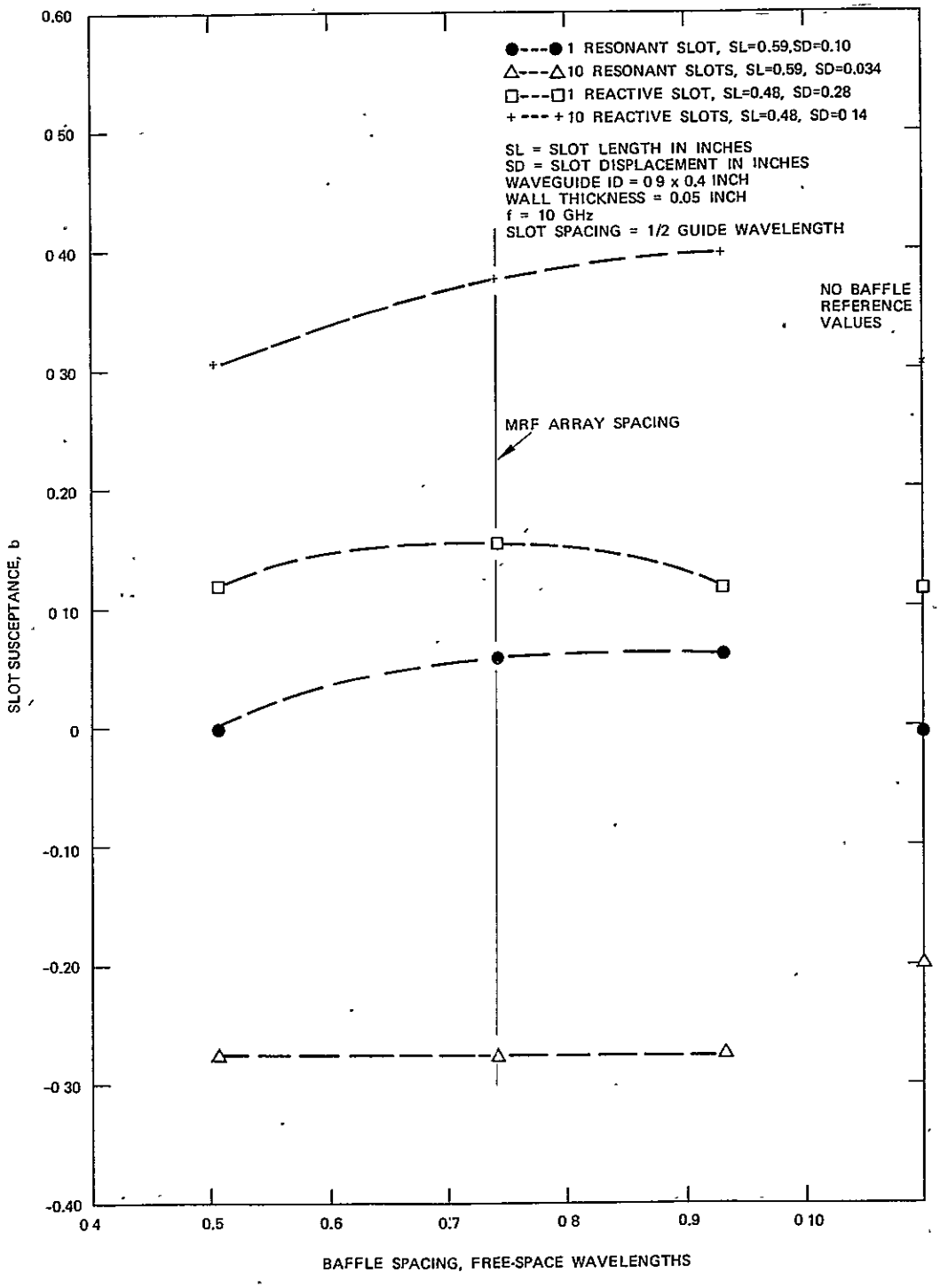

Figure 50. Susceptance of longitudinal shunt slot as a function of baffle spacing.

6.0 SUMMARY, CONCLUSIONS, AND RECOMMENDATIONS

A preliminary MRF array design study was completed in which: (1) The slot element spacing limitations were determined. (2) The aperture impedance change versus scan angle was investigated. (3) The slot conductance requirements were determined. (4) Test slots were selected on the basis of these conductance requirements and the predicted theoretical slot performance. (5) The designs using multiple slots per element were evaluated. (6) Slot conductance error effects were evaluated; and (7) design approaches using variable slot length and variable slot displacement were evaluated with the objective of minimizing aperture phase errors.

On the basis of this preliminary design study, an internal width of 0.835 inch and an external dimension of 0.875 inch was selected for the waveguide composing the linear array sections. Also, it was determined that the spacing between the broadwall, longitudinal, shunt slots could be up to 0.622 inch. The results of the aperture impedance study showed that, for lattice spacings corresponding to this waveguide internal dimension and to these slot spacings, the aperture impedance change with beam scan in the horizontal plane was small; therefore, aperture impedance variations, versus beam scan, would not be expected to result in any serious aperture distribution changes. The results of the slot conductance error study shows that gain, beamwidth, and sidelobe-level performance is quite insensitive to slot conductance errors. It is only when the overall conductance errors are worse than either twice or one half of the design conductance that the array gain degrades by 0.5 dB or more. In this case, an error conductance equal to twice the design conductance results in a gain loss of 0.43 dB due to an increase in the vertical plane beamwidth; and an error conductance equal to one-half the design conductance results in a gain loss of 0.48 dB due to an excess amount of power being dissipated in the terminating loads. A number of design approaches utilizing multiple slots per element were shown to be feasible in that the low-level grating lobes that occurred were either lost in the normal, low-level, sidelobe structure or they occurred above the main lobe, pointing either above the horizon or at long ranges towards the earth. The best performance occurred for the case where the number of slots per element were variable, Figure 14.

A principal design problem area, that has emerged from the preliminary design study, relates to the potential buildup of large, non-linear, aperture phase errors due to the phases of transmission coefficients of the reactive slots (see Figures 15 and 16). The large, non-linear, phase error can occur under either of two circumstances: (1) improper or ineffective slot design in which the transmission coefficient phase accumulation across the aperture is non-linear rather than linear or (2) mutual coupling effects so altering the slot reactance that a proper slot design, providing a linear phase accumulation, is altered to an improper slot design, providing a non-linear phase accumulation. The results of the preliminary design study indicate that an accurate prediction of the susceptance of the slots in the array environment is more crucial than the prediction of slot conductances.

The evaluation of three differenct techniques of slot measurement resulted in the selection of the probe comparison measurement technique as the principal experimental approach with the impedance measurement technique being limited to the measurement of some higher-conductance reference slots. The interference-pattern measurement technique was discarded because of low sensitivity and because of a variety of factors that contribute error.

The performance of 43 slots in standard waveguide with inside dimensions of 0.9 x 0.4 inch and 40 slots in waveguide selected for the MRF design (0.835 x 0.4 inch) was measured. Both the radiation phase and the conductance measurements show good agreement with the theoretical predictions. The largest divergence between the predicted and measured conductances generally occurs at small slot displacements where the longitudinal shunt slot is close to the broadwall centerline of the waveguide. In general, the largest divergence between the predicted and measured results occurs for the slot susceptances. A large portion of this divergence is attributed to the manner of deriving the slot susceptance from the measurements, i.e., $b = g \tan \theta$, where g is the measured conductance and θ is the measured radiation phase angle. Because the radiation phase angle is close to 90 degree, phase angle measurement errors as small as 1 degree can result is susceptance errors as large as 3 dB. The principal consequences of such

susceptance errors in the MRF array design would be a beam broadening and gain loss due to a phase error build-up along the aperture as discussed in Section 3.4.2.

Some limited measurements of the impedance of slots with baffles (or image planes) to simulate mutual coupling effects indicate that mutual coupling effects tend to lower the conductances of reactive slots by as much as 3 dB while the susceptances tended to be increased by about 1 dB. In contrast, measurements on resonant slots showed that the mutual coupling effects generally increased the slot susceptances and conductances, with the conductances rapidly increasing with decreased baffle spacing. For a baffle spacing of one half of a wavelength, the resonant slot conductance increased by as much as 3.8 dB.

On the basis of the measurements and preliminary design results presented in this report, the following conclusions are offered:

1. The study results verify that the proposed MRF array design approach is a feasible one.
2. The conductance data obtained is of sufficient accuracy for the MRF array design, particularly since the array performance is relatively insensitive to conductance design error.
3. The susceptance uncertainty appears to be greater than that desired; however, this uncertainty can be resolved with appropriate linear array breadboard design tests. Also, the uncertainty may be lessened by means of additional experimental tests in which the transmission coefficient phase of a limited number of reactive slots would be measured directly. Since these transmission phases are small (4 degrees and less), it would be necessary to test clusters of about 10 identical slots each to achieve the proper test accuracy. The limited data from these measurements would be used for spot confirmation or correction of the more extensive data in Figures 37, 39, 41 and 43.
4. Mutual coupling effects, as measured by tests of slots with baffles, are indicated to be significant and should be evaluated in more detail. This can be done either by small array modeling or analyses. The analytical approach would be complex and lengthy, especially since the slots are non-resonant.

On the basis of these conclusions, it is recommended that an experimental array design program be carried out next.

7.0 REFERENCES

1. Amitay, Galindo, and Wu, "Theory and Analysis of Phased Array Antennas", Wiley - Interscience, New York, 1972.

2. Andre Dion, "Nonresonant Slotted Arrays", IRE Trans. on Antennas and Propagation, Volume AP-6, No. 4, pp. 360-365, October 1958.

3. "Final Report of MRF Study, Part II Antenna Design", Contract No. NAS 5-22468, February 1976.

4. J. R. Lee, "Traveling-Wave Feed for the Doppler Guidance Phased Array", IDC No. 2767.20/79. Antenna Laboratory, Hughes Aircraft Company, Culver City, California, June 1968.

5. R. W. Breithaupt, G. C. McCormick, "Traveling Wave Arrays of Mismatched Elements", IEEE Trans. Antennas Propagat., Volume AP-19, No. 1, January 1971.

6. L. L. Bailin and M. J. Ehrlich" "Factors Affecting the Performance of Linear Arrays", Proc. IRE, Volume 41, pp. 235-241, 1953.

7. H. F. O'Neil and L. L. Bailin" "Further Effects of Manufacturing Tolerances on the Performance of Linear Shunt Slot Arrays", IRE Trans., PGAP-4, pp. 93-102, December 1952.

8. R. J. Stegen, "Waveguide Slot Measurement Techniques", Hughes Aircraft Company, Technical Memorandum No. 262, December 1951.

9. D. Miller, L. E. Raburn, "An Accurate Technique for Measuring Weakly Coupled Slots in Rectangular Waveguide", The Microwave Journal, pp. 70-74, May 1963.